METEOROLOGICAL OFFICE
125826
23 JAN1978
LIBRARY

MET O 11 Technical Note No. 101

An Implicit Dynamic Initialization Scheme

by

Margaret J Atkins

Met O 11 (Forecasting Research Branch)
Meteorological Office
London Road
BRACKNELL
Berkshire RG12 2SZ
UK

December 1977

NOTE: This paper has not been published. Permission to quote from it should be obtained from the Assistant Director of the above Meteorological Office Branch.

Contents

		PAGE
1.	Introduction.	1
2.	Finite-difference schemes and the damping of gravity waves.	1
3.	A scheme for using the backward-implicit method to initialize the 10-level model.	5
4.	Experiments with a barotropic model.	8
	4.1 The model	9
	4.2 Experiments to simulate the external and first internal modes of the 10-level model.	10
	4.3 Experiments to simulate the second internal mode of the 10-level model with $\underline{\Phi} = 0.25 \times 10^4 \ m^2 \ s^{-2}$.	11
	4.4 Experiment to include in the backward-implicit A dynamic initialization scheme the departure from the constant $\underline{\Phi}$ in the equation for the geopotential, analogous to including the departure from a constant static stability in the 10-level model.	13
5.	The dynamic initialization scheme for the 10-level model fine-mesh rectangle version.	15
6.	A damped integration scheme for the 10-level model octagon.	18
7.	A dynamic initialization scheme for the octagon in which only the external and first internal gravity waves are damped.	20
8.	Computing requirements.	21
9.	Conclusions	22
10.	Acknowledgements.	22
	Bibliography	
	Appendix	

1. Introduction

One of the problems with early experiments in dynamic initialization was that the time-stepping schemes which were used, such as the Euler-backward method required many iterations in order to damp high frequency waves and therefore were expensive in computer time. The Okamura scheme (Nitta 1969) used by Temperton (1976), is more highly damped than previous schemes and requires less computation but it is still an explicit scheme with a restriction on the timestep dependent on the speed of the fastest moving gravity wave. Kurihara (1965) discussed an implicit scheme which highly damps high-frequency waves. This scheme is stable for all values of the timestep. This paper shows how this method was incorporated into the formulation of a dynamic initialization scheme for the semi-implicit version of the 10-level model, as described by Burridge and Gadd (1977), and presents the results of some experiments made with the scheme. The results of some preliminary experiments carried out with a barotropic channel model are also described.

The first experiments using a barotropic channel model were carried out by Helmy in 1973 (personal communication). He demonstrated the effectiveness of the backward implicit method in damping high-frequency oscillations. He was particularly interested in the case where the mass field was restored every cycle and the wind field forced to adjust to the mass field. I have used this barotropic channel model in order to test possible schemes for use with the 10-level model. In view of Temperton's (1973) results which showed that it is necessary to allow both mass and wind fields to adjust to each other to obtain a balance on all scales and of the fact that in the future it is probable that both the mass and the wind field will be analysed it was decided to allow mutual adjustment of the mass and wind in the initialization procedure.

2. Finite Difference Schemes and the Damping of Gravity Waves.

Temperton (1975) has analysed the solutions of a linearized system of equations for barotropic flow. He showed that the general solution consists of a meteorological mode and two gravity-wave modes and showed how these solutions were affected by the Okamura dynamic initialization scheme. He considered the linearized equations

$$\frac{\partial u}{\partial t} = -U\frac{\partial u}{\partial x} + fv - \frac{\partial \phi}{\partial x} \tag{2.1}$$

$$\frac{\partial v}{\partial t} = -U\frac{\partial v}{\partial x} - fu \tag{2.2}$$

$$\frac{\partial \phi}{\partial t} = -U\frac{\partial \phi}{\partial x} + fUv - \Phi\frac{\partial u}{\partial x} \tag{2.3}$$

where u , v , ϕ are perturbations independent of y about a basic state consisting of a zonal current U in geostrophic balance with mean geopotential Φ. Considering a particular wave-number in isolation we may write the equations in matrix form

$$\frac{d}{dt}\begin{pmatrix}\hat{u}\\ \hat{v}\\ \hat{\phi}\end{pmatrix} = \begin{pmatrix}-ikU & f & -ik\\ -f & -ikU & 0\\ -ik\Phi & fU & -ikU\end{pmatrix}\begin{pmatrix}\hat{u}\\ \hat{v}\\ \hat{\phi}\end{pmatrix} \tag{2.4}$$

where $u(x,t) = \sum_k \hat{u}_k(t)\exp(ikx)$ etc.

and the subscript k has been omitted.

(2.4) may be written as

$$\frac{d\underline{z}}{dt} = \underline{\underline{A}}\,\underline{z} \qquad (2.5)$$

Let the eigenvalues of $\underline{\underline{A}}$ be $\lambda_i = ik\sigma_i$ and the eigenvectors be $\underline{\psi}_i$, $i = 1,2,3$. Then if $\underline{\underline{D}}$ is the matrix whose columns are the eigenvectors of $\underline{\underline{A}}$, multiplying (2.5) by $\underline{\underline{D}}^{-1}$

$$\frac{d\underline{\zeta}}{dt} = \begin{pmatrix} ik\sigma_1 & 0 & 0 \\ 0 & ik\sigma_2 & 0 \\ 0 & 0 & ik\sigma_3 \end{pmatrix} \underline{\zeta} \qquad (2.6)$$

where $\underline{\zeta} = \underline{\underline{D}}^{-1}\underline{z}$

and the solutions may be written

$$\zeta_i = P_i \exp(ik\sigma_i t) \quad i = 1,2,3 \qquad (2.7)$$

or

$$\underline{z} = \underline{\underline{D}}\,\underline{\zeta} = P_1\exp(ik\sigma_1 t)\underline{\psi}_1 + P_2\exp(ik\sigma_2 t)\underline{\psi}_2 + P_3\exp(ik\sigma_3 t)\underline{\psi}_3$$

The solution for $\underline{z}$ then consists of the sum of three wave solutions with phase speeds σ_1, σ_2, σ_3 which may be identified with the meteorological mode and two gravity-wave modes. The values of the phase speeds are approximately

$$\left.\begin{aligned} \sigma_1 &= -U + \mu \\ \sigma_{2,3} &= -U \pm c \end{aligned}\right\} \qquad (2.8)$$

where $\mu = \dfrac{f^2 U}{f^2 + k^2\Phi}$ and $c = \left(\Phi + f^2/k^2\right)^{\frac{1}{2}}$

The elements of the eigenvectors give the ratio between the geopotential and the two wind components in each mode. The amplitudes P_i are determined from the initial conditions.

$$\begin{pmatrix} P_1 \\ P_2 \\ P_3 \end{pmatrix} = \underline{\underline{S}}(0) = \underline{\underline{D}}^{-1}\underline{Z}(0) \qquad (2.9)$$

This analysis follows Temperton's and is reproduced here for the sake of completeness.

Now consider the finite difference form of equation (2.5)

$$\underline{Z}_{n+1} = \underline{\underline{B}}\,\underline{Z}_n \qquad (2.10)$$

If the eigenvectors of $\underline{\underline{B}}$ are the same as the eigenvectors of $\underline{\underline{A}}$ we may multiply this equation by $\underline{\underline{D}}^{-1}$ to obtain

$$\underline{S}_{n+1} = \begin{pmatrix} \mu_1 & 0 & 0 \\ 0 & \mu_2 & 0 \\ 0 & 0 & \mu_3 \end{pmatrix} \underline{S}_n \qquad (2.11)$$

or $$S_{i\,n+1} = \mu_i S_{in} \qquad i = 1, 2, 3$$

where μ_i are the eigenvalues of $\underline{\underline{B}}$

Now

$$\underline{Z}_n = \underline{\underline{D}}\,\underline{S}_n = S_{1n}\underline{\Psi}_1 + S_{2n}\underline{\Psi}_2 + S_{3n}\underline{\Psi}_3 \qquad (2.12)$$

and $$\underline{Z}_{n+1} = \underline{\underline{D}}\,\underline{S}_{n+1} = S_{1n+1}\underline{\Psi}_1 + S_{2n+1}\underline{\Psi}_2 + S_{3n+1}\underline{\Psi}_3$$

$$= \mu_1 S_{1n}\underline{\Psi}_1 + \mu_2 S_{2n}\underline{\Psi}_2 + \mu_3 S_{3n}\underline{\Psi}_3 \qquad (2.13)$$

Thus the meteorological and the two gravity wave parts of the solution are multiplied by μ_1, μ_2 and μ_3 respectively each timestep. If we write $\mu_i = R_i e^{i\theta_i}$, $i=1,2,3$ then the amplitude of the solutions is multiplied by R_i and the phase changed by θ_i. In dynamic initialization we are usually concerned with integrating forward one timestep and then backwards one timestep and we consider the equation

$$\underline{\underline{Z}}^{\nu+1} = \underline{\underline{C}}\,\underline{\underline{Z}}^{\nu} \qquad (2.14)$$

where ν is the cycle number. Again if $\underline{\underline{C}}$ has the same eigenvectors as $\underline{\underline{A}}$ we find that the meteorological and gravity waves are multiplied by the eigenvalues of $\underline{\underline{C}}$ each cycle. The finite difference scheme is chosen so that the eigenvalues

are real resulting in no change of phase over the cycle and also, as far as is possible, that the eigenvalue corresponding to the meteorological solution is approximately equal to one while those corresponding to the gravity waves are very much less than one, resulting in the gravity wave solution being damped and the meteorological solution being left unaltered.

If η_i , i=1,2,3, are the eigenvalues of $\underline{\underline{C}}$ and if $\eta_1 \approx 1$ and $\eta_{2,3} \ll 1$ we have

$$\underline{z}^{\nu} = (\eta_1)^{\nu} S_1(0) \underline{\psi}_1 + (\eta_2)^{\nu} S_2(0) \underline{\psi}_2 + (\eta_3)^{\nu} S_3(0) \underline{\psi}_3 \qquad (2.15)$$

then $\underline{z}^{\nu} \rightarrow S_1(0) \underline{\psi}_1$ as $\nu \rightarrow \infty$

or $\underline{z}^{\nu} \rightarrow P_1 \underline{\psi}_1$ as $\nu \rightarrow \infty$

In many finite difference schemes, $\underline{\underline{B}}$ and $\underline{\underline{C}}$ are simple functions of $\underline{\underline{A}}$ and have the same eigenvectors. Two examples are given below.

(i) Okamura's or Nitta's scheme

Equation (2.5) may be approximated for this scheme as follows:-

$$\left.\begin{aligned} \underline{z}^{*} &= \underline{z}^{\nu} + \delta t \, \underline{\underline{A}} \, \underline{z}^{\nu} \\ \underline{z}^{**} &= \underline{z}^{*} - \delta t \, \underline{\underline{A}} \, \underline{z}^{*} \\ \underline{z}^{\nu+1} &= 3\underline{z}^{\nu} - 2\underline{z}^{**} \end{aligned}\right\} \qquad (2.16)$$

which implies

$$\underline{z}^{\nu+1} = \left(\underline{\underline{I}} + 2\delta t^2 \underline{\underline{A}}^2\right) \underline{z}^{\nu} \qquad (2.17)$$

so

$$\underline{\underline{C}} = \underline{\underline{I}} + 2\delta t^2 \underline{\underline{A}}^2 \qquad (2.18)$$

It is easily shown that the eigenvectors of $\underline{\underline{C}}$ are the same as the eigenvectors of $\underline{\underline{A}}$ and that the eigenvalues of $\underline{\underline{C}}$ are given by

$$\eta_i = 1 - 2\delta t^2 \sigma_i^2 k^2 \qquad i = 1, 2, 3$$

From (2.8) $k\sigma_1 \ll k\sigma_{2,3}$ for high frequency gravity waves. Provided the timestep δt is chosen such that $k\sigma_i \delta t < 1$, i=1,2,3 the gravity waves are damped considerably more than the meteorological solution.

(ii) Backward-implicit scheme

If the whole of the right-hand side of equation (2.5) is treated using the backward-implicit method we have, for a forward step

$$\underline{z}_{n+1} = \underline{z}_n + \delta t \, \underline{\underline{A}} \, \underline{z}_{n+1} \qquad (2.19)$$

or

$$\underline{z}_{n+1} = \left(\underline{\underline{I}} - \delta t \underline{\underline{A}}\right)^{-1} \underline{z}_n \qquad (2.20)$$

A complete cycle may be represented by

$$\underline{\underline{z}}^{\nu+1} = \left(\underline{\underline{I}} + \delta t \underline{\underline{A}}\right)^{-1}\left(\underline{\underline{I}} - \delta t \underline{\underline{A}}\right)^{-1} \underline{\underline{z}}^{\nu} \qquad (2.21)$$

so

$$\underline{\underline{C}} = \left(\underline{\underline{I}} + \delta t \underline{\underline{A}}\right)^{-1}\left(\underline{\underline{I}} - \delta t \underline{\underline{A}}\right)^{-1} \qquad (2.22)$$

Again it may be shown that the eigenvectors of $\underline{\underline{C}}$ are the same as the eigenvectors of $\underline{\underline{A}}$ and that the eigenvalues are given by

$$\eta_i = \frac{1}{1 + k\sigma_i^2 \delta t^2} \qquad i = 1, 2, 3$$

and again if $\sigma_1 \ll \sigma_2, \sigma_3$ it can be seen that the gravity waves are damped considerably more than the meteorological solution.

It was this highly damping property of the backward implicit scheme together with the fact that it is stable regardless of the length of the timestep which made it an attractive scheme to use. However in practice it is difficult to use it simply, as described above, and some of the terms on the right-hand side of the equations have to be integrated by other methods, resulting in the matrices $\underline{\underline{A}}$ and $\underline{\underline{C}}$ having different sets of eigenvectors. This is described more fully in the next section.

3. A Scheme for using the backward-implicit method to initialize the 10-level model

The initialization scheme for the 10-level model was designed to be used with the semi-implicit version of the model, described by Burridge (1975) and Burridge and Gadd (1977). In this version the equations are integrated using a split time-differencing scheme. The non-linear terms are integrated using a Lax-Wendroff timestep. The stability criterion for the timestep in this part of the integration depends on the wind speed. The linear terms, which describe the motion of small-amplitude inertio-gravitational oscillations are decoupled, with respect to the ICAO standard atmosphere, into ten independent sets of equations one for each of the ten gravity-wave modes of the model. The external and first internal mode, which involve the two fastest moving gravity waves, are integrated with a semi-implicit timestep and the eight remaining higher-order modes are integrated with an explicit timestep. The stability criterion for the explicit timestep is less stringent than for Lax-Wendroff step. The time integration scheme for the initialization is similar to that of the forecast model. The non-linear terms are integrated using a Lax-Wendroff timestep. The linear equations are again decoupled and this time the external and first internal modes are integrated with a backward-implicit timestep. Several experiments were carried out to find the best way of integrating the eight higher-order modes. At first it was thought pointless to attempt to damp these internal gravity waves at all as any finite-difference scheme, where the damping was frequency dependent, would not damp them very much owing to their low phase speeds and therefore low frequencies. However it was found that the explicit scheme used in the forecast model was unstable when integrated forwards and backwards and after experimenting unsuccessfully with modifications to this it was decided to use an Euler-backward timestep to integrate the eight higher-order modes. After some experiments with the rectangle this scheme was later modified for the octagon so that the higher-order modes were not integrated at all.

The stability and damping properties of a dynamic initialization scheme such as described above may be examined by considering the equations for barotropic flow, as the linear adjustment equations for one mode of the 10-level model are analogous to the linear terms of the equations for barotropic flow, with mean geopotential depth equal to the square of the phase speed of the gravity waves for that mode.

Consider the equations

$$\frac{\partial u}{\partial t} = -U\frac{\partial u}{\partial x} - V\frac{\partial u}{\partial y} - \frac{\partial \phi}{\partial x} + fv \qquad (3.1)$$

$$\frac{\partial v}{\partial t} = -U\frac{\partial v}{\partial x} - V\frac{\partial v}{\partial y} - \frac{\partial \phi}{\partial y} - fu \qquad (3.2)$$

$$\frac{\partial \phi}{\partial t} = -U\frac{\partial \phi}{\partial x} - V\frac{\partial \phi}{\partial y} - \Phi\left(\frac{\partial u}{\partial x} + \frac{\partial v}{\partial y}\right) \qquad (3.3)$$

where u, v and ϕ are perturbations about a steady state solution U, V, Φ with small spatial variation. Again considering a particular wave number in each of the x and y directions in isolation where

$$u(x,y,t) = \sum_{\mu_x \mu_y} \hat{u}_{\mu_x,\mu_y}(t)\exp[i(\mu_x x + \mu_y y)] \quad \text{etc.}$$

we may write these equations in the form

$$\frac{d\underline{z}}{dt} = \underline{\underline{A}}\,\underline{z} \qquad (3.4)$$

where $\underline{z} = (\hat{u}, \hat{v}, \hat{\phi})^T$

The Lax-Wendroff timestep for the advection terms may be represented by

$$\underline{z}_n^* = \underline{\underline{N}}(\delta t)\,\underline{z}_n \qquad (3.5)$$

and the linear adjustment stage may be represented by

$$\underline{z}_{n+1} = \underline{\underline{L}}(\delta t)\,\underline{z}_n^* \qquad (3.6)$$

for a forward timestep. A cycle of initialization may therefore be represented by

$$\underline{z}^{2n+1} = \underline{\underline{L}}(-\delta t)\underline{\underline{N}}(-\delta t)\underline{\underline{L}}(\delta t)\underline{\underline{N}}(\delta t)\,\underline{z}^{2n} \qquad (3.7)$$

and the stability and damping properties of the scheme may be found by considering the matrix.

$$\underline{\underline{C}} = \underline{\underline{L}}(-\delta t)\underline{\underline{N}}(-\delta t)\,\underline{\underline{L}}(\delta t)\underline{\underline{N}}(\delta t) \qquad (3.8)$$

This may be written

$$\underline{\underline{C}} = n(-\delta t)n(\delta t)\,\underline{\underline{L}}(-\delta t)\,\underline{\underline{L}}(\delta t) \qquad (3.9)$$

since it may be shown that $\underline{\underline{N}}(\delta t) = n(\delta t)\underline{\underline{I}}$ and $\underline{\underline{N}}(-\delta t) = n(-\delta t)\underline{\underline{I}}$ where $n(\delta t)$, $n(-\delta t)$ are scalars. The eigenvectors of $\underline{\underline{C}}$ are therefore the eigenvectors of $\underline{\underline{L}}(-\delta t)\underline{\underline{L}}(\delta t)$ and the eigenvalues of $\underline{\underline{C}}$ are $n(-\delta t)n(\delta t)$ times the eigenvalues of $\underline{\underline{L}}(-\delta t)\underline{\underline{L}}(\delta t)$.

For the eight higher-order modes, for which the linear terms are integrated entirely with an Euler-backward timestep the eigenvectors of $\underline{\underline{L}}(-\delta t)\underline{\underline{L}}(\delta t)$ are the same as the eigenvectors of $\underline{\underline{A}}$ and therefore it may be shown that for

these modes the gravity waves are damped and the meteorological solution is left largely unaltered. For the external and first internal mode the linear terms are integrated using the backward-implicit method except for the coriolis terms which are integrated separately in order to facilitate the solution of the resulting Helmholtz equations. The term representing the departure from the ICAO-standard-atmosphere static stability is also integrated separately. This will be described in section 4. This separate treatment of some of the terms in the linear equation causes the eigenvectors of $\underline{\underline{L}}(-\delta t)\,\underline{\underline{L}}(\delta t)$ to be not necessarily the same as the eigenvectors of $\underline{\underline{A}}$. However in many schemes the meteorological mode is an eigenvector. In this case let the eigenvectors of $\underline{\underline{L}}(-\delta t)\,\underline{\underline{L}}(\delta t)$ be $\underline{\psi}_1$, $\underline{\psi}_5$, $\underline{\psi}_6$ and let $\underline{\underline{F}}$ be the matrix whose columns are these eigenvectors. Then multiplying equation (3.7) by $\underline{\underline{F}}^{-1}$ we have

$$\underline{\xi}^{\nu+1} = \begin{pmatrix} \eta_1 & 0 & 0 \\ 0 & \eta_2 & 0 \\ 0 & 0 & \eta_3 \end{pmatrix} \underline{\xi}^{\nu} \qquad (3.10)$$

where $\underline{\xi} = \underline{\underline{F}}^{-1}\underline{z}$ and η_1, η_2, η_3 are the eigenvalues of $\underline{\underline{C}}$. An equation analogous to (2.15) may then be obtained

$$\underline{z}^{\nu} = (\eta_1)^{\nu}\xi_1(0)\underline{\psi}_1 + (\eta_2)^{\nu}\xi_2(0)\underline{\psi}_2 + (\eta_3)^{\nu}\xi_3(0)\underline{\psi}_3$$

If $\eta_1 \approx 1$ and $\eta_2, \eta_3 \ll 1$ we have

$$\underline{z}^{\nu} \Rightarrow \xi_1(0)\underline{\psi}_1 \text{ as } \nu \to \infty$$

Now $\underline{\xi}(0) = \underline{\underline{D}}\,\underline{z}(0)$ and $\underline{\xi}(0) = \underline{\underline{F}}\,\underline{z}(0)$ so in general

$$\xi_1(0) \neq \xi_1(0) \quad \text{i.e.} \quad \xi_1(0) \neq P_1$$

This means that the dynamic initialization will converge to a solution in which the ratio of the geopotential and wind components are those of the meteorological solution but their amplitudes will not be those which exist in the initial data. This fact does not appear to have caused any problems in the dynamic initialization scheme devised for the 10-level model but should perhaps be borne in mind in the planning of any future scheme.

Two methods of including the coriolis terms for the external and first internal modes were considered.

(i) The coriolis terms were evaluated explicitly.

Consider the terms of equations (3.1) to (3.3) which are analogous to the equations for the linear adjustment step of the 10-level model.

$$\frac{\partial u}{\partial t} = -\frac{\partial \phi}{\partial x} + fv \qquad (3.11)$$

$$\frac{\partial v}{\partial t} = -\frac{\partial \phi}{\partial y} - fu \qquad (3.12)$$

$$\frac{\partial \phi}{\partial t} = -\overline{\Phi}\left(\frac{\partial u}{\partial x} + \frac{\partial v}{\partial y}\right) \qquad (3.13)$$

Then the backward-implicit scheme with the coriolis terms evaluated explicitly is given, for a forward step, by

$$u_{n+1} = u_n - \delta t \left(\frac{\partial \phi}{\partial x}\right)_{n+1} + \delta t f v_n \tag{3.14}$$

$$v_{n+1} = v_n - \delta t \left(\frac{\partial \phi}{\partial y}\right)_{n+1} - \delta t f u_n \tag{3.15}$$

$$\phi_{n+1} = \phi_n - \delta t \bar{\Phi} \left(\frac{\partial u}{\partial x} + \frac{\partial v}{\partial y}\right)_{n+1} \tag{3.16}$$

The eigenvalues of $\underline{\underline{L}}(-\delta t)\underline{\underline{L}}(\delta t)$ in this case are

$$1 \quad , \quad \frac{1+\delta t^2 f^2}{1+\delta t^2 k^2 \bar{\Phi}} \quad , \quad \frac{1+\delta t^2 f^2}{1+\delta t^2 k^2 \bar{\Phi}}$$

where $k^2 = \mu_x^2 + \mu_y^2$. When the effect of spatial finite differences is taken into account both f and k^2 are replaced by more complex expressions. It may be shown that the eigenvector corresponding to the eigenvalue 1 is the meteorological mode. The gravity wave modes are stable and damped only if $|k\bar{\Phi}| > |f|$ but unstable for $|k\bar{\Phi}| < f$ i.e. for low frequencies.

(ii) The coriolis terms were evaluated using an Euler-backward timestep.

For a forward step equations (3.11) to (3.13) become

$$u_{n+1} = u_n - \delta t \left(\frac{\partial \phi}{\partial x}\right)_{n+1} + \delta t f v_I \tag{3.17}$$

$$v_{n+1} = v_n - \delta t \left(\frac{\partial \phi}{\partial y}\right)_{n+1} - \delta t f u_I \tag{3.18}$$

$$\phi_{n+1} = \phi_n - \delta t \bar{\Phi} \left(\frac{\partial u}{\partial x} + \frac{\partial v}{\partial y}\right)_{n+1} \tag{3.19}$$

where

$$u_I = u_n - \delta t \left(\frac{\partial \phi}{\partial x}\right)_n + \delta t f v_n \tag{3.20}$$

$$v_I = v_n - \delta t \left(\frac{\partial \phi}{\partial y}\right)_n - \delta t f u_n \tag{3.21}$$

In this case the matrix $\underline{\underline{L}}(-\delta t)\underline{\underline{L}}(\delta t)$ is very complicated and it is it is arduous to calculate all the eigenvalues. However it has been demonstrated that one of the eigenvectors is the meteorological mode with eigenvalue 1. The damping properties have been demonstrated in the experiments which are described in the following section.

4. Experiments with a Barotropic Model.

Several experiments were carried out with Helmy's barotropic channel model in order to test the effective damping of finite difference schemes which could be used in the 10-level model.

(4.1) The model.

The basic equations were

$$\frac{\partial u}{\partial t} + u\frac{\partial u}{\partial x} + v\frac{\partial u}{\partial y} + \frac{\partial \phi}{\partial x} - fv = 0 \qquad (4.1)$$

$$\frac{\partial v}{\partial t} + u\frac{\partial v}{\partial x} + v\frac{\partial v}{\partial y} + \frac{\partial \phi}{\partial y} + fu = 0 \qquad (4.2)$$

$$\frac{\partial \phi}{\partial t} + u\frac{\partial \phi}{\partial x} + v\frac{\partial \phi}{\partial y} + \bar{\Phi}\left(\frac{\partial u}{\partial x} + \frac{\partial v}{\partial y}\right) = 0 \qquad (4.3)$$

where x is positive in the easterly direction, y is positive in the northerly direction, u, v are the eastward and northward components of the wind and ϕ is the geopotential depth with mean $\bar{\Phi}$. In the first experiments the geopotential was assumed constant for the last term of equation (4.3). Later the departure from $\bar{\Phi}$ was also included. The grid consisted of 33 x 31 points with a grid length of 200 km. There were cyclic boundary conditions in the east-west direction and constant boundary conditions on the north and south boundaries. The coriolis parameter was specified as a linear function of y by

$$f = 2.0 \times 10^{-4} + 1.5 \times 10^{-11} y \quad \text{sec}^{-1} \qquad (4.4)$$

where y is in kilometres.

Various different values of $\bar{\Phi}$ were used to simulate the different gravity-wave modes of the 10-level model. Height data were obtained from an analytic function given by Grammelvedt (1969),

$$h(x,y) = H_0 + H_1 \tanh\left\{\frac{9(y-y_0)}{2D}\right\} + H_2 \operatorname{sech}^2\left\{\frac{9(y-y_0)}{D}\right\} \times \left\{0.7 \sin\left(\frac{2\pi x}{L}\right) + 0.6 \sin\left(\frac{6\pi x}{L}\right)\right\} \qquad (4.5)$$

where

$H_0 = \bar{\Phi}/g$

$H_1 = -220$ m

$H_2 = 133$ m

$g = 10$ m sec^{-1}

L is the length = 6600 km

D is the width = 6200 km

$y_0 = D/2$ is middle latitude of the channel.

and the initial geopotential was set equal to gh. The wind field was obtained from the geostrophic approximation. A forward integration with an Euler-backward timestep was made for a period of time sufficient to dissipate all high frequency oscillations. In most cases this was 48 hours. The resulting geopotential and wind fields were then used as initial data. A control run was made by running forwards for 12 hours with a leapfrog timestep. The initial wind field was then replaced by the geostrophic wind and various experiments were performed with different initialization schemes, in each case followed by 12 hours of leapfrog integration which was compared with the control run. We would not expect these integrations to be identical to the control run as both the geopotential and wind fields are free

to adjust to one another during the initialization. A leapfrog integration scheme was used as it would readily show up any imbalance remaining at the end of the initialization. There was averaging introduced into the spatial differencing of the leapfrog scheme to make it consistent with the spatial differencing used in the initialization.

(4.2) Experiments to simulate the external and first internal modes of the 10-level model.

Most of the experiments were run to simulate the external gravity wave. Figure 1 shows the root-mean-square (RMS) divergence plotted every cycle during three different initializations using $\bar{\Phi} = 9 \times 10^4$. Curve 2 is Nitta's or Okamura's scheme. The graph, which is for 108 cycles with a timestep of 200 seconds is equivalent to 12 hours of integration. Curves 1 and 3 are both from experiments using the backward-implicit scheme but with different formulations of the coriolis terms. They both use a timestep of 720 seconds, which is the 10-level model forecast timestep for the rectangle and was thought to be the value which would be used in the 10-level model initialization, and represent an equivalent integration time of 24 hours. The experiment shown by curve 1 uses the Euler-backward formulation of the coriolis terms and will be referred to as the "Backward-Implicit A" scheme. The RMS divergence converges to about the same value as in Nitta's scheme. The experiment shown by curve 3 uses the explicit formulation of the coriolis terms and will be referred to as the "Backward-Implicit B" scheme. The RMS divergence in this case does not tend to a limiting value but after decreasing rapidly at the beginning of the initialization begins to climb slowly again.

Figure 2 shows the RMS vorticity during the initialization. Note that the vertical scale is the same as for the RMS divergence but the origin is displaced. In this case too the backward-implicit A and Okamura schemes behave in a similar fashion, whereas the backward-implicit B scheme behaves rather differently with the RMS vorticity decreasing at the beginning and then increasing again. If the initialization period is extended to 72 hours the RMS vorticity increases to 12.01×10^{-6} sec^{-1}.

Figure 3 shows the RMS height difference between the initial height field and the height field as it adjusts during the initialization. Again Okamura's scheme and the backward-implicit A scheme behave similarly with the RMS height difference increasing rapidly and tending to a steady value. With the backward-implicit B scheme the height difference after reaching what appears to be a balanced value, beings to depart from it more and more as the initialization period is extended.

Figure 4 shows the RMS wind difference between the adjusting wind and the wind field which balances the initial height field. Unfortunately the differences between the initial geostrophic wind and the balanced wind are not available. Okamura's scheme and the backward-implicit A scheme behave in a similar way. The RMS wind difference decreases very slightly and tends to a steady value. In the backward-implicit B scheme the RMS wind difference decreases slightly at the beginning but then begins to increase. Comparing figures 3 and 4 for the Okamura and backward-implicit A schemes it can be seen that with $\bar{\Phi} = 9 \times 10^4$ m^2 s^{-2} the height field is adjusting to balance the initial wind field. These agree well with theory as the critical wavelength given by

$$\lambda = \frac{2\pi}{g}\sqrt{\bar{\Phi}}$$

is approximately equal to 9000 km (which may be compared with the channel dimensions of 6600 and 6200 km). For wavelengths shorter than this we would expect the mass to adjust to the wind field and for longer wavelengths we would expect the wind to adjust to the mass field. In this case most of the wavelengths are shorter than the critical wavelength.

Figure 5 shows the RMS divergence during the subsequent leapfrog integrations. Okamura's and the backward-implicit A scheme give values of the RMS divergence after 12 hours of initialization which are almost identical to each other and similar to the control run. The backward-implict B scheme after 24 hours of initialization gives lower values of the RMS divergence than in the integration with no initialization (curve 4) but has oscillations with about the same amplitude.

These experiments show that the backward-implicit A scheme effectively damps high frequency oscillations and produces results comparable to Okamura's scheme. Since theoretically Okamura's scheme converges to the meteorological solution in the initial data it may be presumed that the backward-implicit A scheme, very nearly does so. However the backward-implicit B scheme, in accordance with the theory, does not converge to the meteorological solution but steadily departs further and further from it. Following these results it was decided to use only the backward-implicit A scheme in the experiments simulating the first internal mode.

Figures 6 to 10 show the results of these experiments using a value of $\overline{\Phi}$ equal to 1×10^4 m^2 s^{-2}. The corresponding curves for the external mode are shown in Figures 6 to 9 for comparison. It can be seen from Figures 6 to 9 that the rate of adjustment is much slower for $\overline{\Phi} = 1 \times 10^4$ than for $\overline{\Phi} = 9 \times 10^4$ as would be expected from theory and also that the height field changes less (Figure 8) and the wind field (Figure 9) in particular the vorticity (Figure 7) changes more as would also be expected from theory. In this case the critical wavelength is approximately 3000 km. Figure 10 shows the RMS divergence during the subsequent 12-hour leapfrog integrations. The values of the divergence and amplitude of the oscillations are much larger, when there is no initialization for this value of $\overline{\Phi}$ than for the previous one and the frequency of the oscillations is lower. After 12 hours of initialization the value of the RMS divergence has been reduced to about that of the control run but there are still quite large amplitude oscillations. These are considerably reduced after 24 hours of initialization again showing that the rate of damping of gravity waves is much less for $\overline{\Phi} = 1 \times 10^4$ than for $\overline{\Phi} = 9 \times 10^4$ given the same wavelength.

(4.3) Experiments to simulate the second internal mode of the 10-level model with $\overline{\Phi} = 0.25 \times 10^4$ m^2 s^{-2}.

The experiments with $\overline{\Phi} = 1 \times 10^4$ were repeated with $\overline{\Phi} = 0.25 \times 10^4$. The results were similar but the dynamic initialization took even longer to converge to a balanced state, the heights changed even less and the winds changed even more. There were still appreciable oscillations in the leapfrog integration after 48 hours of initialization. In a practical scheme it would not be desirable to initialize for such a long period of time so some experiments were carried out to try and find a stable, but not necessarily damped, economical way of integrating the eight higher order modes.

An obvious choice was the explicit scheme used in the 10-level model. However when used to integrate forwards and backwards this turns out to be unstable with eigenvalues, in the notation of section (3), given by

$$1, \quad 1 + \delta t^2 f^2 + k^4 \overline{\Phi}^2 \delta t^4 \pm k^2 \overline{\Phi} \delta t^2 \sqrt{\frac{k^4 \overline{\Phi}^2 \delta t^4}{2} + 1 + \delta t^2 f^2}$$

This scheme was modified so that the heights were evaluated first and substituted into the wind equation on the forward step, and the winds evaluated first and substituted into the height equation on the backward step. Ignoring the coriolis terms this scheme has all its eigenvalues equal to 1 as it simply reverses all operations on the backward step. If the coriolis terms are evaluated explicitly this produces a slightly unstable scheme with eigenvalues $1, 1+\delta t^2 f^2, 1+\delta t^2 f^2$. If the coriolis terms are evaluated with an Euler-backward step, we have for the linear terms of equations (4.1) to (4.3) the forward step.

$$u_1 = u_0^{\nu} - \delta t \frac{\partial \phi_1}{\partial x} + \delta t f v_{IF} \tag{4.6}$$

$$v_1 = v_0^{\nu} - \delta t \frac{\partial \phi_1}{\partial y} - \delta t f u_{IF} \tag{4.7}$$

$$\phi_1 = \phi_0^{\nu} - \delta t \underline{\Phi} \left(\frac{\partial u_0^{\nu}}{\partial x} + \frac{\partial v_0^{\nu}}{\partial y} \right) \tag{4.8}$$

where

$$u_{IF} = u_0^{\nu} - \delta t \frac{\partial \phi_0^{\nu}}{\partial x} + \delta t f v_0^{\nu} \tag{4.9}$$

$$v_{IF} = v_0^{\nu} - \delta t \frac{\partial \phi_0^{\nu}}{\partial y} - \delta t f u_0^{\nu} \tag{4.10}$$

and the backward step

$$u_0^{\nu+1} = u_1 + \delta t \frac{\partial \phi_1}{\partial x} - \delta t f v_{IB} \tag{4.11}$$

$$v_0^{\nu+1} = v_1 + \delta t \frac{\partial \phi_1}{\partial y} + \delta t f u_{IB} \tag{4.12}$$

$$\phi_0^{\nu+1} = \phi_1 + \delta t \underline{\Phi} \left(\frac{\partial u_0^{\nu+1}}{\partial x} + \frac{\partial v_0^{\nu+1}}{\partial y} \right) \tag{4.13}$$

where

$$u_{IB} = u_1 + \delta t \frac{\partial \phi_1}{\partial x} - \delta t f v_1 \tag{4.14}$$

$$v_{IB} = v_1 + \delta t \frac{\partial \phi_1}{\partial y} + \delta t f u_1 \tag{4.15}$$

The eigenvalues are

$$1, \quad 1 - \delta t^2 f^2 + \delta t^4 f^4, \quad 1 - \delta t^2 f^2 + \delta t^4 f^4 + k^2 \underline{\Phi} \delta t^4 f^2$$

which is stable provided that

$$\delta t^2 < \frac{1}{k^2 \underline{\Phi} + f^2}$$

and it may be shown that the meteorological mode is an eigenvector corresponding to the eigenvalue 1. This latter scheme was thought suitable for integrating the eight higher order modes of the 10-level model. However when it was tested using $\underline{\Phi} = 0.25 \times 10^4$ the divergence at first decreased but then steadily increased throughout the initialization and the height difference did not tend to any specific value but also steadily increased. It was thought that this unexpected behaviour might be due to the fact that with a value of $\underline{\Phi}$ as low as 0.25×10^4 the amplitude of the waves in the initial height field was comparable with the depth of the fluid. In order to overcome this problem it was decided to test this finite difference scheme by simulating the external gravity wave using $\underline{\Phi} = 9 \times 10^4$, and then if this were successful to use it in the simulation of the second internal mode starting with an initial height field with smaller amplitude perturbations in it. The results of the experiment using $\underline{\Phi} = 9 \times 10^4$ are shown in Figures 1 to 3. The RMS divergence decreases steadily and appears to level out to a value higher than that for either Okamura's or the backward-implicit A scheme. The RMS vorticity and height difference are only plotted for the first six hours as the curves go off the scale in the second six hours. The RMS wind difference (Figure 4) is not plotted as the curve lies on top of the others. It can be seen from Figure 3 that the height field is not converging to any balanced state and while the RMS divergence is decreasing the RMS vorticity is increasing but the RMS wind difference remains fairly

constant. The RMS divergence during the subsequent leapfrog integration is not shown as it rises very rapidly to values of about 0.6×10^{-6} sec^{-1} and then oscillates between 0.5×10^{-6} sec^{-1} and 0.7×10^{-6} sec^{-1}. Because of the unsatisfactory nature of this scheme, which has not been explained, it was decided to adopt the Euler-backward method to integrate all the linear terms for the eight higher-order modes. The second internal mode with $\underline{\Phi} = 0.25 \times 10^4$ was simulated using an initial field with smaller amplitude waves in it. It was found, when examining the RMS divergence, vorticity, height difference and wind difference during initialization and the RMS divergence during the subsequent leapfrog integration that the Euler-backward scheme used for the linear terms as part of a split scheme produced almost identical results to the backward-implicit A scheme.

(4.4) Experiments to include in the backward-implicit A dynamic initialization scheme the departure from the constant $\underline{\Phi}$ in the equation for the geopotential, analogous to including the departure from a constant static stability in the 10-level model.

In these experiments the first internal mode was simulated with the initial data being defined using $\underline{\Phi} = 1 \times 10^4$ $m^2\ s^{-2}$. The results of 48 hours of Euler-backward integration using a constant value of $\underline{\Phi} = 1 \times 10^4$ in the last term of equation (4.3) were used as initial data. The first experiment was to see what was the effect of using ϕ instead of $\underline{\Phi}$ in this equation in the leapfrog integration starting from these "balanced" fields. The result is shown in Figure 11 ((a) and (b)) and by comparing this with the control run in Figure 10, which is plotted on the same scale and in which $\underline{\Phi}$ was used, it can be seen that the use of ϕ instead of $\underline{\Phi}$ makes very little difference. Experiments were then carried out to see the effect of using in an initialization a value of $\underline{\Phi}$ in equation (4.3) which differed by a rather large amount from the actual value of ϕ. The balanced winds obtained from 48 hours Euler-backward integration with $\underline{\Phi} = 1 \times 10^4$ were replaced by geostrophic winds and the fields were then initialized for the equivalent of 24 hours using a value of $\underline{\Phi} = 9 \times 10^4$ $m^2\ s^{-2}$. This was followed by a leapfrog integration using ϕ in the last term of equation (4.3). The results are shown in Figure 11a. By comparing this with Figure 10 it can be seen that the RMS divergence oscillates with about the same amplitude as if no initialization had been done but that the general level of RMS divergence has been reduced to about the right value. Figure 11b shows the effect of using a value of $\underline{\Phi}$ less than ϕ, in this case $\underline{\Phi} = 0.3 \times 10^4$ $m^2\ s^{-2}$, in the initialization with similar results. Using a constant $\underline{\Phi} = 9 \times 10^4$ $m^2\ s^{-2}$ which is greater than ϕ corresponds in the 10-level model to the case where the atmosphere is more unstable than the ICAO standard atmosphere used in the linear adjustment step and using $\underline{\Phi} = 0.3 \times 10^4$ $m^2\ s^{-2}$, which is less than ϕ, corresponds to the case where the atmosphere is more stable than the ICAO standard atmosphere. Methods were then considered of including the departure from $\underline{\Phi}$ in equation (4.3) in the backward-implicit A dynamic initialization scheme.

(i) The departure from the constant $\underline{\Phi}$ included explicitly.

Considering the linear terms of equations (4.1) to (4.3) we have, for a forward step, in differences

$$u_{n+1} - u_n = -\delta t \left(\frac{\partial \phi}{\partial x}\right)_{n+1} + \delta t f v_I \qquad (4.16)$$

$$v_{n+1} - v_n = -\delta t \left(\frac{\partial \phi}{\partial y}\right)_{n+1} - \delta t f u_I \qquad (4.17)$$

$$\phi_{n+1} - \phi_n = -\delta t \underline{\Phi} \left(\frac{\partial u}{\partial x} + \frac{\partial v}{\partial y}\right)_{n+1} - \delta t (\phi_n - \underline{\Phi}) \left(\frac{\partial u}{\partial x} + \frac{\partial v}{\partial y}\right)_n \qquad (4.18)$$

where u_I and v_I are defined by equation (3.20) and (3.21).
If we write $\phi_n = \bar{\Phi}(1+\gamma)$, the eigenvalues of the amplification matrix $\underline{\underline{L}}(-\delta t)\underline{\underline{L}}(\delta t)$ for this scheme (integrating around a cycle) are

$$1, \quad \frac{1}{1+\omega^2\delta t^2+\gamma^2\frac{\omega^4\delta t^4}{2} \pm \gamma\frac{\omega^2\delta t^2}{2}\sqrt{\gamma^2\omega^4\delta t^4+4(1+\omega^2\delta t^2)}}$$

writing $\omega^2 = (\mu_x^2+\mu_y^2)\bar{\Phi}$ in the notation of section 3 and ignoring the coriolis terms. This scheme is unstable for $|\gamma|>1$. A sketch of these eigenvalues as a function of $\omega^2\delta t^2$ for different values of γ is shown in Figure 12a. In the corresponding case of the 10-level model it has been found that for the external and first internal modes $\gamma<1$ usually. Nevertheless it was decided to look for a scheme which was stable for all possible values of γ. Note that $\gamma<-1$ corresponds to negative values of geopotential in the barotropic model and to the atmosphere being statically unstable in the 10-level model, which is not allowed to occur.

(i) The departure from the constant $\bar{\Phi}$ included with an Euler-backward timestep.

Again considering the linear terms of equations (4.1) to (4.3), for a forward step, we have

$$u_{n+1}-u_n = -\delta t\left(\frac{\partial\phi}{\partial x}\right)_{n+1} + \delta t f v_I \qquad (4.19)$$

$$v_{n+1}-v_n = -\delta t\left(\frac{\partial\phi}{\partial y}\right)_{n+1} - \delta t f u_I \qquad (4.20)$$

$$\phi_{n+1}-\phi_n = -\delta t\bar{\Phi}\left(\frac{\partial u}{\partial x}+\frac{\partial v}{\partial y}\right)_{n+1} - \delta t(\phi_I-\bar{\Phi})\left(\frac{\partial u}{\partial x}+\frac{\partial v}{\partial y}\right)_I \qquad (4.21)$$

where u_I and v_I are again defined by equations (3.20) and (3.21) and

$$\phi_I = \phi_n - \delta t\,\phi_n\left(\frac{\partial u}{\partial x}+\frac{\partial v}{\partial y}\right)_n \qquad (4.22)$$

In this case, writing $\phi = \bar{\Phi}(1+\gamma)$, the eigenvalues of the amplification matrix $\underline{\underline{L}}(-\delta t)\underline{\underline{L}}(\delta t)$, integrating around a cycle are given by

$$1, \quad \frac{1}{1+\frac{\omega^2\delta t^2(1+\gamma)}{1-\gamma\omega^2\delta t^2}}, \quad \frac{1}{1+\frac{\omega^2\delta t^2(1+\gamma)}{1-\gamma\omega^2\delta t^2}}$$

ignoring the coriolis terms.
This is stable for $|\gamma|<1$, and if $\gamma>1$ it is stable provided

$$\delta t \leq \frac{1}{\omega}\sqrt{\frac{2}{\gamma-1}}$$

A sketch of the eigenvalues is shown in Figure 12b.

This second scheme was tested with the barotropic model. Mistakenly in the third equation the last term was included as

$$-\delta t(\phi_n - \bar{\Phi})\left(\frac{\partial u}{\partial x} + \frac{\partial v}{\partial y}\right)_I$$

which does not make any difference in the theoretical analysis. This was corrected for one case and produced results which were virtually indistinguishable from it. The scheme was tested in the initialization with $\bar{\Phi}$ set to 9×10^4 and $\bar{\Phi}$ set to 0.3×10^4. The results are again shown in Figure 11. There is some improvement in both cases but the result is considerably better for the second case of $\bar{\Phi}=0.3\times10^4$. In the first case $\gamma = -8/9$ and in the second case $\gamma = 2\frac{1}{3}$. For this second case the limiting value of δt according to the stability criterion is about 1000 secs. and so the value of δt = 720 secs. which was used for the experiment was well within this. Examining Figure 12 it may be seen that for $\gamma = 2\frac{1}{3}$ the eigenvalue lies between $\pm$ 1 depending on the wavelength, but for $\gamma = -8/9$ the eigenvalue lies very near + 1 for all wavelengths. This probably explains why the scheme is better for $\gamma = 2\frac{1}{3}$. The effects of including the departure from $\bar{\Phi}$ on the rate of damping of the dynamic initialization are also illustrated in Figure 13 which shows the RMS divergence during initialization. Graphs are shown both for initializations where the constant $\bar{\Phi}$ was used and also for those where the departure from $\bar{\Phi}$ was also included. In the case of the latter the results for $\bar{\Phi} = 0.3 \times 10^4$ are very similar to $\bar{\Phi} = 1\times10^4$ but for $\bar{\Phi} = 9\times10^4$ the convergence is much slower and the RMS divergence tends to the wrong value. The curve for $\bar{\Phi} = 1\times10^4$ including the departure from $\bar{\Phi}$ is very similar to that using constant $\bar{\Phi} = 1\times10^4$ which is not shown in Figure 13 but which is the one shown in Figure 6.

5. The dynamic initialization scheme for the 10-level model fine-mesh rectangle version.

A detailed mathematical description of the dynamic initialization scheme for the rectangle version of the 10-level model is contained in the appendix. To summarize this briefly in words, it is a "split" scheme with the non-linear terms of all the equations, except the humidity equation, integrated using a Lax-Wendroff timestep. The linear terms are decoupled into the ten normal modes of the model. The external and first internal mode are integrated using a backward-implicit timestep, with the coriolis terms and the term representing the departure from the ICAO-standard-atmosphere static stability integrated with an Euler-backward timestep. The eight higher-order modes are all integrated with an Euler-backward timestep. The timestep is limited by the speed of the second internal gravity wave and is set at 9 minutes. The equations are integrated one timestep forwards and then the sign of δt is reversed and the equations are integrated one timestep backwards, making one cycle. This process is repeated until the gravity waves have been sufficiently damped. Both the height and wind are free to adjust to one another. There is no diffusion or friction and no physical processes are included except the effect of topography, which is included in a similar way to that in the forecast model (Hayes 1976). An essential part of this process is the setting of the horizontal wind to zero beneath topography every timestep. In the initialization this has been done at the end of every cycle.

The first experiments were to try to improve the balance between the height and wind fields after the operational diagnostic initialization. This scheme was written for the original explicit version of the 10-level model. It is not possible to solve the equations in a manner entirely consistent with the semi-implicit version of the model which uses a different arrangement of the wind components on the horizontal grid. This problem was overcome by performing the initialization on the original "explicit grid" and interpolating on to the "semi-implicit" grid. It has been suggested that this interpolation might be the cause of the gravity waves apparent during the first few hours of the rectangle forecasts and demonstrated on cine films made of some of these forecasts. The

first experiments with the dynamic initialization scheme were made to try to improve these results.

The date used for these experiments was chosen at random. The surface pressure and 500 mb fields are shown in Figure 14. At first it was decided to use the same diagnostics as in the barotropic experiments, that is the root-mean-square divergence, vorticity, height and wind differences during initialization and the root-mean-square divergence during the subsequent forecast. In order to examine the effects of the different finite difference schemes on the different gravity-wave modes these diagnostics were calculated for each of the modes separately by transforming from the variables

$$\underline{u} = \begin{pmatrix} u_1^* \\ u_2^* \\ \vdots \\ u_{10}^* \end{pmatrix}, \quad \underline{v} = \begin{pmatrix} v_1^* \\ v_2^* \\ \vdots \\ v_{10}^* \end{pmatrix}, \quad \underline{h} = \begin{pmatrix} h_1 \\ h_2 \\ \vdots \\ h_{10} \end{pmatrix}$$

where the elements are the height and wind components (in the notation of the appendix) at the 10 levels of the model, to the variables

$$\underline{a} = \begin{pmatrix} a_1 \\ a_2 \\ \vdots \\ a_{10} \end{pmatrix} = \underline{\underline{E}}^{-1}\underline{u}, \quad \underline{b} = \begin{pmatrix} b_1 \\ b_2 \\ \vdots \\ b_{10} \end{pmatrix} = \underline{\underline{E}}^{-1}\underline{v}, \quad \underline{y} = \begin{pmatrix} y_1 \\ y_2 \\ \vdots \\ y_{10} \end{pmatrix} = \underline{\underline{E}}^{-1}\underline{h}$$

where the elements represent the height and wind components for each of the ten normal modes and $\underline{\underline{E}}^{-1}$ is the inverse of the 10 x 10 matrix whose columns are the eigenvectors of a 10 x 10 matrix $\underline{\underline{G}}_0$ whose elements depend on the static stability of the ICAO standard atmosphere. For more details see the appendix and Burridge and Gadd (1977). Only the RMS divergence is illustrated. Figure 15 shows the RMS divergence during initialization for the external (mode 1), first internal (mode 2) and second internal (mode 3) modes. There is a large jump between the first and second cycle because the wind was not forced to zero beneath topography until the end of the first cycle, after the diagnostics were output. Figure 15 shows that the RMS divergence is behaving in the way we would expect during initialization. The adjustment is taking place much more quickly for the external mode than for the first internal mode which in turn has a faster rate of adjustment than the second internal mode. Figure 16 shows the RMS divergence at every timestep during the first four hours of the subsequent forecast, for each of the three modes. This forecast was made after 15 cycles or $4\frac{1}{2}$ hours of initialization by which time it appeared from Figure 15 that most of the adjustment had taken place for at least the external and first internal modes. The corresponding values from the operational forecast, with no dynamic initialization, are shown for comparison. The forecast following dynamic initialization does not show any obvious improvement. The RMS divergence for the external mode increases sharply at the beginning of the forecast indicating that it is too low at the end of the initialization. Similar but less marked behaviour is apparent for the first and second internal modes. In order to see what kind of oscillations might be present later in the forecast the RMS divergence was plotted from the operational forecast for the period 24 to 28 hours after the initial time. Figure 17 compares this with the 0 to 4 hour values from the operational forecast. However the results are still rather inconclusive and do not really give any indication of how we should expect the RMS divergence to behave at the beginning of the forecast.

In order to try to see more clearly the effects of dynamic initialization on the subsequent forecast we decided to examine the vertical velocity and geopotential

height at specific points. The points chosen are shown in Figure 14. Figure 18 shows the vertical velocity $\omega = \frac{Dp}{Dt}$ at two points during the first four hours of the forecasts run with and without $4\frac{1}{2}$ hours of dynamic initialization. For point A which is near the surface low there is not much difference between the forecasts. The large oscillation at about 13 timesteps has been shown to be caused by the physical processes (possibly the deep convection scheme) and disappears when these are removed. For point B which is at the tip of Greenland there is considerable improvement in the forecast following dynamic initialization. This shows that the height and wind fields are adjusting to the topography in a manner consistent with the forecast model. Figure 19 shows the heights at all ten levels, relative to their initial values, at the point C which is almost at the centre of the surface low, at every timestep for the first six hours of forecasts with and without dynamic initialization. The amplitude of the oscillations present in the operational forecast has been reduced in this case but increasing the number of cycles of initialization beyond 15 did not produce any further improvement. The improvement is not apparent at some other points as is shown in Figure 20. Some of the oscillations disappear when the physical processes, which are absent in the initialization, are removed from the forecast as illustrated in Figure 21 which shows the heights at point C. Further experiments were made with changes to the initialization to alter the formulation of the coriolis terms to a straightforward explicit evaluation and also to leave out the term representing the departure from the ICAO-standard-atmosphere static stability but these did not produce any significant effect. The greatest improvement was found when the boundary values of the rectangle were not updated during the forecast. This is illustrated by Figure 22 which shows the heights at point C and may be compared with Figure 19. However when the boundary tendencies were incorporated into the dynamic initialization there was not a similar improvement.

It is apparent from these experiments that many of the oscillations present in the forecast are not caused by an imbalance between the initial height and wind fields but by the physical processes and the boundary updating procedure. In any event their amplitude is not excessively large and such gravity wave activity is not unduly harmful to the forecast. In order to see whether the dynamic initialization would have a good effect on really unbalanced data analysed heights and geostrophic winds were used as the starting point for the initialization. It is recognized that this would not be a practical means of providing initial data for a forecast as during initialization much of the adjustment is taking place in the height field and the systematic error in the geostrophic assumption in areas of strong curvature around highs and lows means that depressions are deepened and highs become less intense during the initialization procedure. Nevertheless such experiments give an idea as to how much the dynamic initialization removes gravitational oscillations in the subsequent forecast. Figure 23 shows the height at each timestep during the first six hours of forecasts with no or varying amounts of initialization for two points. There were no physical processes included in any of the forecasts but the boundary values were updated. Twenty-five cycles, that is $7\frac{1}{2}$ hours, of initialization removes most of the oscillation. At point C, near the centre of the depression, the initialization lowers the height at all levels. 105 cycles, that is $31\frac{1}{2}$ hours of initialization lowers the height slightly more but does not make much difference to the short period oscillations. It seems to be having some effect on a longer period wave, which is in agreement with theory. The effects of the boundary updating can still be seen at twelve timesteps.

The same experiments were made with another case, 00Z 18/11/76, giving broadly similar results. This case was one in which there was a jet with strong anticyclonic curvature. It is known that the elliptization in the diagnostic initialization acts to remove excessive anticyclonic vorticity and that this has the effect of sometimes producing rather too weak jets in the wind field. It was hoped that the use of analysed heights and gradient winds together with dynamic initialization might improve this. It was found necessary to do 50 cycles of initialization

to remove the gravitational oscillations. Figure 24 compares the oscillations in the 1000 mb height at a grid point during the first six hours of

(a) the operational forecast

(b) a forecast from 15 cycles (4½ hours) of dynamic initialization starting from the operational initialization,

(c) a forecast from 25 cycles (7½ hours) of dynamic initialization starting from analysed heights and gradient winds

and

(d) a forecast from 50 cycles (15 hours) of dynamic initialization starting from analysed heights and gradient winds.

The gradient winds were calculated by adjusting the geostrophic winds according to the curvature of the contours of the height field which is an approximation to the curvature of the trajectories. After 15 hours of initialization the forecast from analysed heights and gradient winds is comparable, in the amount of gravity-wave activity present, with the operational forecast. Such waves left are in phase with those in (b) indicating some other cause than the initial imbalance of the height and wind fields. It is interesting to compare the forecasts from the operational initialization and from 15 hours of dynamic initialization. Figures 25, 26 and 27 show the surface pressure, 300 mb height, 300 mb isotachs and accumulated rain for the two initializations and the 12-and 24-hour forecasts. Figure 28 shows the verfiying analyses. The winds in the jet cores are stronger in the dynamic initialization. The surface pressure and 300 mb height fields are very similar after initialization. At 12 hours it can be seen that both forecasts are beginning to go wrong in that the depression in the Atlantic is forecast to go to the east of Greenland whereas it actually went to the west. At 300 mb the ridge is more intense in the forecast following dynamic initialization and the main jet as seen on the isotach chart is about 10 knots stronger and somewhat further north and east. In fact in this case this is probably slightly worse than the operational forecast. There is about 25% more accumulated rain near Greenland in the first 12 hours of the forecast following dynamic initialization but slightly less in the trailing front to the south. It is not possible to say which is the more correct. At 24 hours there are similar kinds of differences between the two forecasts but these are small when compared with the difference from the actual. Between 12 and 18 hours (not shown) there is about 25% more rain near Greenland in the operational forecast. This experiment does not show that the use of analysed heights and gradient winds together with dynamic initialization is better than the current operational procedures but it does show that the backward-implicit dynamic initialization scheme used with some other wind field than currently used is a possible alternative and that the forecasts are quite sensitive to the initial wind field.

6. A damped integration scheme for the 10-level model octagon.

In the work on data assimulation with the 10-level model octagon, height and wind data are assimilated into the forecast height and wind fields every three hours by the use of the optimum interpolation method of objective analysis. This work has been described by Maryon (1977). There is no initialization performed after each update and although steps are taken to adjust the wind field to the updated height field by means of geostrophic increments (Cattle 1976) and to modify the updated wind field to remove excessive values of divergence (Dickinson 1976), some gravity-wave activity remains particularly when large quantities of data are assimilated. If these gravity waves are not dissipated within three hours they will contaminate the next analysis. There are two possible means of overcoming this problem. One is to use dynamic initialization to damp the gravity waves and then to run the usual forecast forwards three hours

to the next assimilation time. (A dynamic initialization scheme for the octagon is described in section 7). This approach would be necessary if one wished to run a longer period forecast. The alternative is to use a damped forward integration scheme for integrating between the assimilation times. This is obviously more economical in terms of computing time.

With dynamic initialization one varies the amount of damping by varying the number of cycles of initialization performed. In order to have the facility of being able to vary the amount of damping when integrating forwards over a fixed period of three hours we decided to adopt a generalization of the semi-implicit and backward-implicit methods, which was also discussed by Kurihara (1965) and which he termed "partly-implicit".

Considering equation (2.5), that is

$$\frac{d\underline{z}}{dt} = \underline{\underline{A}}\,\underline{z} \tag{6.1}$$

we may represent the partly-implicit scheme by

$$\underline{z}_{n+1} = \underline{z}_n + \delta t\,\underline{\underline{A}}\left(\alpha\,\underline{z}_n + (1-\alpha)\underline{z}_{n+1}\right) \tag{6.2}$$

where $0 \le \alpha \le 1$. When $\alpha = 0$ this becomes the backward-implicit scheme, when $\alpha = \frac{1}{2}$ it is the semi-implicit scheme and when $\alpha = 1$ it is a simple forward timestep. The amplification matrix

$$\underline{\underline{B}} = \left(\underline{\underline{I}} - (1-\alpha)\delta t\,\underline{\underline{A}}\right)^{-1}\left(\underline{\underline{I}} + \alpha\,\delta t\,\underline{\underline{A}}\right)$$

and has eigenvalues

$$\frac{1 + i\alpha k\sigma_j \delta t}{1 - i(1-\alpha)k\sigma_j \delta t} \qquad j = 1, 2, 3$$

The modulus of the eigenvalues are

$$R_j = \sqrt{\frac{1 + \alpha^2 k^2 \sigma_j^2 \delta t^2}{1 + (1-\alpha)^2 k^2 \sigma_j^2 \delta t^2}} \qquad j = 1, 2, 3$$

The scheme is stable provided $\alpha \le \frac{1}{2}$ and damped if $\alpha < \frac{1}{2}$. The amount of damping may be varied by varying α between 0 and $\frac{1}{2}$. This scheme was used for the linear terms of the external and first internal mode of the 10-level model. The remaining eight higher-order modes were integrated using the undamped explicit adjustment scheme used in the semi-implicit forecast model itself. This was because it appeared that it was mainly the external gravity wave that was giving trouble in the data assimilation experiments. The mathematical details of the partly-implicit scheme as applied to the 10-level model octagon may be found in the appendix. Apart from the use of the "partly-implicit" method for the external and first internal modes, the remaining equations, including all the physical processes, are the same as in the semi-implicit version of the 10-level model.

The first experiment was to run a 12-hour forecast with the damped scheme and compare this with an undamped forecast to see if any of the meteorological features were being harmed. With the maximum damping of $\alpha = 0$ for both modes there was no significant deterioration in the forecast so we used this value in subsequent experiments.

One of the problems in the data assimilation was the assimilation of wind data. If these data were used to update the wind field and no further modification was made to it, large amplitude gravity waves were generated in the forecast, mainly caused by spurious values of divergence in the analysed wind field, although imbalances between the height and wind fields would also have a small effect. Figure 29 shows these gravity waves in the surface pressure at a grid point plotted at every timestep after a wind update had been performed. This problem was largely overcome in the assimilation experiments by modifying the updated divergence field to make it the same as the divergence field before the assimilation of the data. We decided to test the damped integration scheme by using it on the updated wind field with no modification. The result, also illustrated in Figure 29, shows that the gravity wave has been almost completely removed. Also shown in Figure 29 is the result of using the damped integration scheme for three hours and then reverting to the undamped scheme. This experiment was performed partly to see how quickly the oscillations were removed and partly to see if there was any fundamental inconsistency between the damped scheme and the undamped scheme. The experiment shows that the gravity waves had been almost completely damped after three hours and there was no large discontinuity when the damping was removed. This was encouraging since there was some concern that the failure to damp the oscillations in the rectangle beyond a certain point might be due to a fundamental inconsistency between the backward-implicit and semi-implicit finite difference schemes.

7. A dynamic initialization scheme for the octagon in which only the external and first internal gravity waves are damped.

The forecasts run in conjunction with the dynamic initialization experiments with the rectangle version of the 10-level model showed that the physical processes present in the forecast model itself generated internal gravity waves. This further supports the suggestion that it is unnecessary and wasteful in computing time to damp the higher-order internal gravity waves in an initialization. A dynamic initialization scheme has been devised for the semi-implicit octagon version of the 10-level model, in which the advective terms are integrated with a Lax-Wendroff timestep as before, the linear terms are decoupled into the model's ten normal modes, the external and first internal modes are integrated with a backward-implicit timestep to damp these gravity waves but the equations for the eight higher-order modes are not integrated at all. For the external and first internal mode the coriolis terms are included with an Euler-backward timestep which has a slightly different form of spatial averaging from that in the rectangle initialization and the departure from the ICAO-standard-atmosphere static stability is included explicitly to save computation time. After one timestep forwards the sign of δt is changed and a backward timestep made to complete a cycle. The mathematical details of this scheme may be found in the appendix. As in the case of the rectangle initialization there is no diffusion or friction and no physical processes are included except the effects of topography.

Not many experiments have been made with this scheme as the computer program has only been recently made to work. Indeed it is apparent from the results that there is still a problem with the "top left-hand sloping" boundary, which may be seen in Figure 31b, and possibly others also. This may be caused by a programming mistake but it seems more likely to be some kind of formulation error, possibly the lack of any kind of diffusion around the boundary. It should be noted however that this gave no similar trouble with the rectangle initialization. Nevertheless the program is giving generally sensible and encouraging results.

The first experiment was to use an operational initialization as a starting point. Figure 30 compares the surface pressure at a grid point in the Atlantic during 12 hour forecasts with and without dynamic initialization. The forecast without dynamic initialization shows some small amplitude gravity waves typical of operational semi-implicit forecasts. The other forecast follows twenty fifteen-minute timesteps or 5 hours of dynamic initialization and shows a

considerable reduction in the amplitude of the gravity waves. Figure 31 shows the surface pressure field before and after dynamic initialization. Apart from near the "top left-hand sloping" boundary there is very little difference between them except after the dynamic initialization there is a slight loss in the depths of depressions and in the intensity of the anticyclones.

In order to see how dynamic initialization would deal with large amplitude gravity waves the result of the wind update, used in section 6, was also used as a starting point. Figure 32 shows the sufrace pressure at a grid point at every timestep for three 12-hour forecasts following

(a) no initialization

(b) twenty 15-minute timesteps or 5 hours of dynamic initialization

(c) six 24-minute timesteps or 2.4 hours of dynamic initialization.

Twenty-four minutes is the theoretical limit for the timestep. Both initializations have effectively damped the gravity waves. The second (c) shows that this may be achieved in the equivalent of 2.4 hours of integration time which is about the time Temperton (1976) found was required to damp the external gravity wave when using Okamura's scheme.

The dynamic initialization scheme has also been used in conjunction with some of the data assimilation experiments and some results are presented by Maryon (1977).

8. Computing Requirements

The timestep for the rectangle dynamic initialization is limited by the Euler-backward scheme for the second internal mode and is set at 9 minutes. The CPU time on the Meteorological Office IBM 360/195 computer for 30 timesteps or 4½ hours of initialization is about 84 seconds. This compares with the operational initialization CPU time of about 90 seconds and the rectangle semi-implicit forecast which takes about 13 minutes CPU time for 36 hours.

The damped integration scheme for the octagon requires the same amount of CPU time as the semi-implicit forecast, about 206 seconds for a 12-hour forecast. It has been run with a 15 minute timestep because this was found desirable, in order to prevent severe time truncation, for the semi-implicit forecast model. No experiments have been done increasing the timestep to the theoretical limit of 24 minutes.

The theoretical limit on the timestep for the octagon dynamic initialization is also 24 minutes resulting from the Lax-Wendroff part of the integration. With this timestep the CPU time required for the equivalent of 2.4 hours integration is about 20 seconds. This compares with the operational initialization CPU time of about 60 seconds.

Okamura's scheme on the 11-level model takes 217 seconds CPU time for the equivalent of three hours of integration. A 24 minute timestep for the backward-implicit scheme allows for a 220 km mesh as in the 11-level model and it requires about 25 seconds to do the equivalent of three hours integration. Allowing for the increased number of grid points in the 11-level model, both horizontally and vertically, we need to multiply this by 1.8 to give a comparison with the Okamura scheme and this gives about 45 seconds. This implies a ratio of 4.8:1 in favour of the backward-implicit method. However one must remember that the program for the Okamura scheme is written in FORTRAN while that for the backward-implicit scheme is in ASSEMBLER langauge. Even if we could halve the time of the Okamura scheme by writing it in ASSEMBLER language this still gives a ratio of between two and three to one in favour of the backward-implicit scheme. It must be remembered also that the backward-implicit program is not absolutely optimized, in fact the routines to advect the humidity

mixing ratio are still present in it.

9. Conclusions

The experiments with the octagon version of the 10-level model show that the backward-implicit method can provide a fast practical way of performing dynamic initialization. It appears to damp the external gravity wave as quickly as the Okamura scheme and is between two and three times as fast if only two gravity-wave modes are damped. It seems unnecessary to attempt to damp the higher-order internal modes as any frequency-dependant damping scheme could only damp them very slowly and also they are generated by the 10-level model's physical processes. The rectangle initialization scheme did not give as satisfactory results as that for the octagon and it is suspected that this is due to the effects of the boundaries on a limited area model.

These experiments have been made with a semi-implicit forecasting model which has pressure as a vertical co-ordinate. The backward-implicit method is restricted to spatial grids on which the Helmholtz equation may be solved in a manner consistent with the forecast equations. This means that it may be used with a semi-implicit model but that it may not be possible to use it with explicit models without some final horizontal interpolation. It is not clear what the effects would be of using this scheme with a σ-coordinate model. In this case the model atmosphere would depart more substantially from the standard atmosphere than with a p-co-ordinate model. The experiments with the barotropic model and theoretical considerations suggest that the rate of damping could be reduced or the scheme could even become unstable, depending on which formulation is used.

It has also been demonstrated that the backward-implicit method could be useful as a damped integration scheme for use in data assimilation. The same restrictions apply as in the case of the dynamic initialization.

A number of further experiments need to be made with the octagon dynamic initialization scheme, using several different cases, both varying the timestep and the number of cycles of initialization. It would be particularly interesting to examine whether the use of wind data in a separate wind analysis together with dynamic initialization produces better forecasts than the current operational scheme where the initial wind field is derived from the height analysis. Such an experiment could be made in conjunction with the data assimilation experiments making use of the optimum interpolation objective analysis of height and wind fields which is part of the data assimilation scheme. Experiments could also be made using an atmospheric profile somewhat different from the ICAO standard atmosphere, to decouple the linear terms of the equations in order to test the effect of having a model atmosphere which departed more substantially from the constant profile as would be the case with a σ-co-ordinate model.

10. Acknowledgements

I should like to acknowledge the preliminary work carried out for this study by Mr S Helmy, who, besides performing some early experiments, wrote all the programs for the barotropic initialization, and also the contribution of Mrs P Carver who carried out all the necessary work to amend the 10-level model forecast programs in order to produce the dynamic initialization and damped integration programs. I should also like to express my appreciation and thanks to Dr D M Burrdige for his advice and encouragement, especially during the early stages of this work.

Bibliography

Burridge, D.M. 1975 A split semi-implicit reformulation of the Bushby-Timpson 10-level model. Q.J.R. Met S. Vol 101 pp777-792.

Burridge, D.M. and Gadd, A.J. 1977 The Meteorological Office 10-level numerical weather prediction model (December 1975) Meteorological Office Scientific Paper No 34. (Also Met O 11 Tech Note No 48/Met O 2b Tech Note No 12)

Cattle, H. 1976 Data assimilation experiments with the Meteorological Office 10-level model. GARP WGNE Report No 11 Proceedings of JOC study group conference on data assimilation Paris Nov 1975.

Dickinson, A. 1976 The balancing of updated wind fields by removing excessive divergences. Personal communication.

Grammelvedt, A. 1969 A survey of finite-difference schemes for the primitive equations of a barotropic fluid. Monthly Weather Review Vol 97 No 5.

Hayes, F.R. 1976 A representation of topography and the surface boundary layer in the Meteorological Office 10-level model. Met O 11 Tech Note No 57.

Kurihara, Y. 1965 On the use of implicit and iterative methods for the time integration of the wave equation. Monthly Weather Review Vol 93 No 1.

Maryon, R.H. 1977 The Met O 11 four dimensional data assimilation scheme: pilot experiment. Met O 11 Tech Note No 102

Nitta, T. 1969 Initialization and analysis for the primitive equation model. Proceedings of the WMO/IUGG Symposium on Numerical Weather Prediction, Tokyo, Japan, Nov 26-Dec 4 1968. Japan Meteorological Agency Tokyo 1969 pp VI 11-20.

Temperton, C. 1973 Some experiments in dynamic initialization for a simple primitive equation model. Q.R.J. Met S. Vol 99 pp303-319

1975 Dynamic initialization for multi-level models. Met O 20 Tech Note II/39.

1976 Dynamic initialization for multi-level models. Q.J.R. Met S. Vol 102 pp297-312.

APPENDIX

This appendix contains the mathematical description of (i) the backward-implicit dynamic initialization scheme for the fine-mesh rectangle version of the 10-level model, (ii) the partly-implicit damped integration scheme for the octagon version of the 10-level model and (iii) the backward implicit dynamic initialization scheme for the 10-level model octagon. The spatial distribution of the variables for all three schemes is the same as for the semi-implicit version of the 10-level model as described by Burridge and Gadd (1977). The notation throughout is as far as possible the same as that used by Burridge and Gadd, and a list appears at the end of the appendix. All three schemes are split and the advective terms are integrated using a Lax-Wendroff timestep in a manner identical to that described in section (4.3) of Burridge and Gadd, with the exception that there is no humidity equation in schemes (i) and (iii).

(i) Backward-implicit dynamic initialization scheme for the 10-level model rectangle. The equations for the linear-adjustment step are

$$\frac{\partial u^*}{\partial t} - fv^* + g\frac{\partial h}{\partial x} = 0 \tag{A1}$$

$$\frac{\partial v^*}{\partial t} + fu^* + g\frac{\partial h}{\partial y} = 0 \tag{A2}$$

$$\frac{\partial h'}{\partial t} + \beta w = 0 \tag{A3}$$

$$\frac{\partial h_{10}}{\partial t} + \left(\frac{\partial h}{\partial p}\right)_{10}\omega_{10} - \mu\left(u_{10}\frac{\partial H}{\partial x} + v_{10}\frac{\partial H}{\partial y}\right) = 0 \tag{A4}$$

which are equations (4.14) to (4.16) of Burridge and Gadd. They may be written

$$\frac{\partial a_k}{\partial t} + g\frac{\partial y_k}{\partial x} = fv_k \tag{A5}$$

$$\frac{\partial v_k}{\partial t} + g\frac{\partial y_k}{\partial y} = -fa_k \tag{A6}$$

$$\frac{\partial y_k}{\partial t} + \frac{\mu c_{ok}^2}{g}\left(\frac{\partial a_k}{\partial x} + \frac{\partial v_k}{\partial y}\right) = -\left\{\underline{\underline{E}}^{-1}\left[\frac{\mu}{g}\left(\underline{\underline{G}} - \underline{\underline{G}}_o\right)\left(\frac{\partial \underline{u}}{\partial x} + \frac{\partial \underline{v}}{\partial y}\right) + \mu\,\underline{\underline{T}}\left(\underline{u}\frac{\partial H}{\partial x} + \underline{v}\frac{\partial H}{\partial y}\right)\right]\right\}_k \tag{A7}$$

for k = 1 to 10, where $\underline{u}$ and $\underline{v}$ are vectors

$$\begin{pmatrix} u_1^* \\ u_2^* \\ \vdots \\ u_{10}^* \end{pmatrix} \quad \text{and} \quad \begin{pmatrix} v_1^* \\ v_2^* \\ \vdots \\ v_{10}^* \end{pmatrix}$$

respectively, $\underline{\underline{G}}$ is a 10x10 matrix which is a function of the static stability of the model atmosphere and $\underline{\underline{G}}_o$ is the corresponding matrix for the ICAO standard atmosphere, c_{ok}^2 are the eigenvalues of $\underline{\underline{G}}_o$ and are the squares of the phase speeds of the ten gravity waves of the model, $\underline{\underline{E}}$ is the matrix whose columns are the eigenvectors of $\underline{\underline{G}}_o$ and

a_k, v_k, y_k are elements of the vectors.

$$\underline{a} = \underline{\underline{E}}^{-1}\underline{u}$$

$$\underline{v} = \underline{\underline{E}}^{-1}\underline{v}$$

and $\underline{y} = \underline{\underline{E}}^{-1}\underline{h}$ respectively.

$\underline{\underline{T}}$ is the 10x10 matrix diag (0, 0, 0, ... 0. -1)

The phase speeds c_{0k} are ordered so that $c_{01} > c_{02} > \cdots\cdots > c_{010}$
For k = 3 to 10, the eight higher-order gravity-wave modes, we use an Euler-backward scheme

$$(a_k)_{n+1} - (a_k)_n = -\delta t g \delta_x (y_k)_I + \delta t f (\bar{v}_k^{xy})_I \tag{A8}$$

$$(v_k)_{n+1} - (v_k)_n = -\delta t g \delta_y (y_k)_I - \delta t f (\bar{a}_k^{xy})_I \tag{A9}$$

$$(y_k)_{n+1} - (y_k)_n = -\frac{\delta t \mu c_{0k}^2}{g}\left(\delta_x (a_k)_I + \delta_y (v_k)_I\right) + (\Delta_T y_k)_I + (y'_k)_I \tag{A10}$$

where

$$(a_k)_I = (a_k)_n - \delta t g \delta_x (y_k)_n + \delta t f (\bar{v}_k^{xy})_n \tag{A11}$$

$$(v_k)_I = (v_k)_n - \delta t g \delta_y (y_k)_n - \delta t f (\bar{a}_k^{xy})_n \tag{A12}$$

$$(y_k)_I = (y_k)_n - \frac{\delta t \mu c_{0k}^2}{g}\left(\delta_x (a_k)_n + \delta_y (v_k)_n\right) + (\Delta_T y_k)_n + (y'_k)_n \tag{A13}$$

and

$$\Delta_T y_k = -\delta t \left\{ \underline{\underline{E}}^{-1} \mu \underline{\underline{T}} \left[\left(\delta_x \bar{H}^{xyy}\right) \bar{\underline{u}}^x + \left(\delta_y \bar{H}^{xyx}\right) \bar{\underline{v}}^y \right] \right\}_k \tag{A14}$$

$$y'_k = -\delta t \left\{ \underline{\underline{E}}^{-1} \left[\frac{\mu}{g} (\underline{\underline{G}} - \underline{\underline{G}}_0)(\delta_x \underline{u} + \delta_y \underline{v}) \right] \right\}_k \tag{A15}$$

For k = 1,2 we use the backward-implicit scheme

$$(a_k)_{n+1} - (a_k)_n = -\delta t g \delta_x (y_k)_{n+1} + \delta t f (\bar{v}_k^{xy})_I \tag{A16}$$

$$(v_k)_{n+1} - (v_k)_n = -\delta t g \delta_y (y_k)_{n+1} - \delta t f (\bar{a}_k^{xy})_I \tag{A17}$$

$$(y_k)_{n+1} - (y_k)_n = -\frac{\delta t \mu c_{0k}^2}{g}\left(\delta_x (a_k)_{n+1} + \delta_y (v_k)_{n+1}\right) + (\Delta_T y_k)_n + (y'_k)_I \tag{A18}$$

where $(a_k)_I$, $(v_k)_I$, $\Delta_T y_k$ and y'_k are defined as above.

Eliminating $(a_k)_{n+1}$ and $(v_k)_{n+1}$ from equation (A18) we obtain the Helmholtz equation

$$-\nabla^2 (y_k)_{n+1} + \frac{1}{\delta t^2 \mu c_{0k}^2} (y_k)_{n+1} = \frac{1}{\delta t^2 \mu c_{0k}^2} \left\{ (y_k)_I - \frac{\delta t \mu c_{0k}^2}{g} \left[\delta_x \left(\delta t f (\bar{v}_k^{xy})_I \right) - \delta_y \left(\delta t f (\bar{a}_k^{xy})_I \right) \right] + (y'_k)_I - (y'_k)_n \right\} \tag{A19}$$

corresponding to equation (4.35) of Burridge and Gadd, which may be solved to give $(y_k)_{n+1}$ with $(y_k)_{n+1}$ specified on the boundaries. We may write the solution to the complete set of equations as

$$\underline{y}_{n+1} = \underline{y}_n - \frac{\delta t \mu \underline{\underline{c_o}}^2}{g}\left(\delta_x \underline{u}_I + \delta_y \underline{v}_I\right) + \left(\Delta_T \underline{y}\right)_I + \underline{y}'_I + \left((y_1)_{n+1} - f_1\right)\underline{e}_1 + \left((y_2)_{n+1} - f_2\right)\underline{e}_2 \qquad (A20)$$

where $\underline{e}_1 = (1,0,0,\cdots\cdots 0)^T$, $\underline{e}_2 = (0,1,0,\cdots\cdots 0)^T$,

$\underline{\underline{c_o}}^2 = \mathrm{diag}\left(c_{o1}^2, c_{o2}^2, \cdots\cdots c_{o10}^2\right)$ and

$$f_k = (y_k)_n - \frac{\delta t \mu c_{ok}^2}{g}\left(\delta_x (a_k)_I + \delta_y (b_k)_I\right) + \left(\Delta_T y_k\right)_I + \left(y'_k\right)_I \qquad k = 1,2 \qquad (A21)$$

which is the solution of the explicit part plus a correction.
Multiplying (A20) by $\underline{\underline{E}}$ gives

$$\underline{h}_{n+1} = \underline{h}_n - \frac{\delta t \mu \underline{\underline{G_o}}}{g}\left(\delta_x \underline{u}_I + \delta_y \underline{v}_I\right) + \left(\Delta_T \underline{h}\right)_I + \left(\underline{h}'\right)_I + \left((y_1)_{n+1} - f_1\right)\underline{\hat{y}}_1 + \left((y_2)_{n+1} - f_2\right)\underline{\hat{y}}_2 \qquad (A22)$$

where $\underline{\hat{y}}_1$, $\underline{\hat{y}}_2$ are eigenvectors of $\underline{\underline{G_o}}$ corresponding to the eigenvalues c_{o1}^2, c_{o2}^2

$$\Delta_T \underline{h} = \underline{\underline{E}}\left(\Delta_T \underline{y}\right) = -\delta t \mu \underline{\underline{I}}\left[\left(\delta_x \bar{H}^{xy\delta}\right)\bar{\underline{u}}^x + \left(\delta_y \bar{H}^{xy\delta}\right)\bar{\underline{v}}^y\right]$$

and $$\underline{h}' = \underline{\underline{E}}\,\underline{y}' = -\frac{\delta t \mu}{g}\left(\underline{\underline{G}} - \underline{\underline{G_o}}\right)\left(\delta_x \underline{u} + \delta_y \underline{v}\right)$$

(A22) may be written as

$$\underline{h}_{n+1} = \underline{h}^* + \left((y_1)_{n+1} - f_1\right)\underline{\hat{y}}_1 + \left((y_2)_{n+1} - f_2\right)\underline{\hat{y}}_2 \qquad (A23)$$

where $$\underline{h}^* = \underline{h}_n - \frac{\delta t \mu \underline{\underline{G_o}}}{g}\left(\delta_x \underline{u}_I + \delta_y \underline{v}_I\right) + \left(\Delta_T \underline{h}\right)_I + \underline{h}'_I$$

$$= \underline{h}_n - \frac{\delta t \mu \underline{\underline{G}}_I}{g}\left(\delta_x \underline{u}_I + \delta_y \underline{v}_I\right) + \left(\Delta_T \underline{h}\right)_I \qquad (A24)$$

The sequence of computations is as follows:

(i) Compute $\underline{u}_I$, $\underline{v}_I$ and $\underline{h}_I$ from

$$\underline{u}_I = \underline{u}_n - \delta t g \delta_x \underline{h}_n + \delta t f \bar{\underline{v}}_n^{xy} \qquad (A25)$$

$$\underline{v}_I = \underline{v}_n - \delta t g \delta_y \underline{h}_n - \delta t f \bar{\underline{u}}_n^{xy} \qquad (A26)$$

$$\underline{h}_I = \underline{h}_n - \frac{\delta t \mu}{g}\underline{\underline{G}}_n\left(\delta_x \underline{u}_n + \delta_y \underline{v}_n\right) + \left(\Delta_T \underline{h}\right)_n \qquad (A27)$$

(ii) Compute $\delta t f \underline{\bar{u}}_I^{xy}$, $\delta t f \underline{\bar{v}}_I^{xy}$, $\underline{h}_I' - \underline{h}_n'$, and $\underline{h}^*$

(iii) Compute $\underline{f}_k = \underline{X}_k^T \cdot \underline{h}^*$ and $(\underline{y}_k)_I = \underline{X}_k^T \cdot \underline{h}_I$ for k = 1,2

where $\underline{X}_k^T$ is the k^{th} row of $\underline{\underline{E}}^{-1}$

(iv) Compute the right hand side of the Helmholtz equation

$$\underline{X}_k^T \cdot \left\{ \underline{h}_I - \frac{\delta t \mu G_0}{g} \left(\delta_x (\delta t f \underline{\bar{u}}_I^{xy}) - \delta_y (\delta t f \underline{\bar{u}}_I^{xy}) \right) + \underline{h}_I' - \underline{h}_n' \right\}$$

(v) Solve the Helmholtz equation for $(y_1)_{n+1}$ and $(y_2)_{n+1}$

(vi) Adjust $\underline{h}^*$ to give $\underline{h}_{n+1}$ according to equation (A23)

(vii) Compute $\underline{u}_{n+1}$ and $\underline{v}_{n+1}$ from the following equations.

$$\underline{u}_{n+1} = \underline{u}_n - \delta t g \delta_x \underline{h}_I + \delta t f (\underline{\bar{v}}^{xy})_I - \delta t g \delta_x ((y_1)_{n+1} - (y_1)_I) \hat{\underline{y}}_1 - \delta t g \delta_x ((y_2)_{n+1} - (y_2)_I) \hat{\underline{y}}_2 \quad \text{(A28)}$$

$$\underline{v}_{n+1} = \underline{v}_n - \delta t g \delta_y \underline{h}_I - \delta t f (\underline{\bar{u}}^{xy})_I - \delta t g \delta_y ((y_1)_{n+1} - (y_1)_I) \hat{\underline{y}}_1 - \delta t g \delta_y ((y_2)_{n+1} - (y_2)_I) \hat{\underline{y}}_2 \quad \text{(A29)}$$

The equations for the backward step are the same except that δt is set equal to $-\delta t$.

The computational stability criterion for the Lax-Wendroff step is given by

$$\delta t < \frac{a}{m\sqrt{u^2+v^2}}$$

where a is the grid-length on the polar stereographic projection, m is the map factor and (U, V) is the mean wind. Restricting the horizontal wind to 100 ms^{-1}, this allows a timestep of 12 mins or 720 secs.
For the linear adjustment step assume a vertical structure such that $\underline{G}_I = (1+\gamma)\underline{G}_0$. The stability criterion for the Euler-backward timestep is given by

$$\delta t \leq \frac{a}{2\sqrt{2} m c_{01} (1+\gamma)}$$ ignoring the coriolis terms.

This is only half that allowed by the explicit adjustment step of the 10-level model. It limits the timestep to 9 mins or 540 secs. The stability criterion for the backward implicit step including the departure from $\underline{G}_0$ for $\gamma > 1$ is given by

$$\delta t \leq \frac{a}{2m c_{01} (\gamma - 1)}$$

It is unconditionally stable for $|\gamma| \leq 1$. In practice $|\gamma| \leq 1$ and therefore the timestep is limited by the speed of the 2nd internal mode and is set at 9 min.

(ii) The partly-implicit damped integration scheme.

The equations for the linear adjustment step may be written as (A5) to (A7).

For k = 3 to 10 we use the explicit scheme which is used in the semi-implicit version of the 10-level model.

$$(a_k)_{n+1} - (a_k)_n = -\delta t g \delta_x (y_k)_{n+1} + \Delta_c a_{kn} \qquad (A30)$$

$$(b_k)_{n+1} - (b_k)_n = -\delta t g \delta_y (y_k)_{n+1} + \Delta_c b_{kn} \qquad (A31)$$

$$(y_k)_{n+1} - (y_k)_n = -\frac{\delta t \mu c_{ok}^2}{g}\left(\delta_x (a_k)_n + \delta_y (b_k)_n\right) + (\Delta_T y_k)_n + (y'_k)_n \qquad (A32)$$

where $\Delta_c a_{kn}$ and $\Delta_c b_{kn}$ are the coriolis terms given by

$$\Delta_c a_{kn} = \delta t f\left((\bar{b}_k^i)_n - \frac{\delta t}{2}\left(g \delta_y (\bar{y}_k^{xy})_n + f (a_k)_n\right)\right) \qquad (A33)$$

$$\Delta_c b_{kn} = -\delta t f\left((\bar{a}_k^i)_n - \frac{\delta t}{2}\left(g \delta_x (\bar{y}_k^{xy})_n - f (b_k)_n\right)\right) \qquad (A34)$$

where $(\bar{a}_k^i)_n$, $(\bar{b}_k^i)_n$ indicates that these terms have been obtained by a bicubic interpolation.
For k = 1, 2 we use the partly implicit scheme

$$(a_k)_{n+1} - (a_k)_n = -\delta t g \delta_x\left(\alpha (y_k)_n + (1-\alpha)(\tilde{y}_k)_{n+1}\right) - \delta t g \delta_x (y'_k)_n + \Delta_c a_{kn} \qquad (A35)$$

$$(b_k)_{n+1} - (b_k)_n = -\delta t g \delta_y\left(\alpha (y_k)_n + (1-\alpha)(\tilde{y}_k)_{n+1}\right) - \delta t g \delta_y (y'_k)_n + \Delta_c b_{kn} \qquad (A36)$$

$$(y_k)_{n+1} - (y_k)_n = -\frac{\delta t \mu c_{ok}^2}{g}\left\{\delta_x\left(\alpha (a_k)_n + (1-\alpha)(a_k)_{n+1}\right) + \delta_y\left(\alpha (b_k)_n + (1-\alpha)(b_k)_{n+1}\right)\right\} + (\Delta_T y_k)_n + (y'_k)_n \qquad (A37)$$

where $$(\tilde{y}_k)_{n+1} = (y_k)_{n+1} - (y'_k)_n$$

NB. Burridge and Gadd use $(y'_k)_{n+1}$ to mean the same thing as this $(y'_k)_n$. I have changed the notation to make it more consistent as the term is actually evaluated at time level n. Eliminating $(a_k)_{n+1}$ and $(b_k)_{n+1}$ from equation (A37) we have

$$(y_k)_{n+1} - (y_k)_n = -\frac{\delta t \mu c_{ok}^2}{g}\left(\delta_x (a_k)_n + \delta_y (b_k)_n\right) + \delta t^2 \mu c_{ok}^2 (1-\alpha) \nabla^2 \left[\alpha (y_k)_n + (1-\alpha)(\tilde{y}_k)_{n+1} + (y'_k)_n\right] - (1-\alpha)\frac{\delta t \mu c_{ok}^2}{g}\left(\delta_x (\Delta_c a_{kn}) + \delta_y (\Delta_c b_{kn})\right) + (\Delta_T y_k)_n + (y'_k)_n \qquad (A38)$$

Define $\psi_k = \alpha (y_k)_n + (1-\alpha)(\tilde{y}_k)_{n+1} + (y'_k)_n$, multiply equation (A38) by $(1-\alpha)$ and add $\alpha\left((y_k)_n + (y'_k)_n\right)$ to each side. We then obtain the Helmholtz equation

$$\psi_k - \delta t^2 \mu c_{ok}^2 (1-\alpha)^2 \nabla^2 \psi_k = (y_k)_n + (y'_k)_n - \frac{\delta t \mu c_{ok}^2}{g}(1-\alpha)\left(\delta_x (a_k)_n + \delta_y (b_k)_n\right) - (1-\alpha)^2 \frac{\delta t \mu c_{ok}^2}{g}\left(\delta_x (\Delta_c a_{kn}) + \delta_y (\Delta_c b_{kn})\right) + (1-\alpha)(\Delta_T y_k)_n \qquad (A39)$$

Define

$$f_k = (y_k)_n + (y'_k)_n + \frac{\delta t \mu c_{ok}^2}{g}(1-\alpha)\left(\delta_x (a_k)_n + \delta_y (b_k)_n\right) + (1-\alpha)(\Delta_T y_k)_n \qquad (A40)$$

Equation (A39) may then be written

$$-\nabla^2\psi_k + \frac{1}{\delta t^2 \mu c_{o_k}^2 (1-\alpha)^2}\psi_k =$$

$$\frac{1}{\delta t^2 \mu c_{o_k}^2 (1-\alpha)^2}\left\{ f_k - \frac{\delta t \mu c_{o_k}^2}{g}(1-\alpha)^2\left(\delta_x(\Delta c a_{k_n}) + \delta_y(\Delta c v_{k_n})\right)\right\} \quad \text{(A41)}$$

If we set $\alpha = \frac{1}{2}$ and write $\psi_k = \frac{\psi_k'}{2}$ and $f_k = \frac{1}{2} f_k'$ this becomes equation (4.35) of Burridge and Gadd. This equation may be solved for ψ_k with ψ_k specified on the boundaries. The complete solution may be written as

$$\underline{y}_{n+1} = \underline{y}_n - \frac{\delta t \mu \underline{\underline{c}}_o^2}{g}\left(\delta_x \underline{a}_n + \delta_y \underline{v}_n\right) + \left(\Delta_T \underline{y}\right)_n + \left(\underline{y}'\right)_n + \frac{1}{1-\alpha}(\psi_1 - f_1)\underline{e}_1 + \frac{1}{1-\alpha}(\psi_2 - f_2)\underline{e}_2 \quad \text{(A42)}$$

which is the solution for the explicit equations plus a correction.

Multiplying (A42) by $\underline{\underline{E}}$ we have

$$\underline{h}_{n+1} = \underline{h}_n - \frac{\delta t \mu \underline{\underline{G}}_n}{g}\left(\delta_x \underline{a}_n + \delta_y \underline{v}_n\right) + \left(\Delta_T \underline{h}\right)_n + \frac{1}{1-\alpha}(\psi_1 - f_1)\hat{\underline{y}}_1 + \frac{1}{1-\alpha}(\psi_2 - f_2)\hat{\underline{y}}_2$$

$$= \underline{h}^* + \frac{1}{1-\alpha}(\psi_1 - f_1)\hat{\underline{y}}_1 + \frac{1}{1-\alpha}(\psi_2 - f_2)\hat{\underline{y}}_2 \quad \text{(A43)}$$

where $$\underline{h}^* = \underline{h}_n - \frac{\delta t \mu \underline{\underline{G}}_n}{g}\left(\delta_x \underline{a}_n + \delta_y \underline{v}_n\right) + \left(\Delta_T \underline{h}\right)_n \quad \text{(A44)}$$

The sequence of computations is as follows

(i) Calculate $\underline{h}^*$, $(\underline{h}')_n$, $\Delta_c \underline{u}_n$, $\Delta_c \underline{v}_n$ where

$$\Delta_c \underline{u}_n = \delta t f\left(\bar{\underline{v}}_n^{xy} - \frac{\delta t}{2}\left(g\delta_y \bar{\underline{h}}_n^{xy} + f\underline{u}_n\right)\right)$$

$$\Delta_c \underline{v}_n = -\delta t f\left(\bar{\underline{u}}_n^{xy} - \frac{\delta t}{2}\left(g\delta_x \bar{\underline{h}}_n^{xy} - f\underline{v}_n\right)\right)$$

(ii) Compute $f_k = \underline{X}_k^T \cdot \left((1-\alpha)\underline{h}^* + \alpha \underline{h}_n + \alpha \underline{h}_n'\right)$ and $\underline{X}_k^T \cdot \underline{h}^*$ $k = 1, 2$

(iii) Compute right-hand side of Helmholtz equation

$$f_k - \underline{X}_k^T \cdot \frac{\delta t \mu}{g}(1-\alpha)^2 \underline{\underline{G}}_o\left(\delta_x(\Delta c \underline{u}_n) + \delta_y(\Delta c \underline{v}_n)\right) \qquad k = 1, 2$$

(iv) Solve the Helmholtz equation for ψ_1 and ψ_2

(v) Calculate $\underline{u}_{n+1}$ and $\underline{v}_{n+1}$ from

$$\underline{u}_{n+1} = \underline{u}_n - \delta t g \delta_x \underline{h}^* + \Delta c \underline{u}_n - \delta t g \delta_x (\psi_1 - \underline{X}_1^T \cdot \underline{h}^*)\hat{\underline{y}}_1 - \delta t g \delta_x (\psi_2 - \underline{X}_2^T \cdot \underline{h}^*)\hat{\underline{y}}_2 \quad \text{(A45)}$$

$$\underline{v}_{n+1} = \underline{v}_n - \delta t g \delta_y \underline{h}^* + \Delta c \underline{v}_n - \delta t g \delta_y (\psi_1 - \underline{X}_1^T \cdot \underline{h}^*)\hat{\underline{y}}_1 - \delta t g \delta_y (\psi_2 - \underline{X}_2^T \cdot \underline{h}^*)\hat{\underline{y}}_2 \quad \text{(A46)}$$

(vi) Adjust $\underline{h}^*$ to give $\underline{h}_{n+1}$ according to equation (A43).

On the octagon the computational stability criterion for the Lax-Wendroff timestep

$$\delta t < \frac{a}{m\sqrt{u^2+v^2}}$$

allows a timestep of 24 min restricting the mean wind to 150 ms^{-1}.
It was found with the semi-implicit version of the octagon that it was necessary to reduce the timestep to 15 min to avoid excessive time truncation and the same thing has been done with the partly-implicit scheme.
For the explicit adjustement the stability criterion is

$$\delta t < \frac{a}{m c_{o3}\sqrt{2}(1+\gamma)}$$

assuming a vertical structure such that $\underline{G} = (1+\gamma)\underline{G}_o$
For the partly-implicit step with the departure from the constant-static stability included the eigenvalues of the amplification matrix are

$$1, \quad \frac{1-\alpha(1-\alpha)\omega^2\delta t^2 - \frac{\gamma\omega^2\delta t^2}{2} \pm \frac{1}{2}\sqrt{\gamma\omega^4\delta t^4(\gamma+4\alpha(1-\alpha)) - 4\omega^2\delta t^2(1+\gamma)}}{1+(1-\alpha)^2\omega^2\delta t^2}$$

For $\alpha = 0$, which has been used in the experiments, this may be shown to be unconditionally stable for $|\gamma| \le 1$. As this is generally true in practice, the limiting timestep is provided by the Lax-Wendroff step and is set at 15 min.

(iii) Backward-implicit dynamic initialization scheme for the 10-level model octagon, damping only the external and first internal gravity waves.

The equations for the linear adjustment step may be written as (A5) to (A7).

For k = 3 to 10 do not perform the linear adjustment step.

For k = 1,2 we use the backward-implicit scheme given by

$$(a_k)_{n+1} - (a_k)_n = -\delta t g \delta_x (y_k)_{n+1} + \Delta_c a_{kI} \qquad (A47)$$

$$(b_k)_{n+1} - (b_k)_n = -\delta t g \delta_y (y_k)_{n+1} + \Delta_c b_{kI} \qquad (A48)$$

$$(y_k)_{n+1} - (y_k)_n = -\frac{\delta t \mu c_{ok}^2}{g}\left(\delta_x (a_k)_{n+1} + \delta_y (b_k)_{n+1}\right) + (\Delta_\tau y_k)_n + (y'_k)_n \qquad (A49)$$

where $\Delta_c a_{kI} = \delta t f\left((\bar{b}_k^i)_n - \delta t\left(g\delta_y(\bar{y}_k^{xy})_n + f(a_k)_n\right)\right)$ (A50)

$$\Delta_c b_{kI} = -\delta t f\left((\bar{a}_k^i)_n - \delta t\left(g\delta_x(\bar{y}_k^{xy})_n - f(b_k)_n\right)\right) \qquad (A51)$$

This is similar to the formulation of the coriolis term in the rectangle initialization except that $-i$ represents a bicubic interpolation instead of the straightforward four-point average used for the rectangle and the last term in each equation is not averaged whereas it is a sixteen point average in the rectangle initialization.

Eliminating $(a_k)_{n+1}$ and $(b_k)_{n+1}$ from equation (A49) we have the Helmholtz equation

$$-\nabla^2(y_k)_{n+1} + \frac{1}{\delta t^2 \mu c_{0k}^2}(y_k)_{n+1} = \frac{1}{\delta t^2 \mu c_{0k}^2}\left\{(y_k)_n - \frac{\delta t \mu c_{0k}^2}{g}(\delta_x(a_k)_n + \delta_y(b_k)_n)\right.$$
$$\left. - \frac{\delta t \mu c_{0k}^2}{g}\left(\delta_x(\Delta_c a_{kI}) + \delta_y(\Delta_c b_{kI})\right) + (\Delta_t y_k)_n + (y'_k)_n\right\} \qquad (A52)$$

This equation may be solved for $(y_k)_{n+1}$ with $(y_k)_{n+1}$ specified on the boundaries. The complete solution may be written

$$\underline{y}_{n+1} = \underline{y}_n + ((y_1)_{n+1} - (y_1)_n)\underline{e}_1 + ((y_2)_{n+1} - (y_2)_n)\underline{e}_2 \qquad (A53)$$

or multiplying by $\underline{\underline{E}}$

$$\underline{h}_{n+1} = \underline{h}_n + ((y_1)_{n+1} - (y_1)_n)\hat{\underline{y}}_1 + ((y_2)_{n+1} - (y_2)_n)\hat{\underline{y}}_2 \qquad (A54)$$

that is the height is left unchanged except for a correction for the external and first internal modes.

The sequence of computations is as follows

(i) Compute $\Delta_c \underline{u}_I$ and $\Delta_c \underline{v}_I$ from

$$\Delta_c \underline{u}_I = \delta t f\left(\underline{\bar{v}}^i_n - \delta t\left(g\delta_y \underline{\bar{h}}^{xy}_n + f\underline{u}_n\right)\right)$$
$$\Delta_c \underline{v}_I = -\delta t f\left(\underline{\bar{u}}^i_n - \delta t\left(g\delta_x \underline{\bar{h}}^{xy}_n - f\underline{v}_n\right)\right)$$

(ii) Compute $\Delta_c a_{kI} = \underline{X}_k^T \cdot \Delta_c \underline{u}_I$, $\Delta_c b_{kI} = \underline{X}_k^T \cdot \Delta_c \underline{v}_I$ $\quad k = 1, 2$

(iii) Compute the right hand side of the Helmholtz equation

$$\underline{X}_k^T \cdot \left\{\underline{h}_n - \frac{\delta t \mu}{g}\underline{\underline{G}}_n\left(\delta_x \underline{u}_n + \delta_y \underline{v}_n\right) + (\Delta_t \underline{h})_n - \frac{\delta t \mu}{g}\underline{\underline{G}}_0\left(\delta_x(\Delta_c \underline{u}_I) + \delta_y(\Delta_c \underline{v}_I)\right)\right\}$$

(iv) Solve the Helmholtz equation for $(y_1)_{n+1}$ and $(y_2)_{n+1}$

(v) Adjust $\underline{h}_n$ to give $\underline{h}_{n+1}$ according to equation (A54)

(vi) Compute the winds from

$$\underline{u}_{n+1} = \underline{u}_n - \left\{\delta t g \delta_x (y_1)_{n+1} - \Delta_c a_{1I}\right\}\hat{\underline{y}}_1 - \left\{\delta t g \delta_x (y_2)_{n+1} - \Delta_c a_{2I}\right\}\hat{\underline{y}}_2 \qquad (A55)$$

$$\underline{v}_{n+1} = \underline{v}_n - \left\{\delta t g \delta_y (y_1)_{n+1} - \Delta_c b_{1I}\right\}\hat{\underline{y}}_1 - \left\{\delta t g \delta_y (y_2)_{n+1} - \Delta_c b_{2I}\right\}\hat{\underline{y}}_2 \qquad (A56)$$

The computational stability criterion for the Lax-Wendroff timestep

$$\delta t < \frac{a}{m\sqrt{u^2+v^2}}$$

allows a timestep of 24 mins restricting the mean wind to 150ms $^{-1}$. Assuming a vertical structure such that $\underline{\underline{G}} = (1+\gamma)\,\underline{\underline{G}}_0$ the backward-implicit timestep, including the departure from constant static stability explicitly, is unconditionally stable for $|\gamma| \leq 1$ and unstable for $\gamma > 1$. In practice $|\gamma| \leq 1$ so the timestep is limited by the Lax-Wendroff stability criterion. Experiments have been carried out with 15 min and 24 min timesteps.

NOTATION USED IN APPENDIX

a	horizontal grid length on polar stereographic projection
$c_{\omega k}$	phase speed of gravity wave, mode k
f	coriolis parameter
g	acceleration due to gravity
h	height of an isobaric surface
h'	thickness of a 100mb layer
H	height of topography
m	map magnification factor = $\frac{2}{1+\sin\phi}$
p	pressure
t	time
u, v	horizontal velocity components
u^*, v^*	u/m, v/m
x, y	co-ordinates on polar-stereographic map projection
z	height
β	static stability parameter
δt	timestep of integration
μ	m^2
ϕ	latitude
ω	$\frac{Dp}{Dt}$
suffices x,y	partial differentiation
i, j	horizontal grid-point indices
1 to 10	level number 100 to 1000 mb

Finite difference approximations

$$(\delta_x z)_i = \frac{1}{a}\left(z_{i+\frac{1}{2}} - z_{i-\frac{1}{2}}\right)$$

$$(\overline{z}^x)_i = \frac{1}{2}\left(z_{i+\frac{1}{2}} + z_{i-\frac{1}{2}}\right)$$

With similar notation for y derivatives and averages

$$\nabla^2 \equiv \delta_{xx} + \delta_{yy}$$

FIGURE 1. RMS DIVERGENCE DURING INITIALIZATION FOR DIFFERENT SCHEMES $\bar{\phi} = 9 \times 10^4$

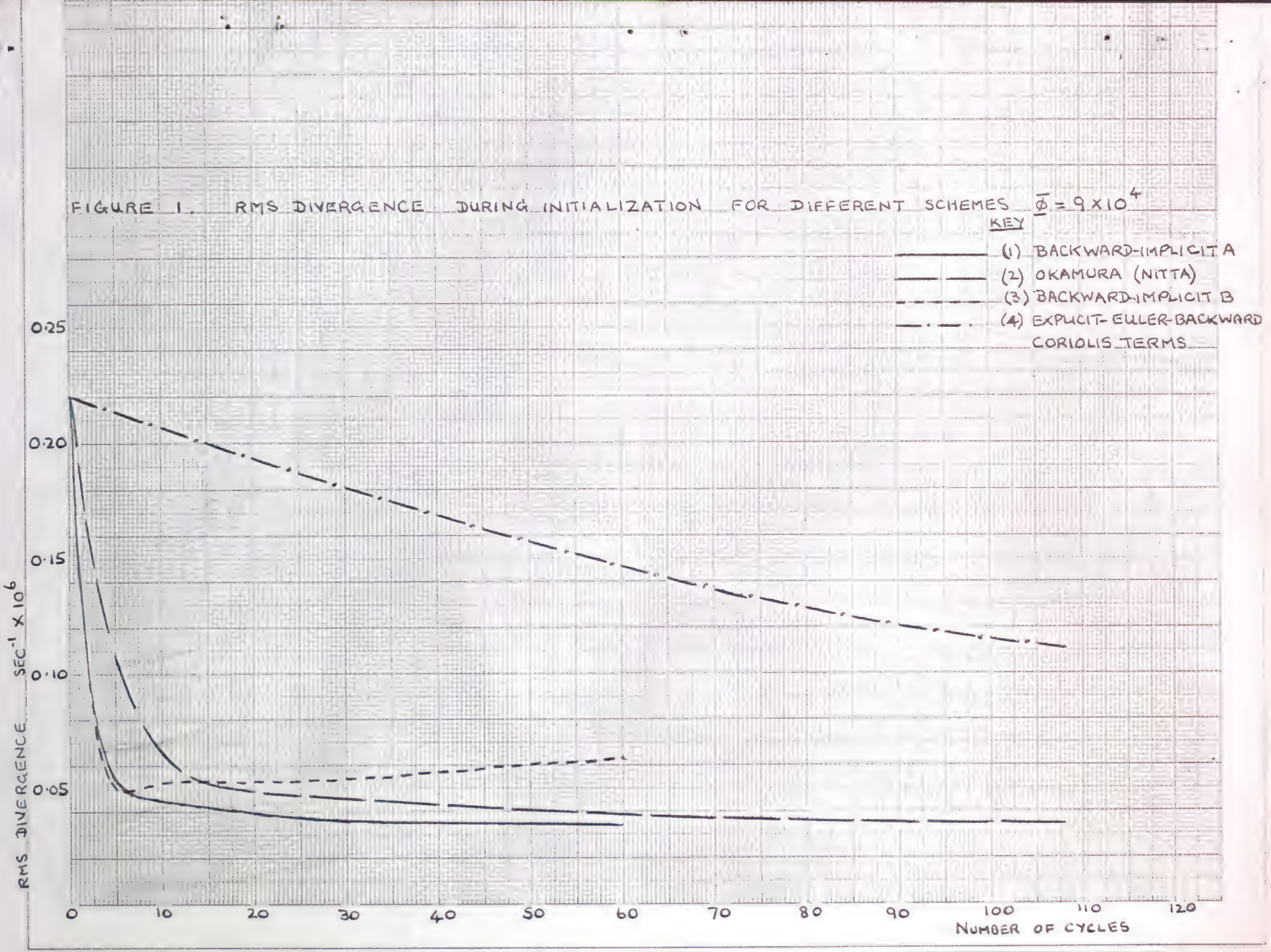

FIGURE 2. RMS VORTICITY DURING INITIAIZATION FOR DIFFERENT SCHEMES $\Phi = 9 \times 10^4$

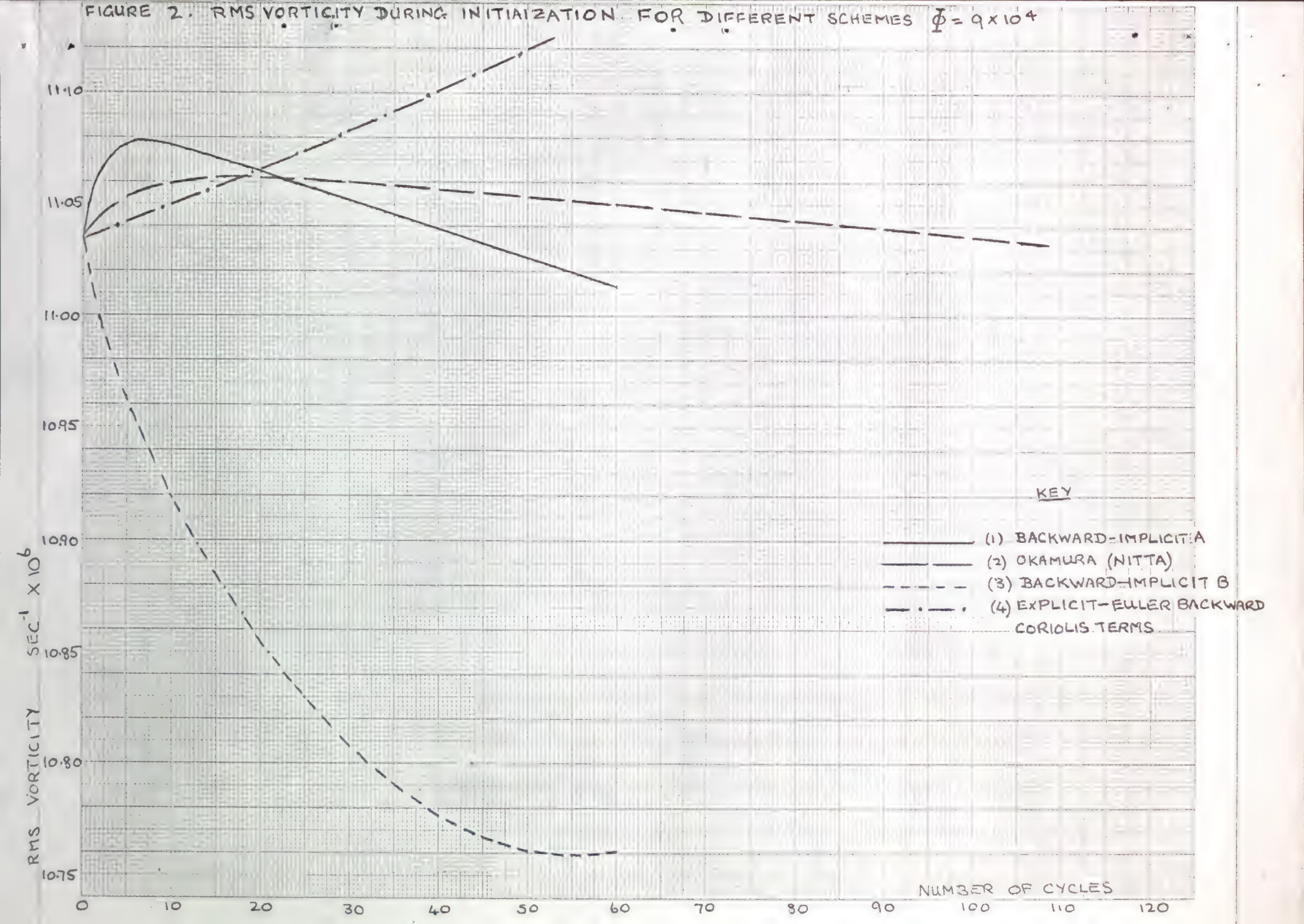

FIGURE 3 RMS HEIGHT DIFFERENCE BETWEEN INITIAL AND ADJUSTING HEIGHT FIELDS DURING INITIALIZATION FOR DIFFERENT SCHEMES. $\Phi = 9 \times 10^4$

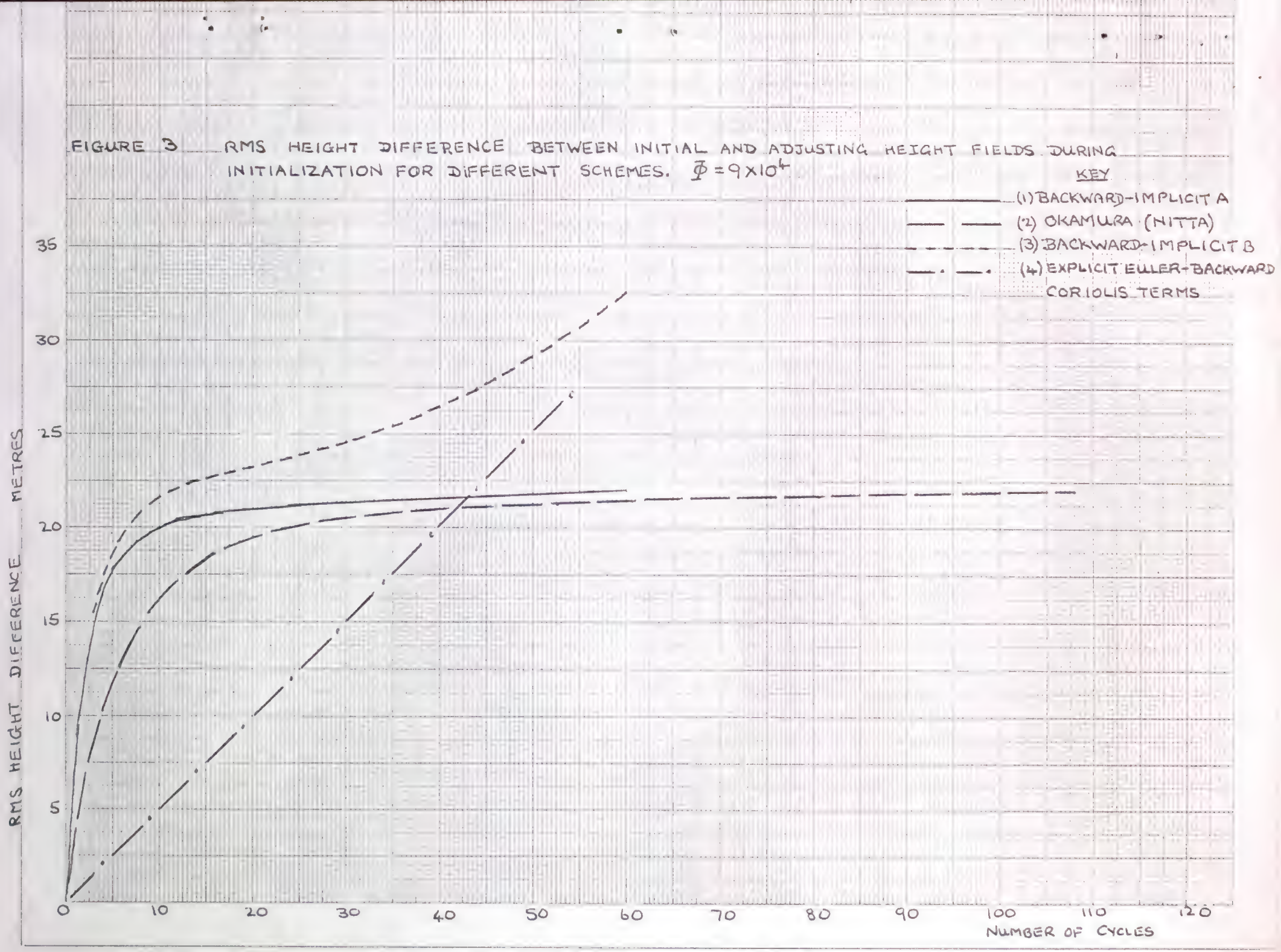

FIGURE 4. RMS DIFFERENCE BETWEEN ADJUSTING WIND FIELD AND WIND FIELD WHICH BALANCES INITIAL HEIGHT FIELD DURING INITIALIZATION FOR DIFFERENT SCHEMES $\bar{\Phi} = 9 \times 10^4$

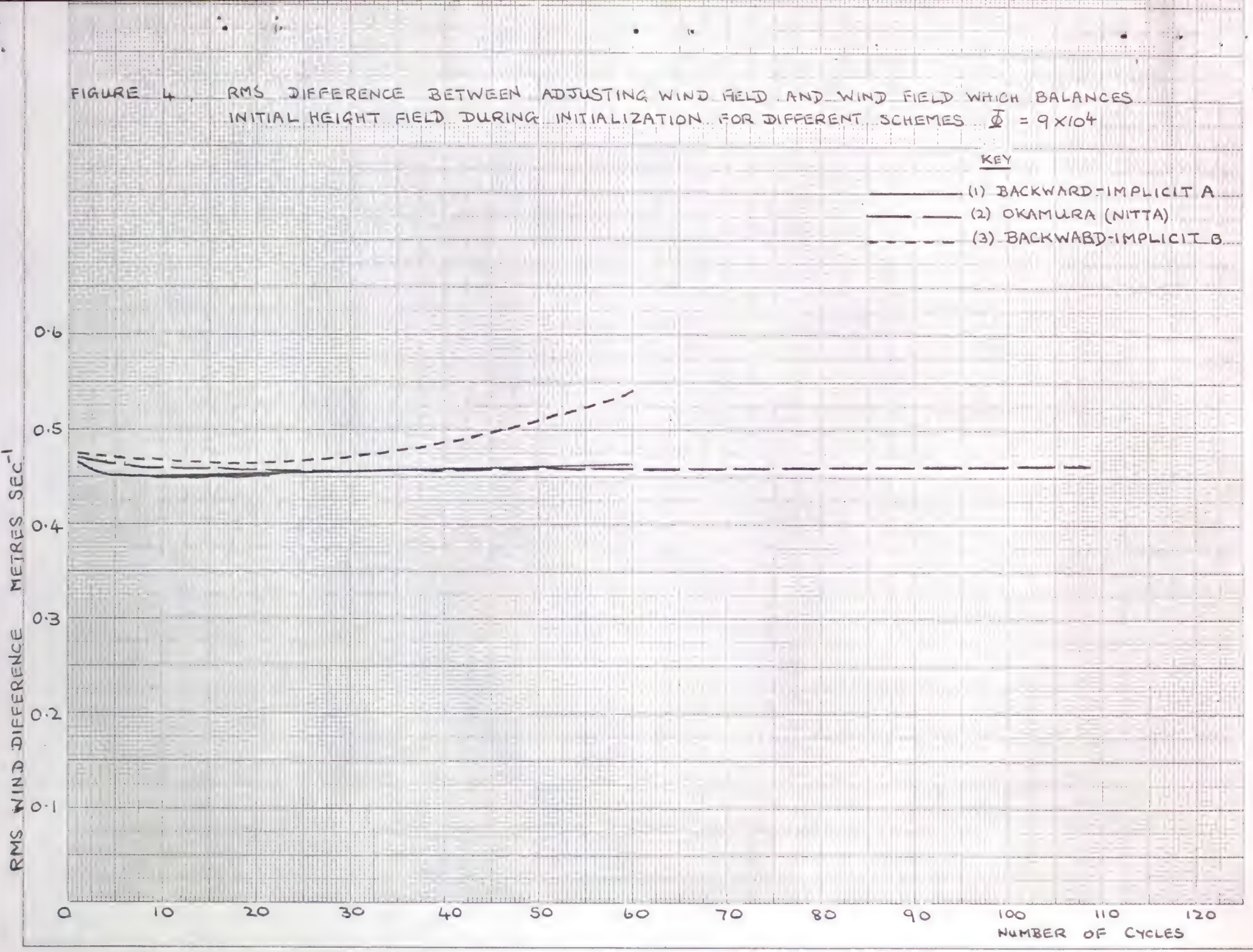

FIGURE 5. RMS DIVERGENCE DURING LEAPFROG INTEGRATION FOLLOWING DIFFERENT INITIALIZATION SCHEMES.
$\bar{D} = 9 \times 10^4$

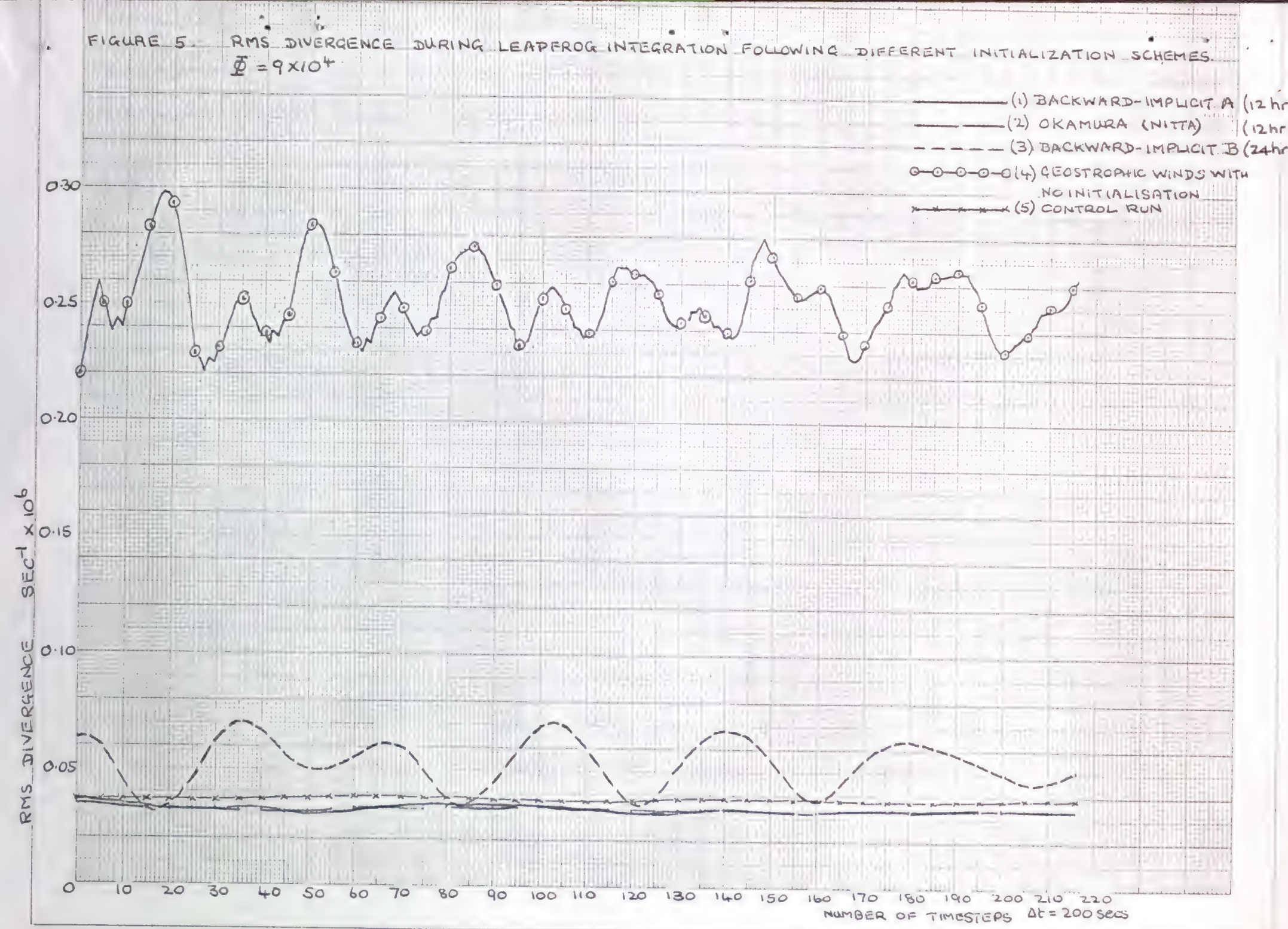

FIGURE 6. RMS DIVERGENCE $SEC^{-1} \times 10^6$ DURING INITIALIZATION BACKWARD-IMPLICIT A SCHEME

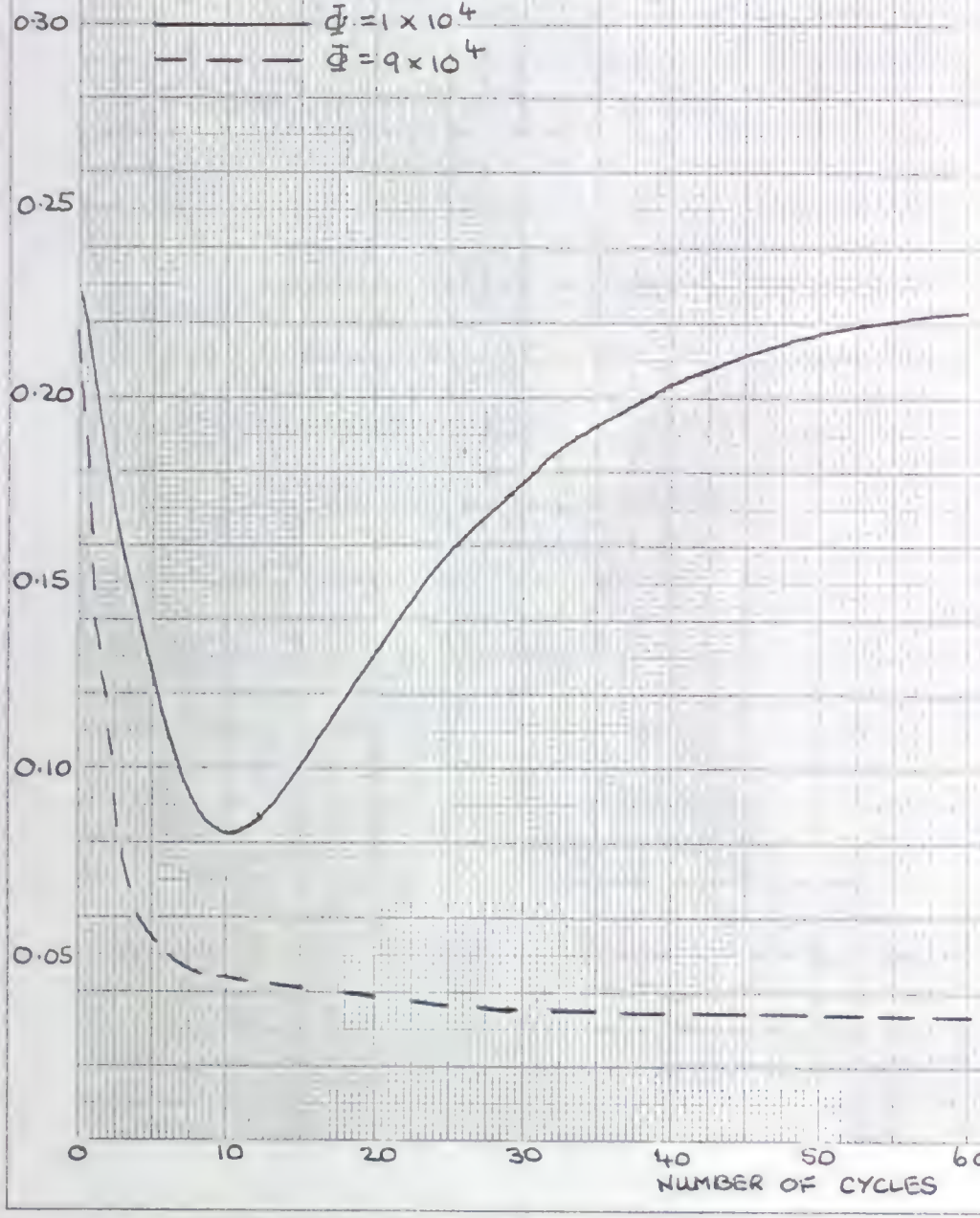

FIGURE 7. RMS VORTICITY $SEC^{-1} \times 10^4$ DURING INITIALIZATION . BACKWARD-IMPLICIT A SCHEME

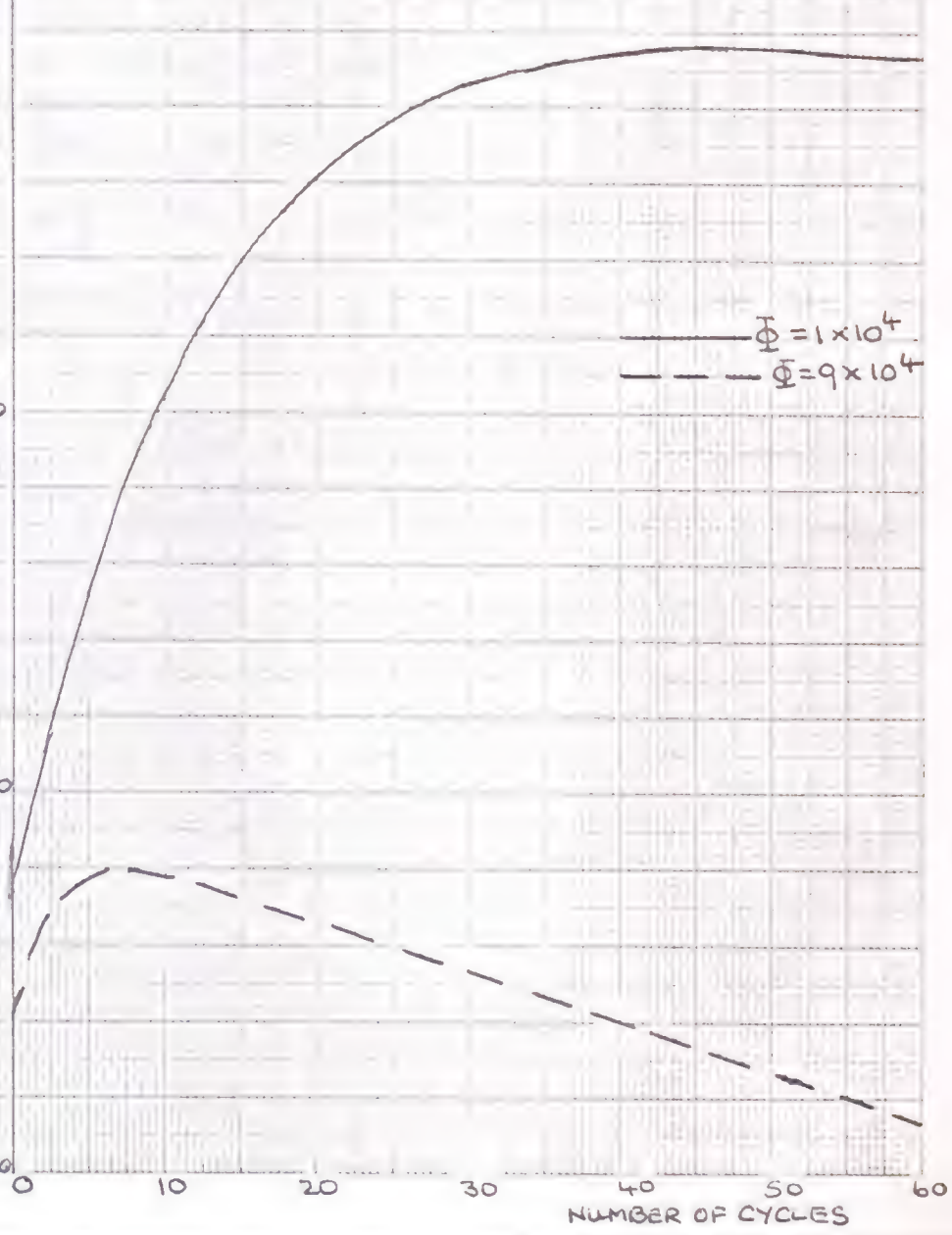

FIGURE 8. RMS DIFFERENCE BETWEEN INITIAL AND ADJUSTING HEIGHT. BACKWARD-IMPLICIT A SCHEME

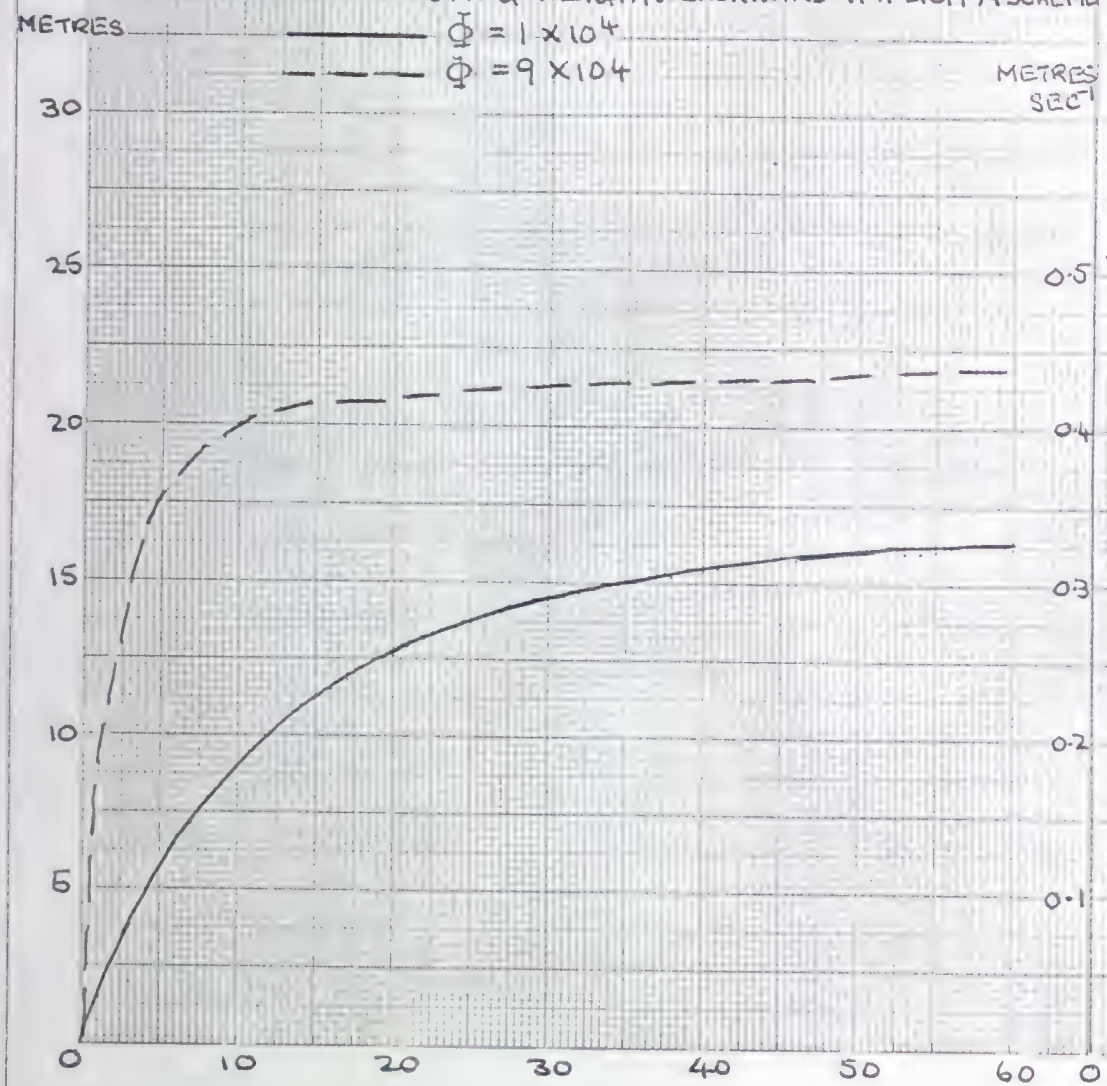

FIGURE 9. RMS DIFFERENCE BETWEEN ADJUSTING WIND AND WIND FIELD BALANCING INITIAL HEIGHT FIELD BACKWARD-IMPLICIT A SCHEME

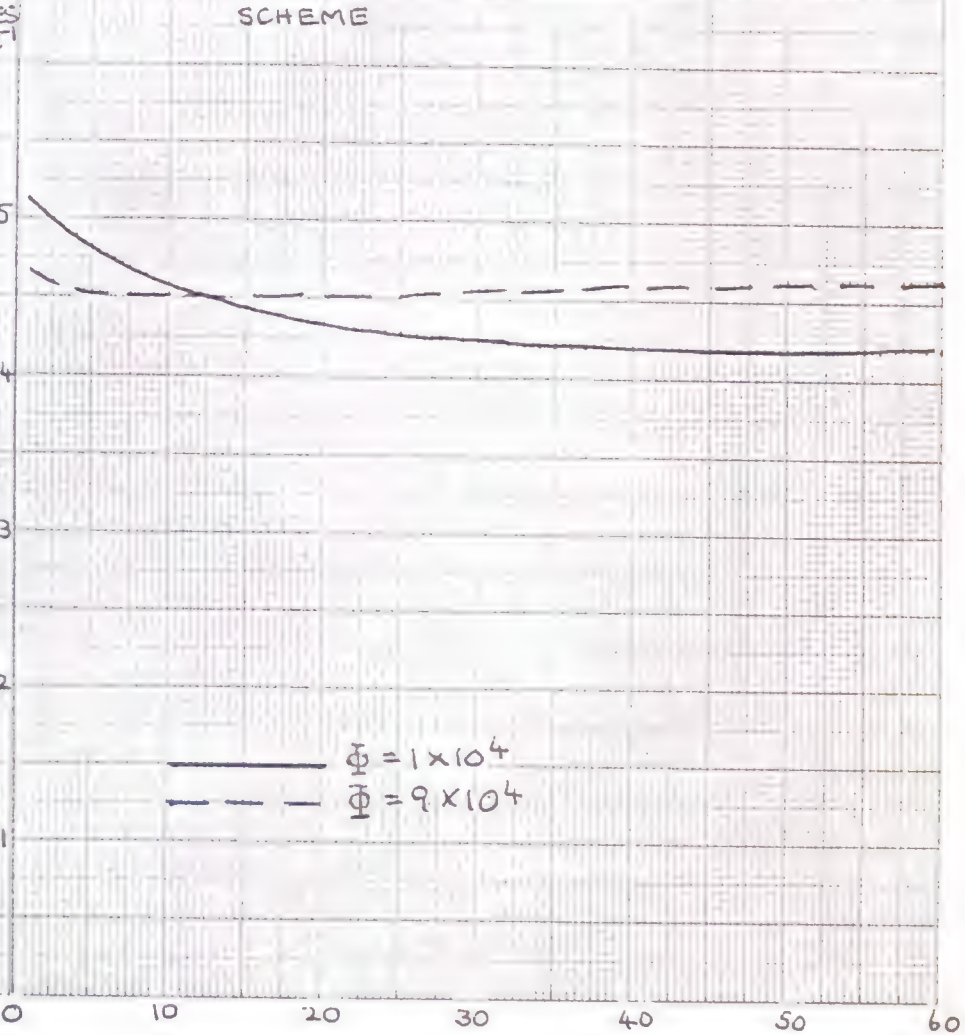

FIGURE 10 RMS DIVERGENCE DURING LEAPFROG INTEGRATION FOLLOWING DIFFERENT INITIALIZATIONS.

$\Phi = 1 \times 10^4$

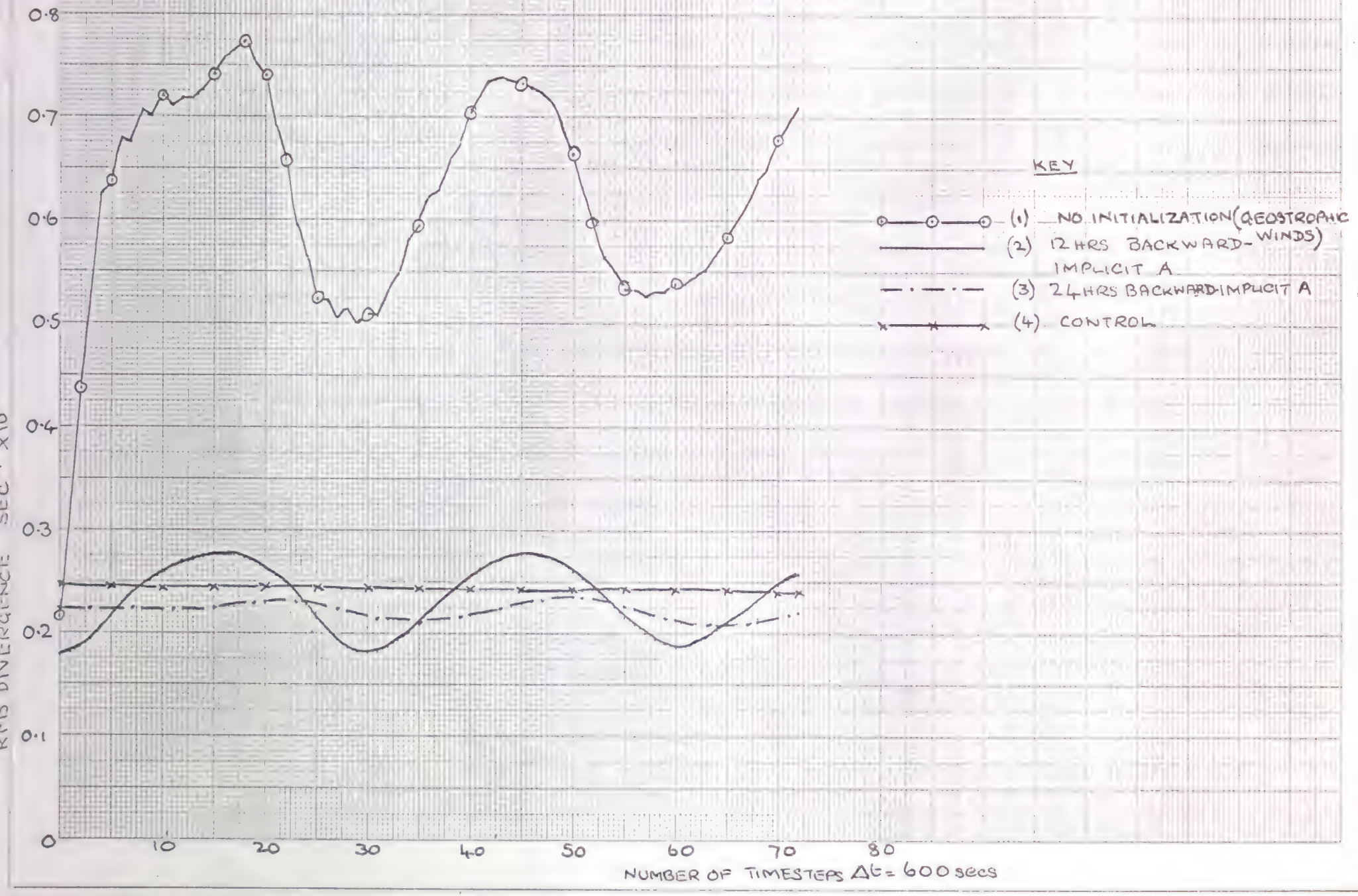

FIGURE 11a RMS DIVERGENCE DURING LEAPFROG INTEGRATION INCLUDING DEPARTURE FROM 'MEAN' GEOPOTENTIAL $\bar{\Phi} = 1 \times 10^4$ FOLLOWING DIFFERENT INITIALIZATION PROCEDURES

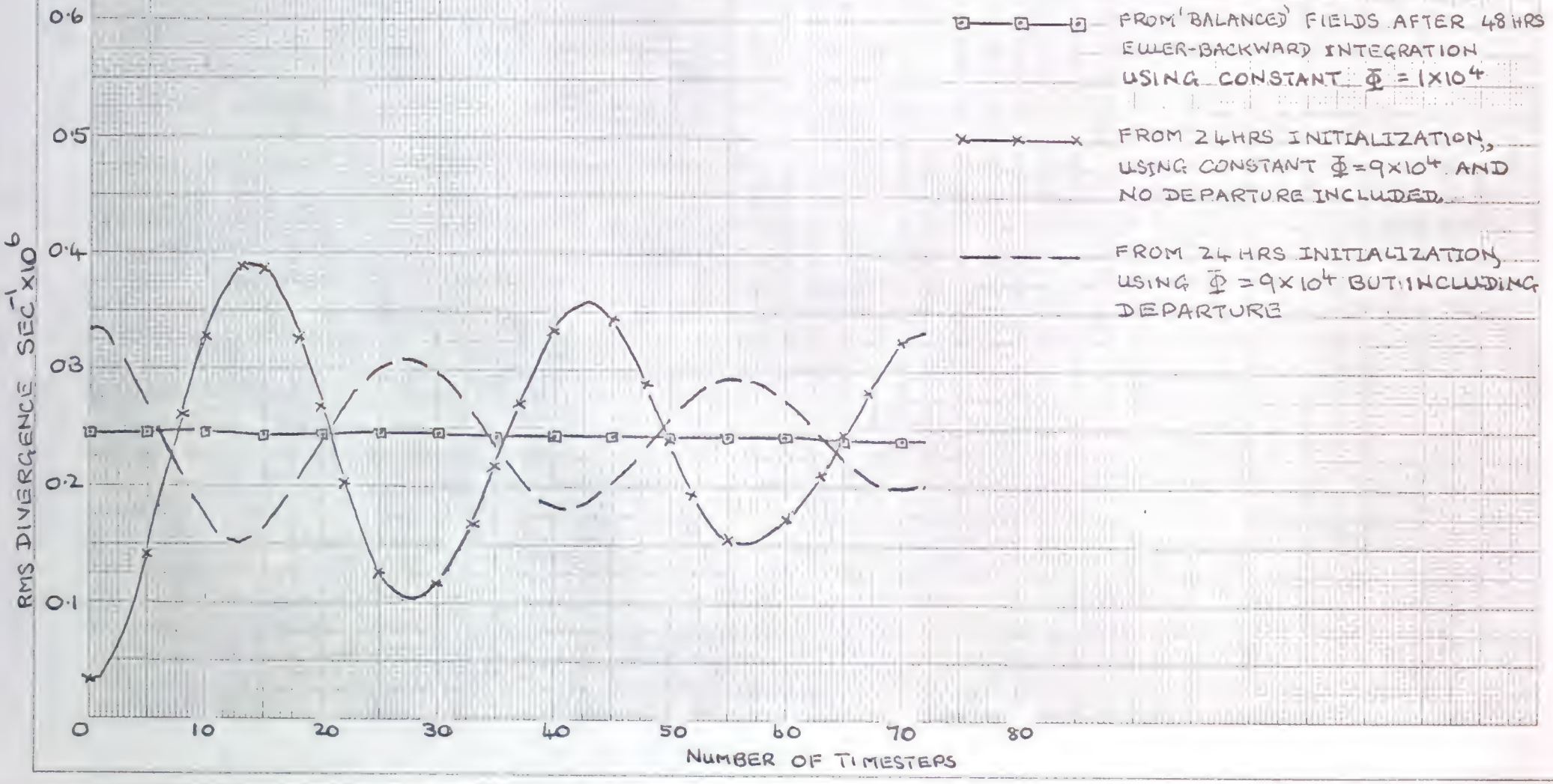

FIGURE 11.6 RMS DIVERGENCE DURING LEAPFROG INTEGRATION INCLUDING DEPARTURE FROM 'MEAN' GEOPOTENTIAL $\bar{\Phi} = 1 \times 10^4$ FOLLOWING DIFFERENT INITIALIZATION PROCEDURES

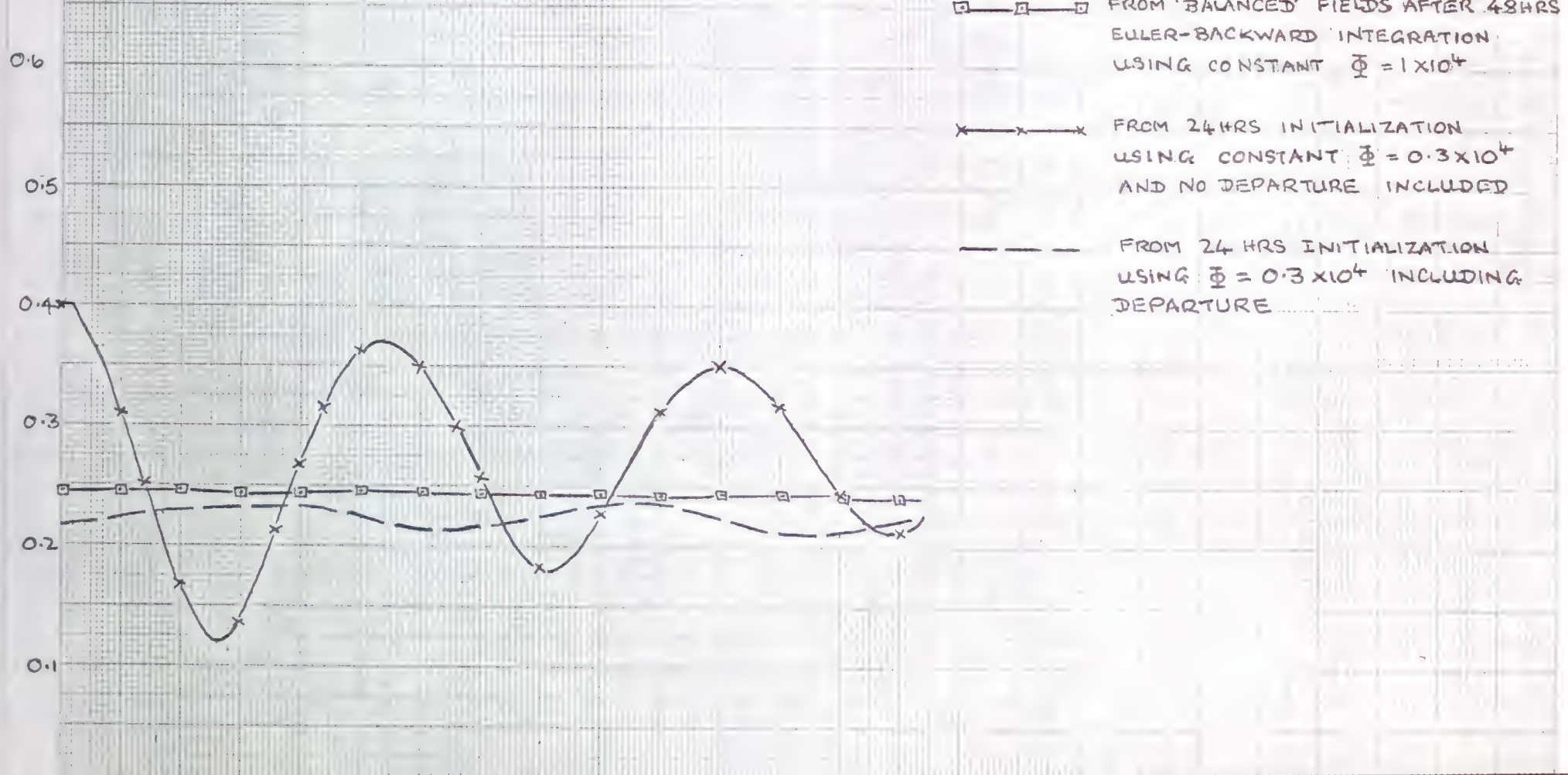

FIGURE 12a Sketch of Eigenvalues ρ_2, ρ_3 of $\underline{\underline{L}}(-\Delta t)\,\underline{\underline{L}}(\Delta t)$ or method (i) of including departure from Φ

$$\rho_2 = \frac{1}{1+\omega^2\Delta t^2+\frac{\gamma^2\omega^4\Delta t^4}{2} + \gamma\frac{\omega^2\Delta t^2}{2}\sqrt{\gamma^2\omega^4\Delta t^4+4(1+\omega^2\Delta t^2)}}$$

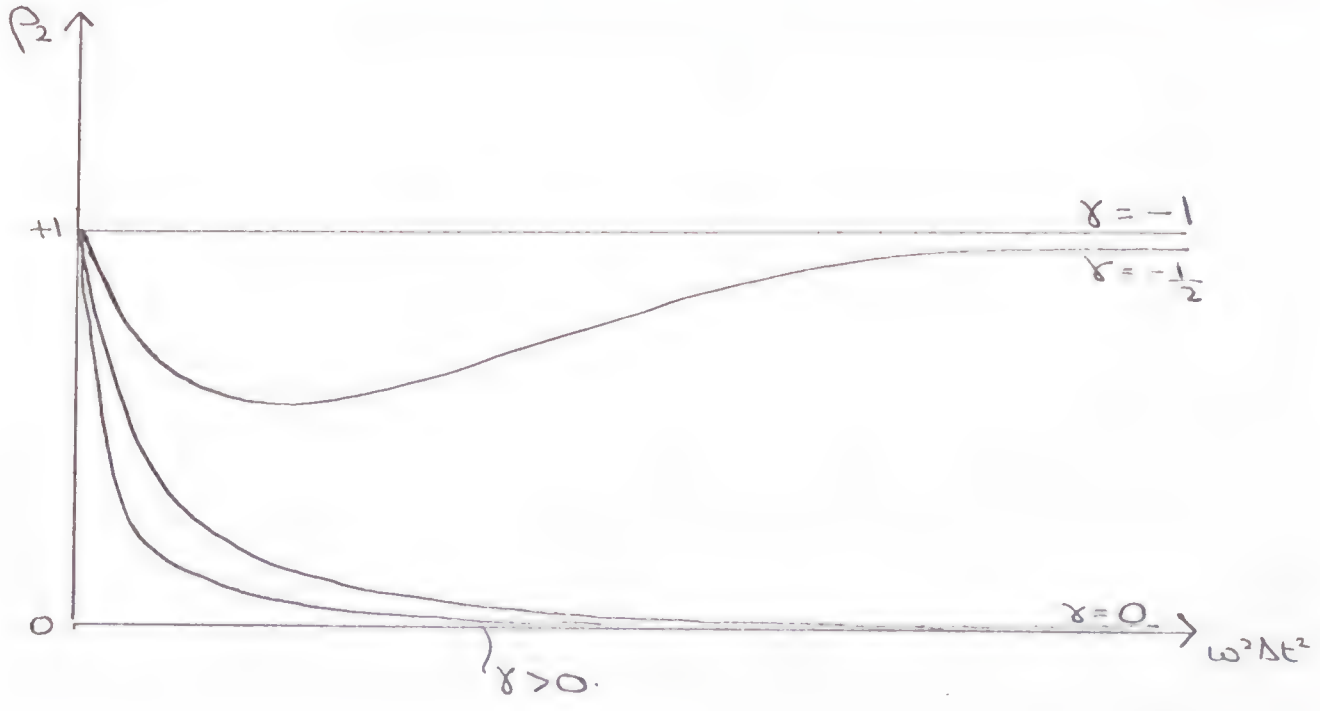

$$\rho_3 = \frac{1}{1+\omega^2\Delta t^2+\frac{\gamma^2\omega^4\Delta t^4}{2} - \gamma\frac{\omega^2\Delta t^2}{2}\sqrt{\gamma^2\omega^4\Delta t^4+4(1+\omega^2\Delta t^2)}}$$

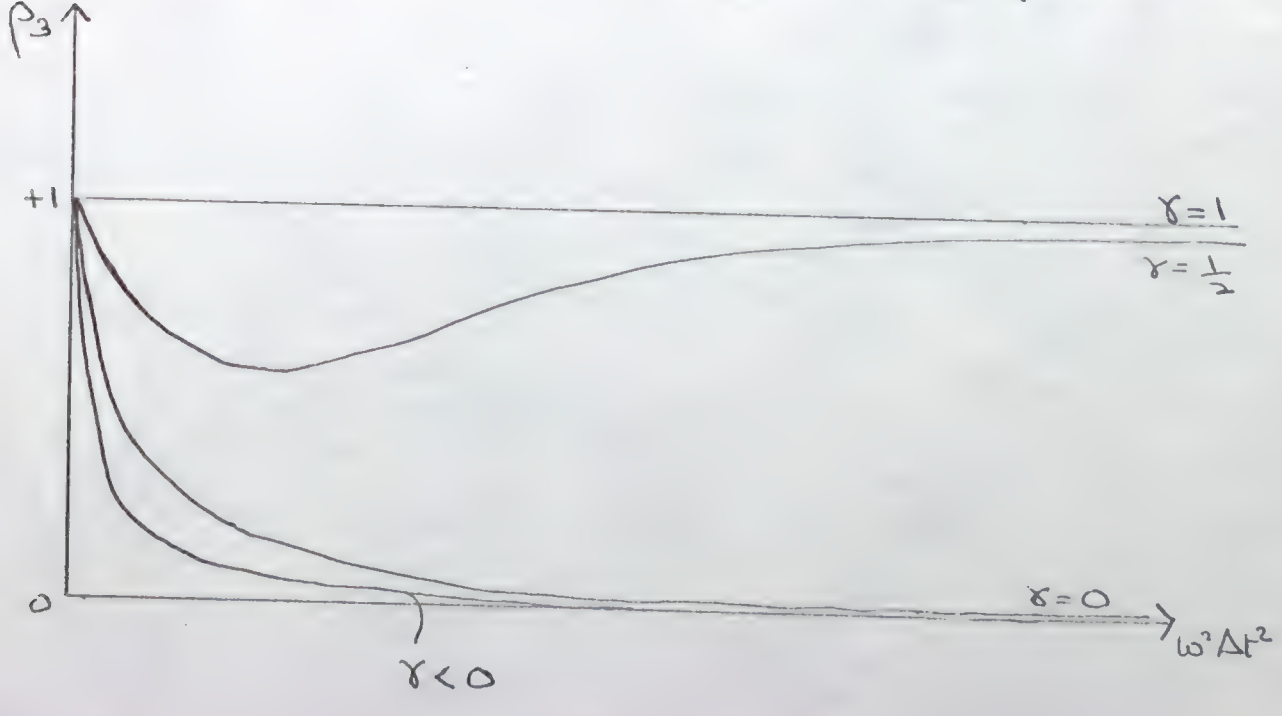

FIGURE 12b. Sketch of eigenvalues $\rho_{2,3}$ of $\underline{\underline{L}}(-\Delta t)\,\underline{\underline{L}}(\Delta t)$ for method (ii) of including departure from $\underline{\underline{\Phi}}$

$$\rho_{2,3} = \frac{1 - \gamma\omega^2\Delta t^2}{1 + \omega^2\Delta t^2}$$

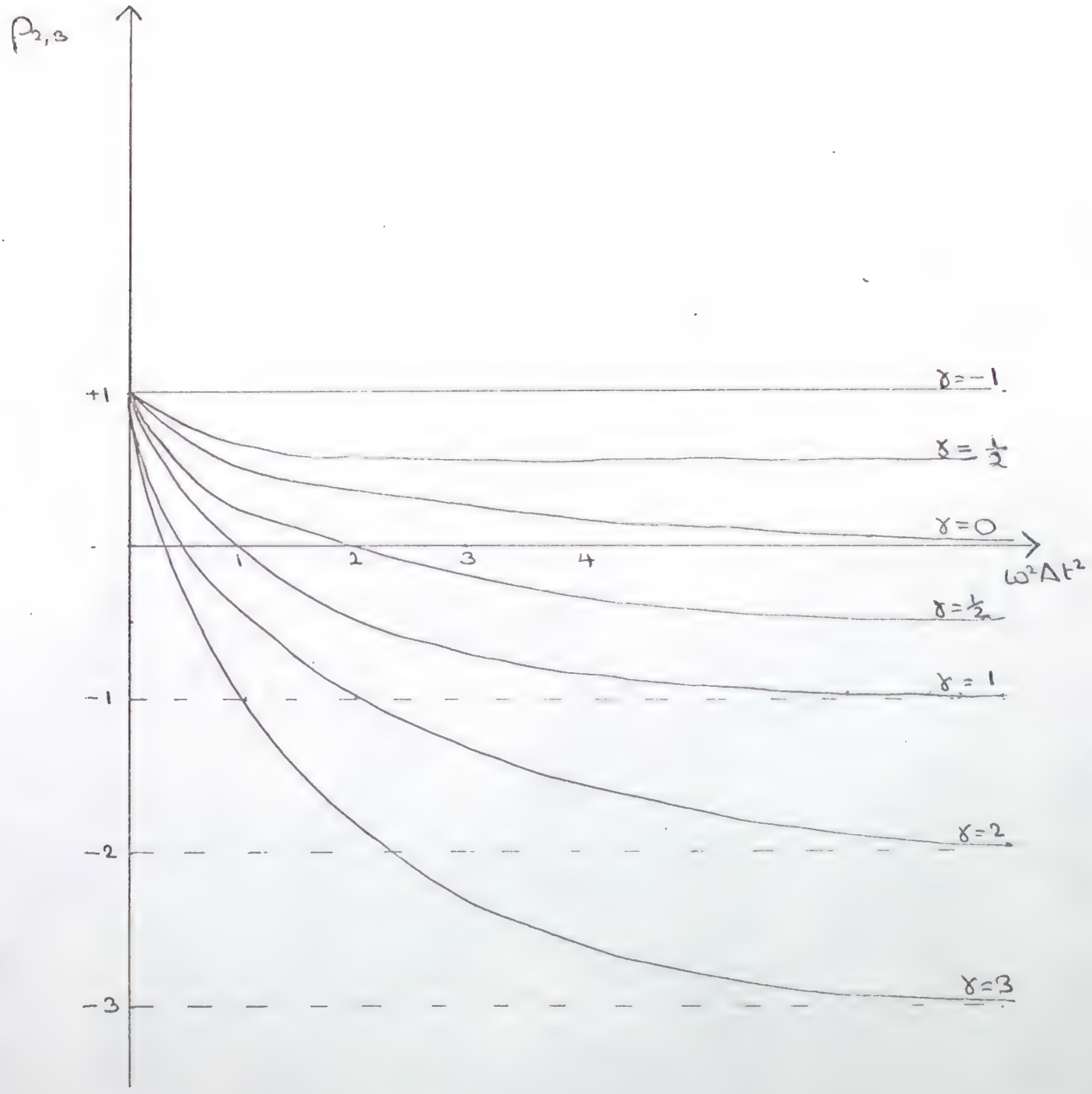

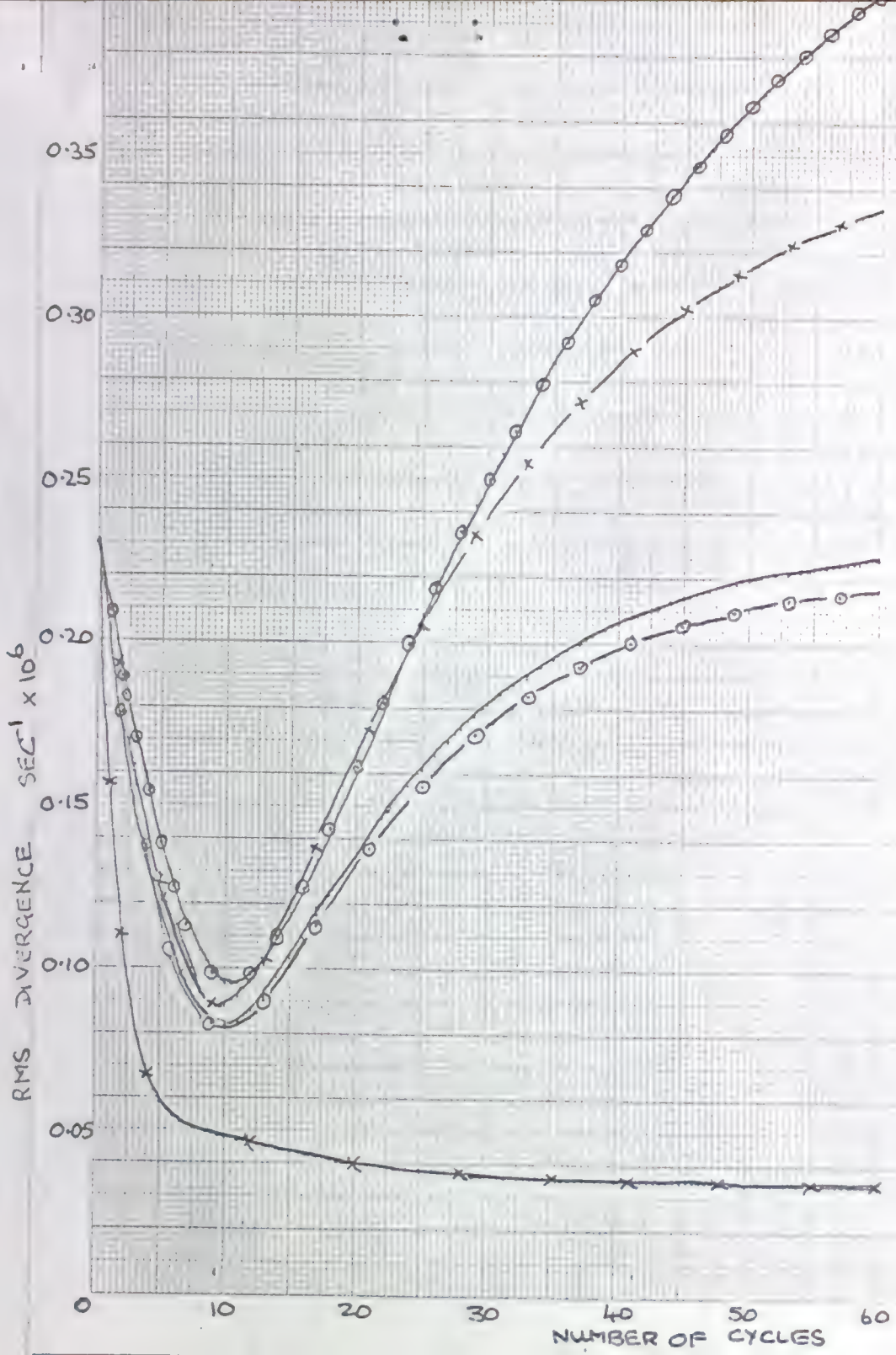

FIGURE 13

RMS DIVERGENCE DURING INITIALIZATION WITH AND WITHOUT DEPARTURE FROM CONSTANT GEOPOTENTIAL $\bar{\Phi}$ INCLUDED

ACTUAL GEOPOTENTIAL $\phi = 1 \times 10^4 + \phi'$

———— $\phi = 1 \times 10^4 + \phi'$

x——x——x $\bar{\phi} = 9 \times 10^4$

x——x——x $\phi = 9 \times 10^4 + \phi''$

⊙——⊙——⊙ $\phi = 0.3 \times 10^4$

⊙——⊙——⊙ $\phi = 0.3 \times 10^4 + \phi'''$

FIGURE 14.

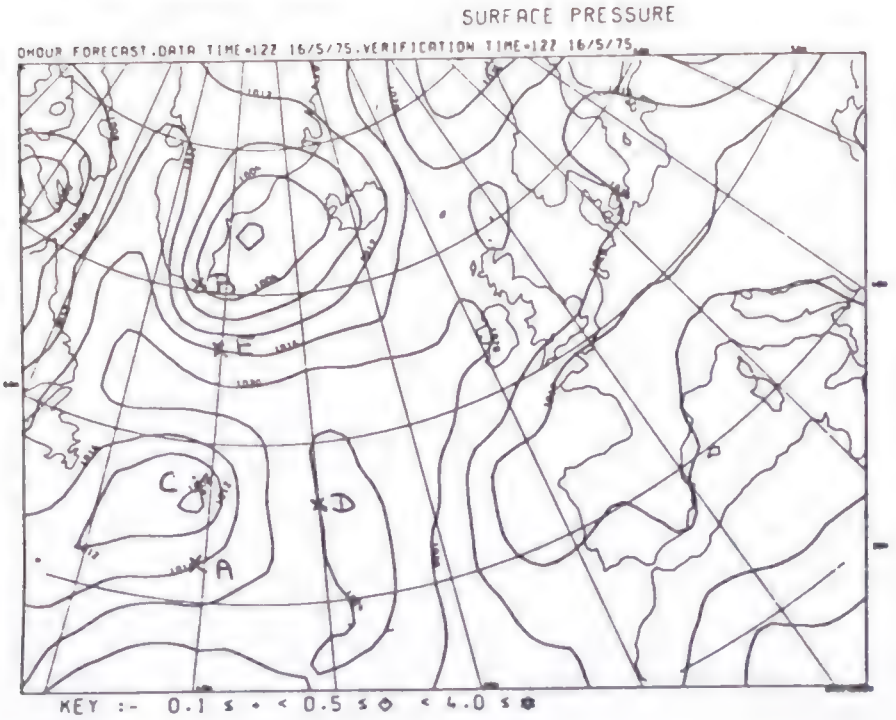
SURFACE PRESSURE
OMOUR FORECAST.DATA TIME=122 16/5/75.VERIFICATION TIME=122 16/5/75
B
E
C
D
A
KEY :- 0.1 ≤ • < 0.5 ≤ ◇ < 4.0 ≤ ◆

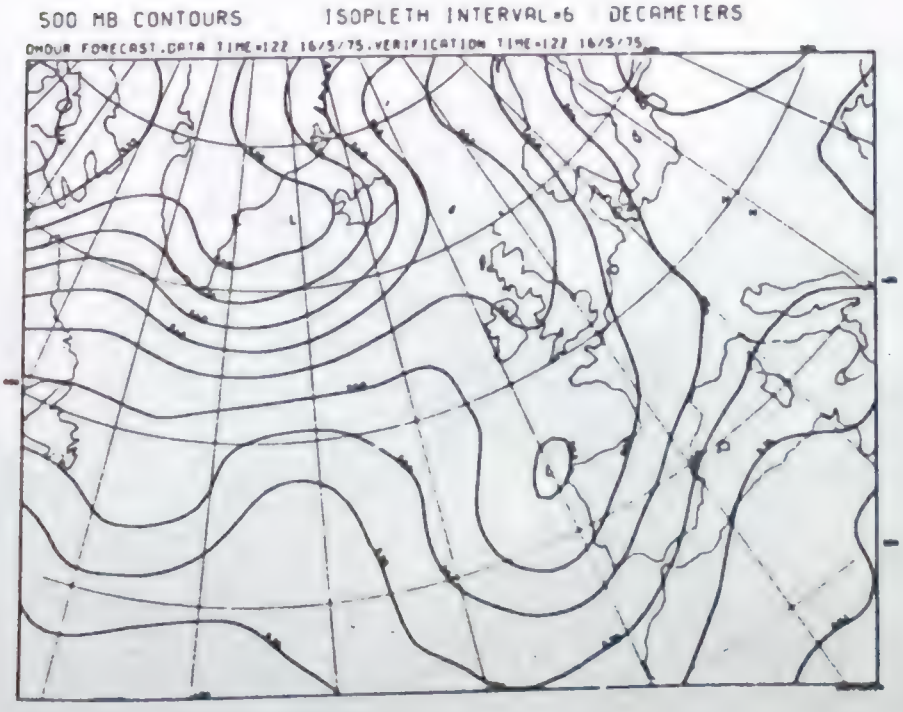
500 MB CONTOURS ISOPLETH INTERVAL=6 DECAMETERS
OMOUR FORECAST.DATA TIME=122 16/5/75.VERIFICATION TIME=122 16/5/75

FIGURE 15a. RMS DIVERGENCE DURING INITIALIZATION. EXTERNAL MODE 12Z 16/5/75

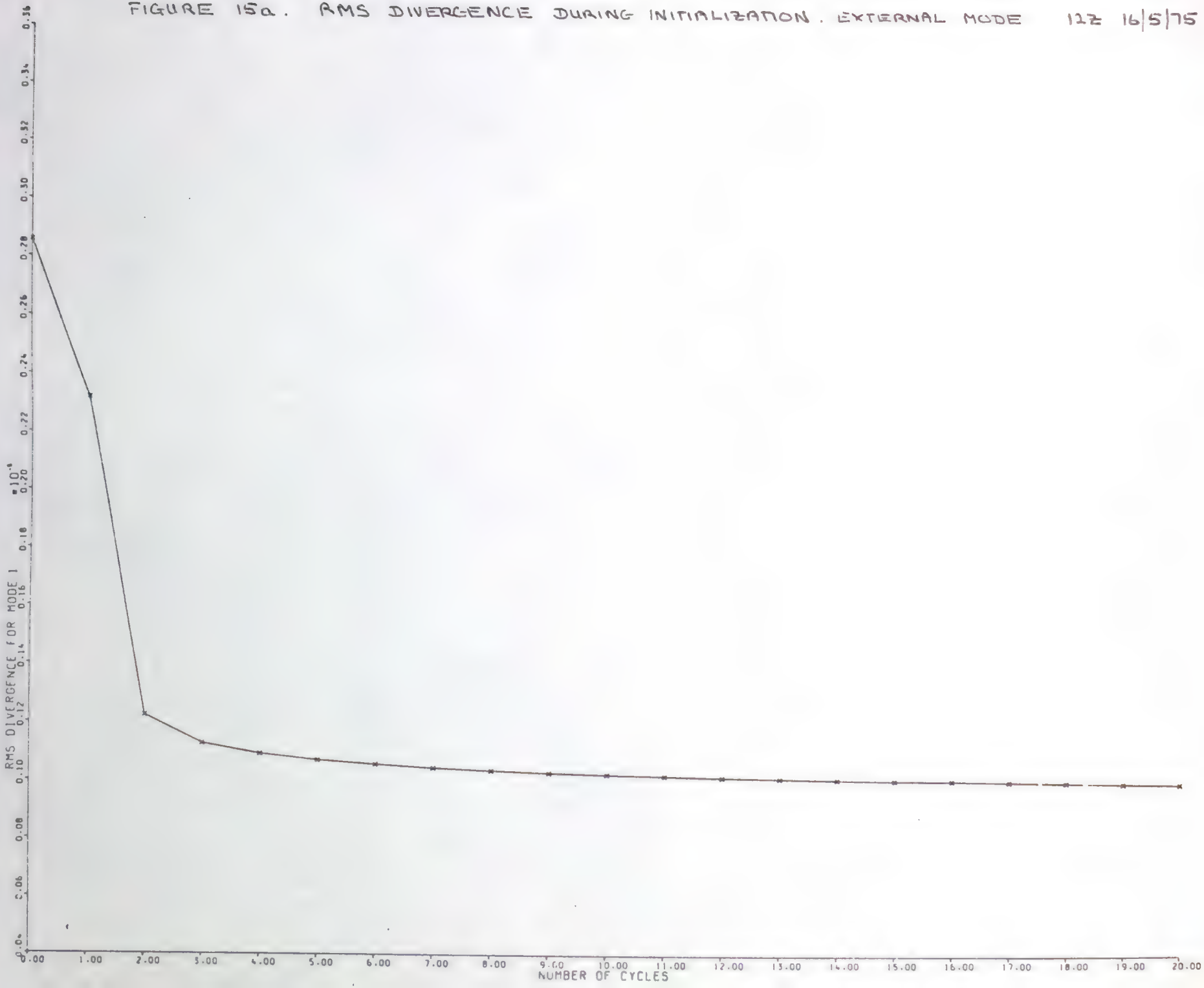

FIGURE 15G RMS DIVERGENCE DURING INITIALIZATION 1ST INTERNAL MODE. 12Z 16/5/75

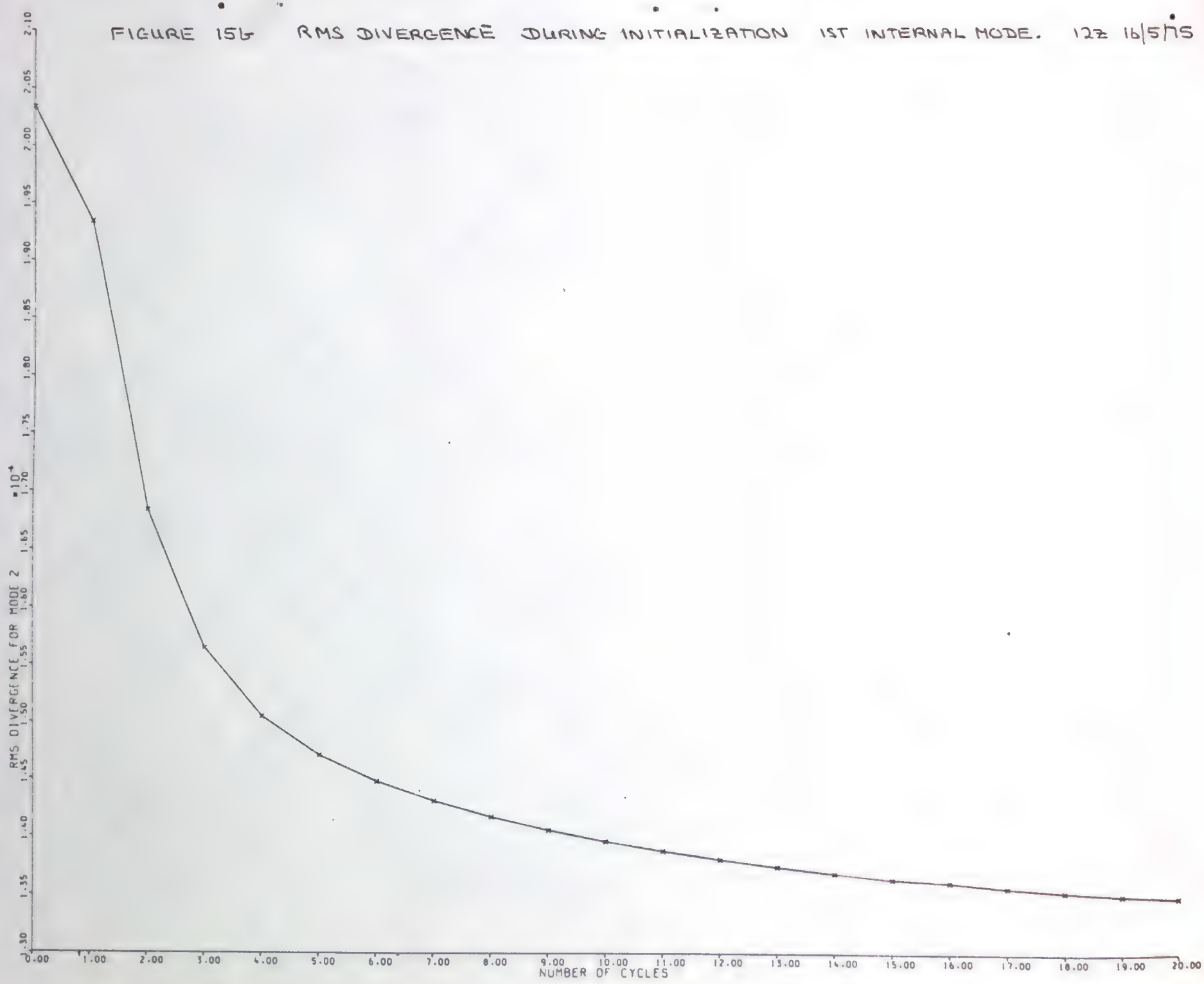

FIGURE 15c. RMS DIVERGENCE DURING INITIALIZATION 2ND INTERNAL MODE 12Z 16/5/75

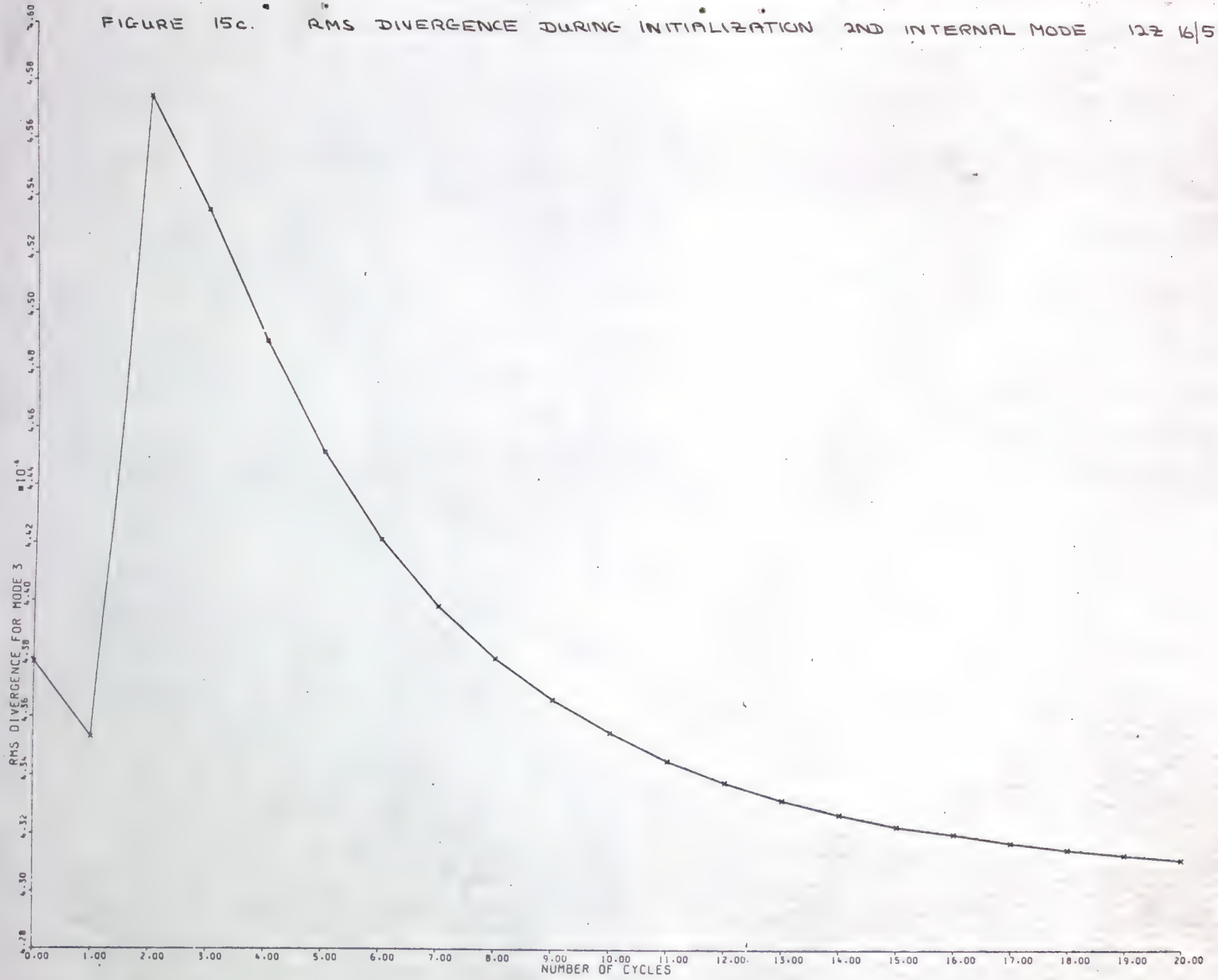

FIGURE 16a RMS DIVERGENCE DURING THE FIRST FOUR HOURS OF FORECASTS

EXTERNAL MODE DATA TIME 12Z 16/5/75

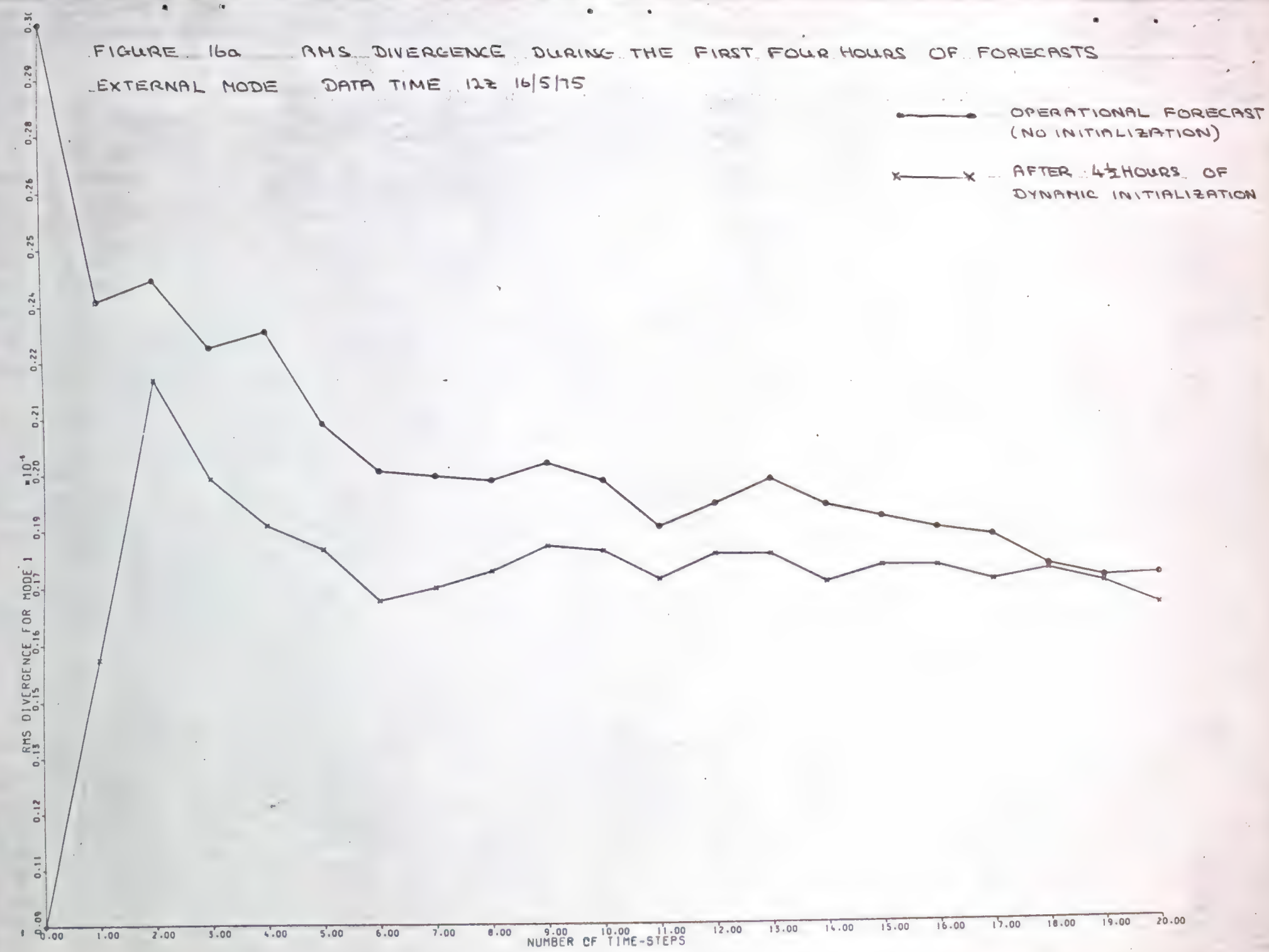

FIGURE 16b RMS DIVERGENCE DURING FIRST FOUR HOURS OF FORECASTS

1ST INTERNAL MODE DATA TIME 12Z 16/5/75

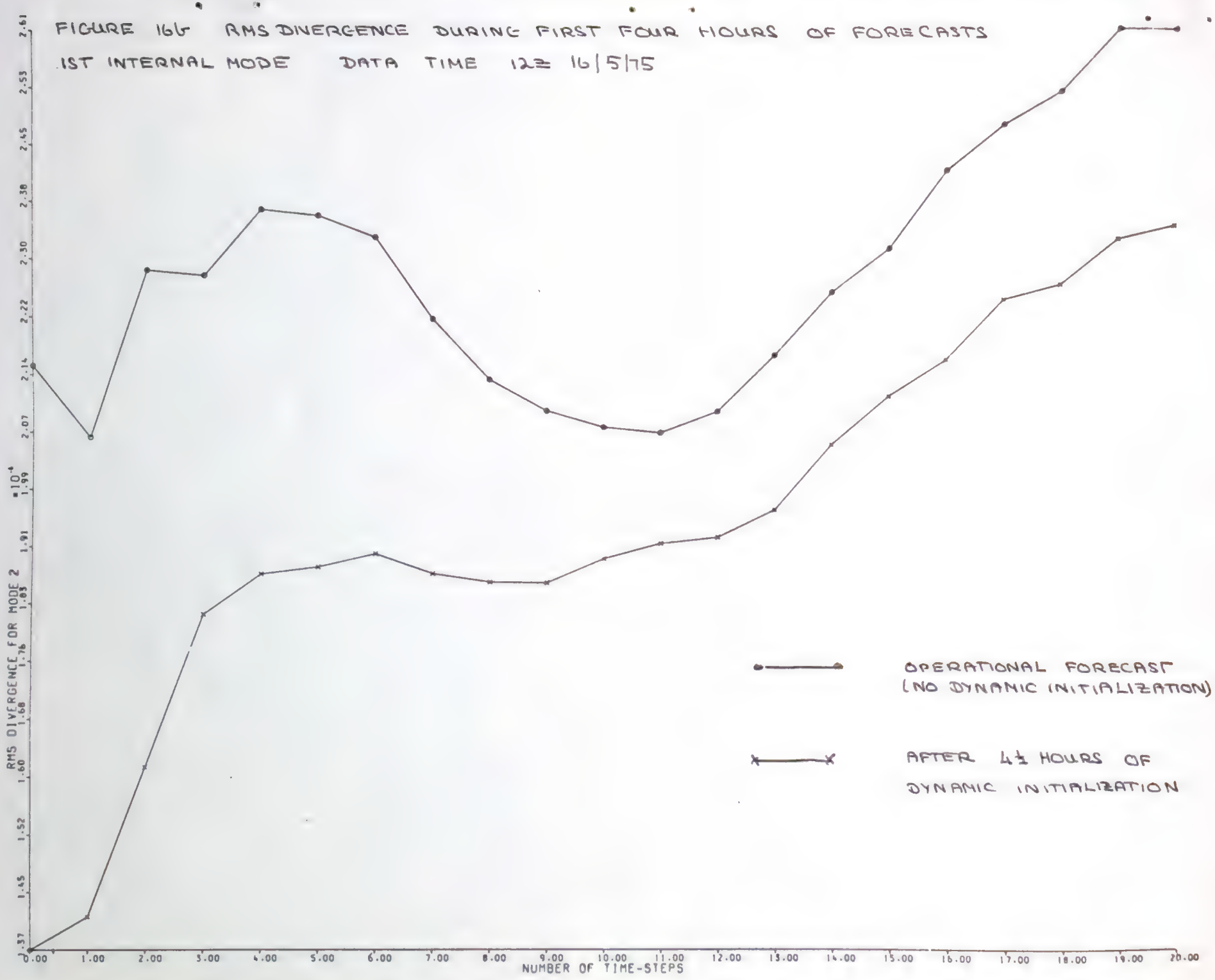

FIGURE 16c. RMS DIVERGENCE DURING FIRST FOUR HOURS OF FORECASTS. 2ND INTERNAL MODE DATA TIME 12Z 16/5/75

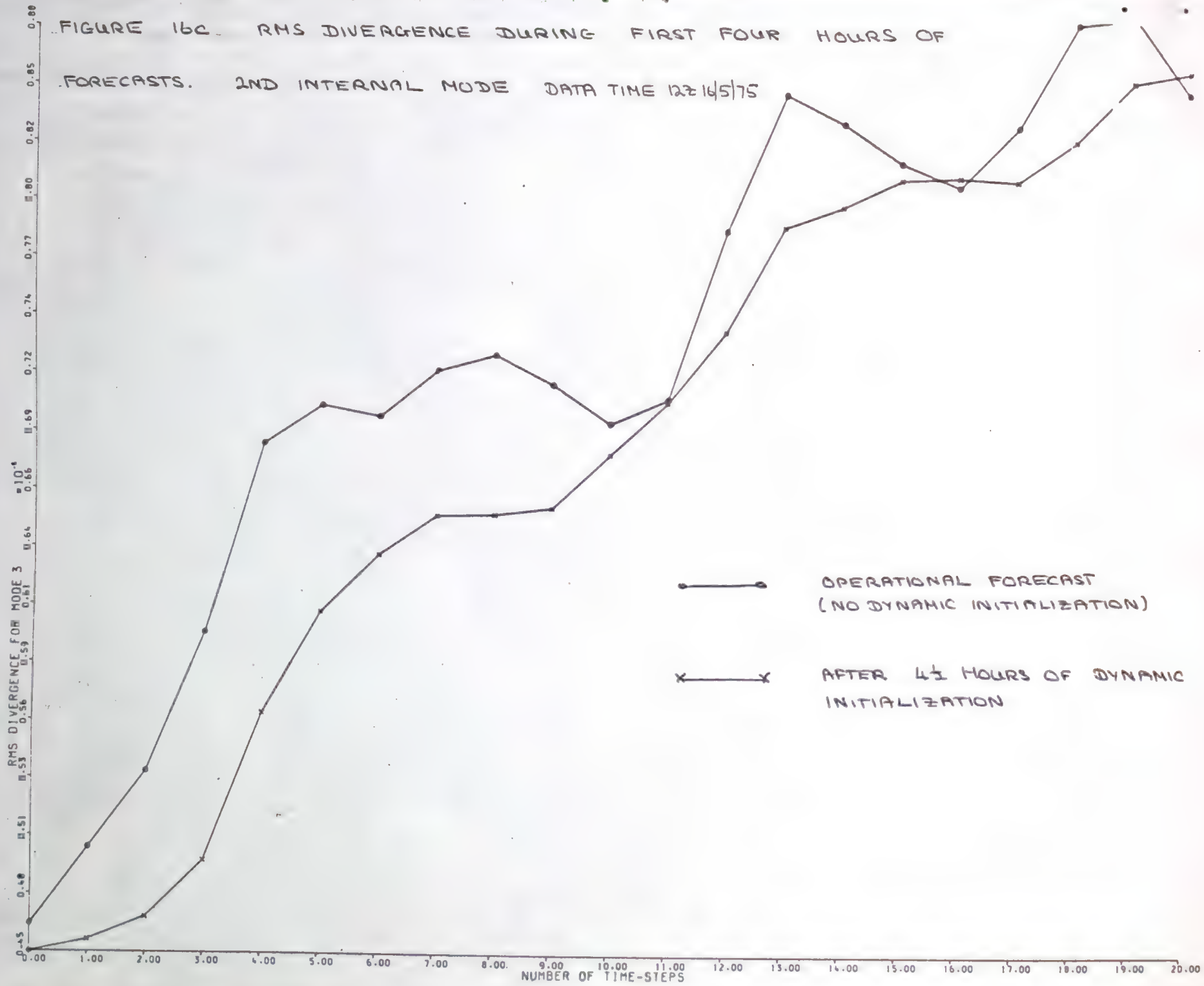

FIGURE 17a RMS DIVERGENCE DURING OPERATIONAL FORECAST . EXTERNAL MODE
INITIAL DATA TIME 12Z 16/5/75

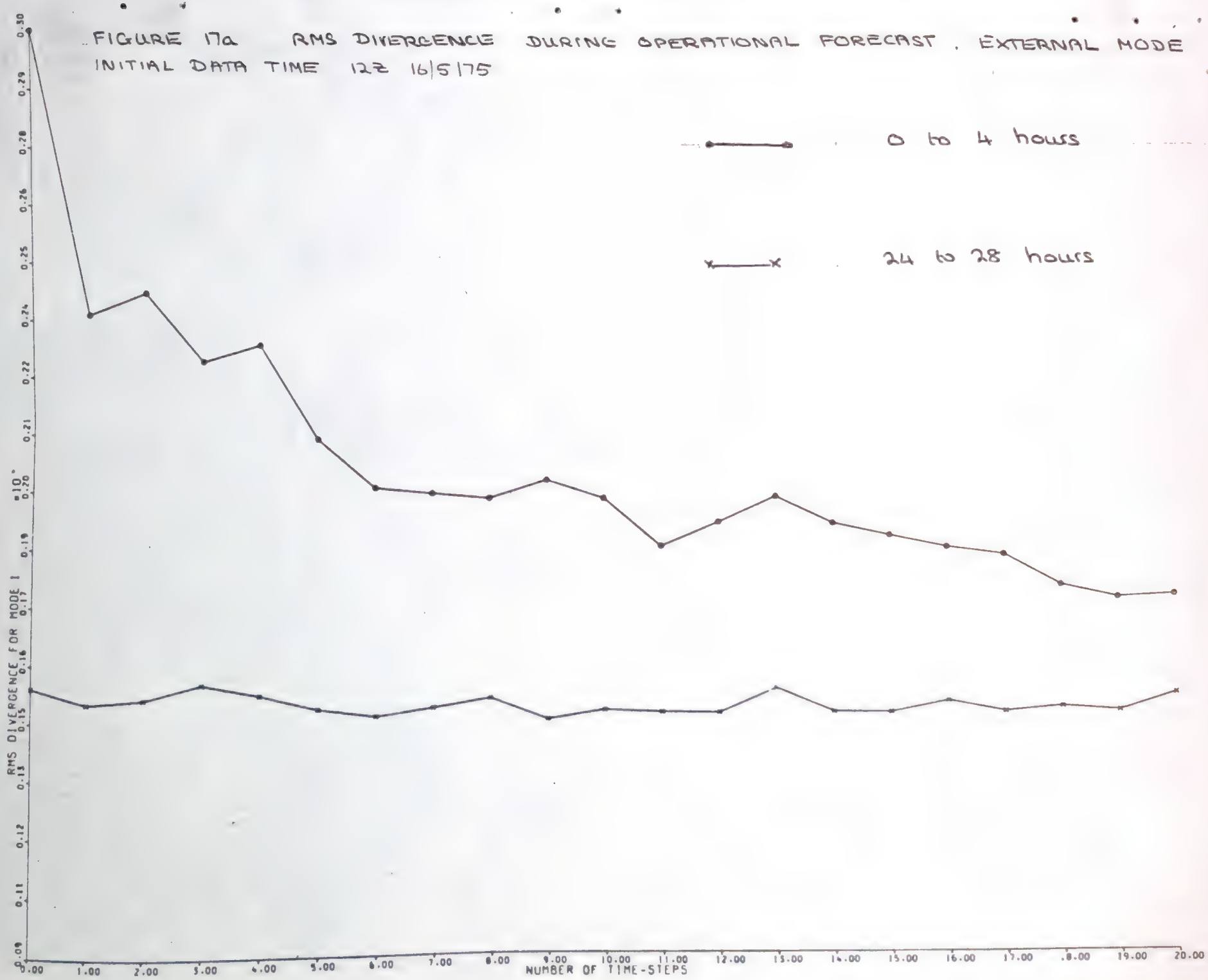

FIGURE 116 RMS DIVERGENCE DURING OPERATIONAL FORECAST

1ST INTERNAL MODE INITIAL DATA TIME 12Z 16/5/75

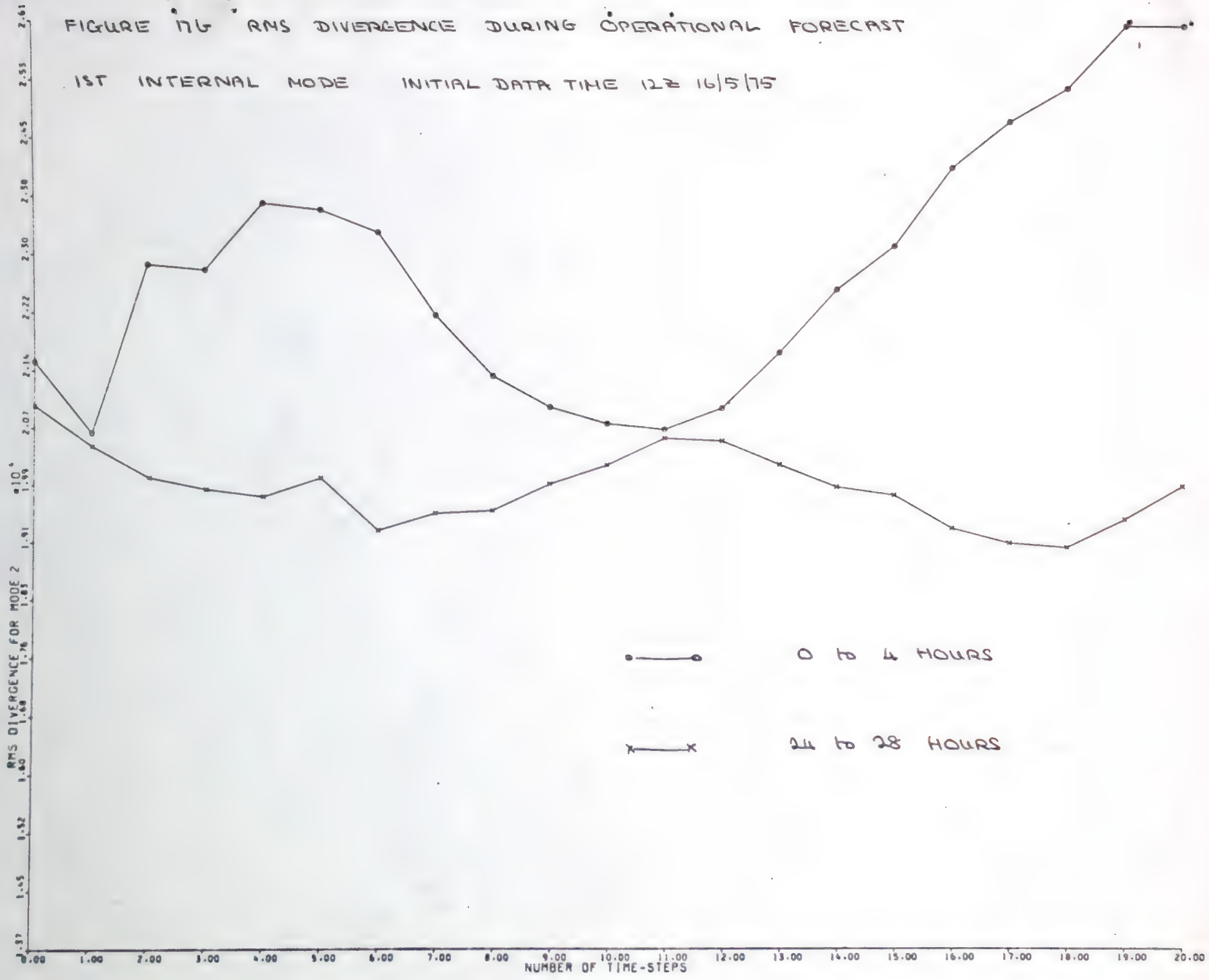

FIGURE 17c

RMS DIVERGENCE DURING OPERATIONAL FORECAST. 2ND INTERNAL MODE DATA TIME 12Z 16/5/75

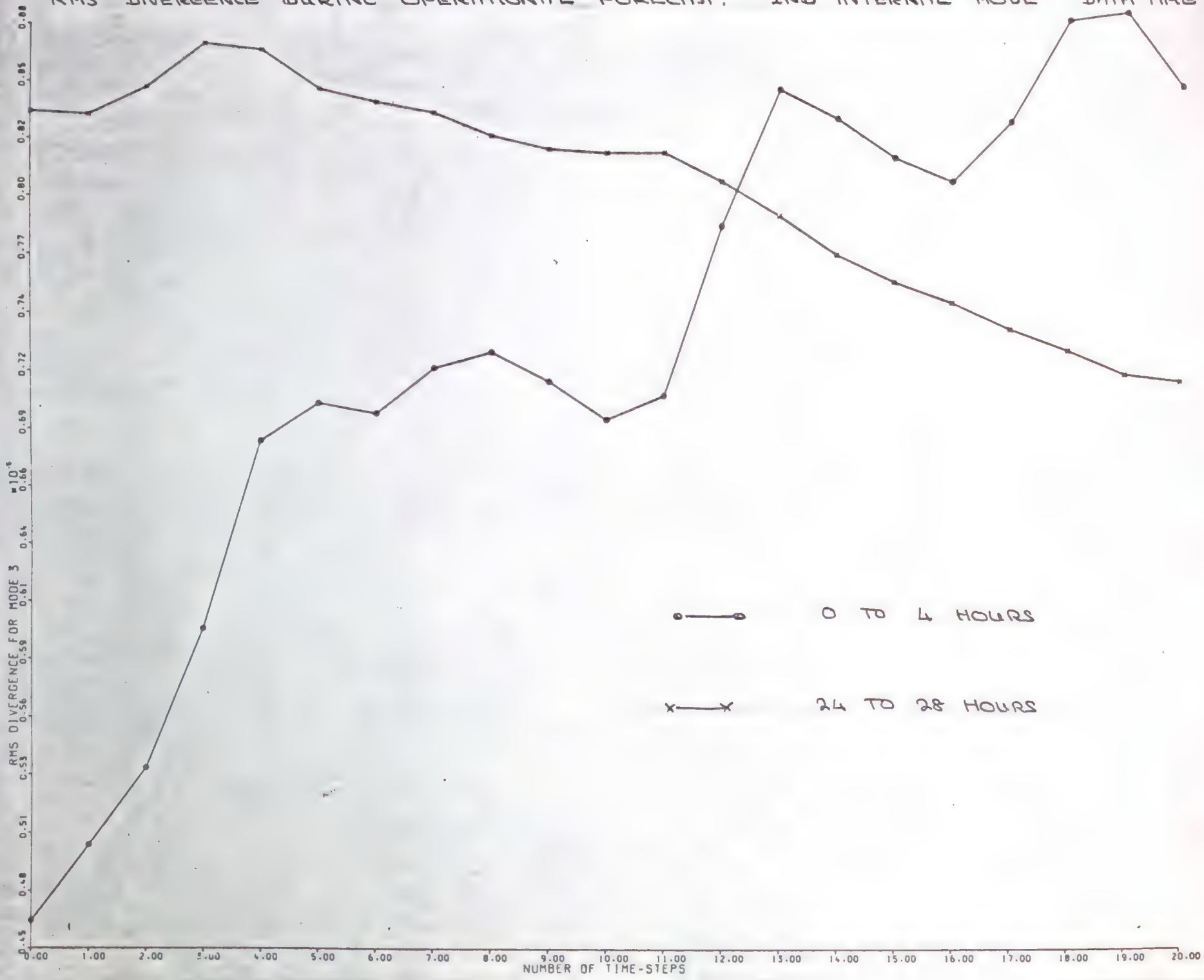

FIGURE 18a VERTICAL VELOCITY $\omega = \frac{Dp}{Dt}$ AT POINT A DURING 1ST FOUR HOURS OF FORECAST FOLLOWING 4½ HOURS DYNAMIC INITIALIZATION. DATA TIME 12Z 16/5/75

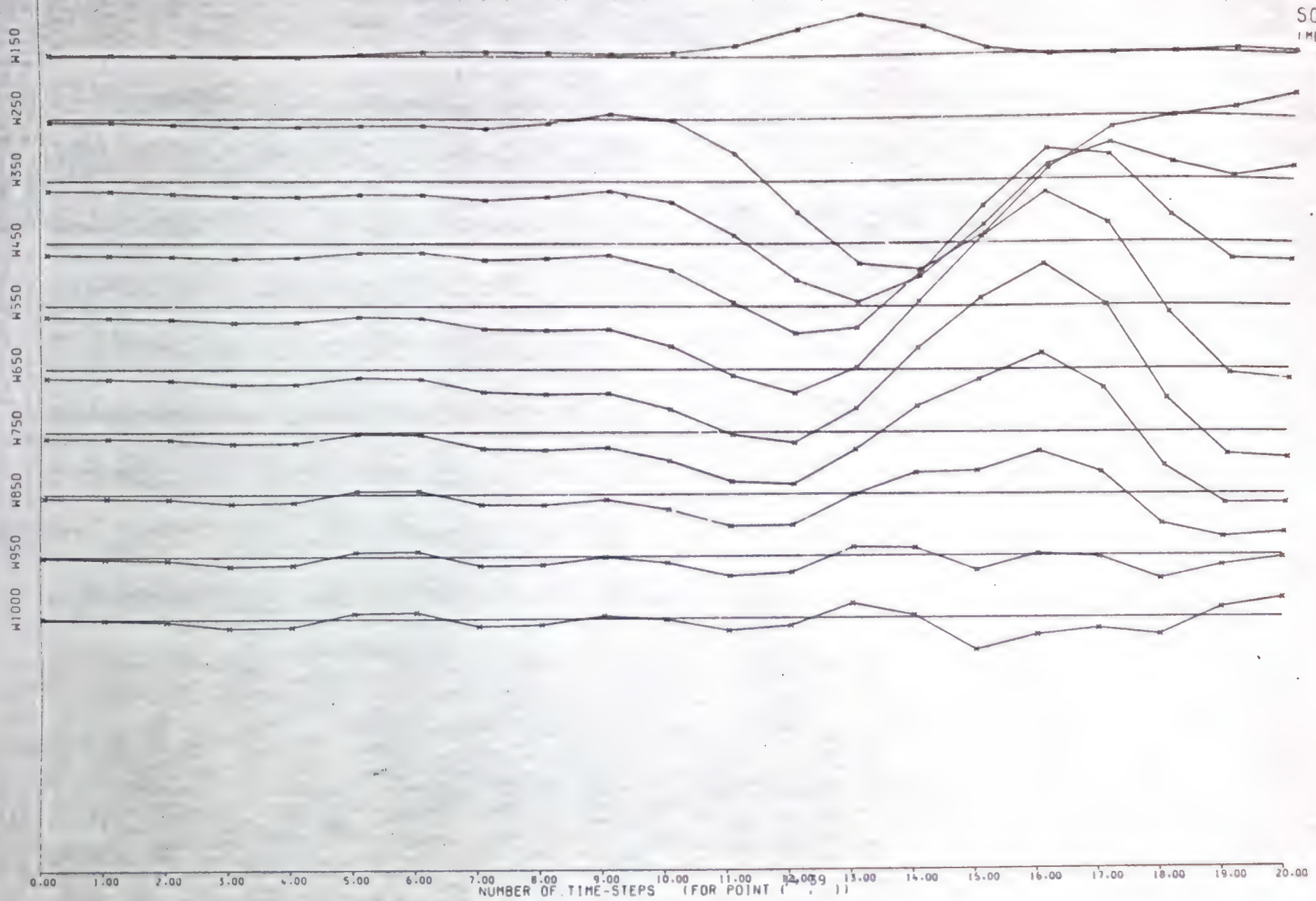

HORIZONTAL LINES REPRESENT ZERO VALUES FOR EACH LEVEL

FIGURE 18b VERTICAL VELOCITY $\omega = \frac{Dp}{Dt}$ AT POINT A DURING 1ST FOUR HOURS OF

OPERATIONAL FORECAST DATA TIME 12Z 16/5/75

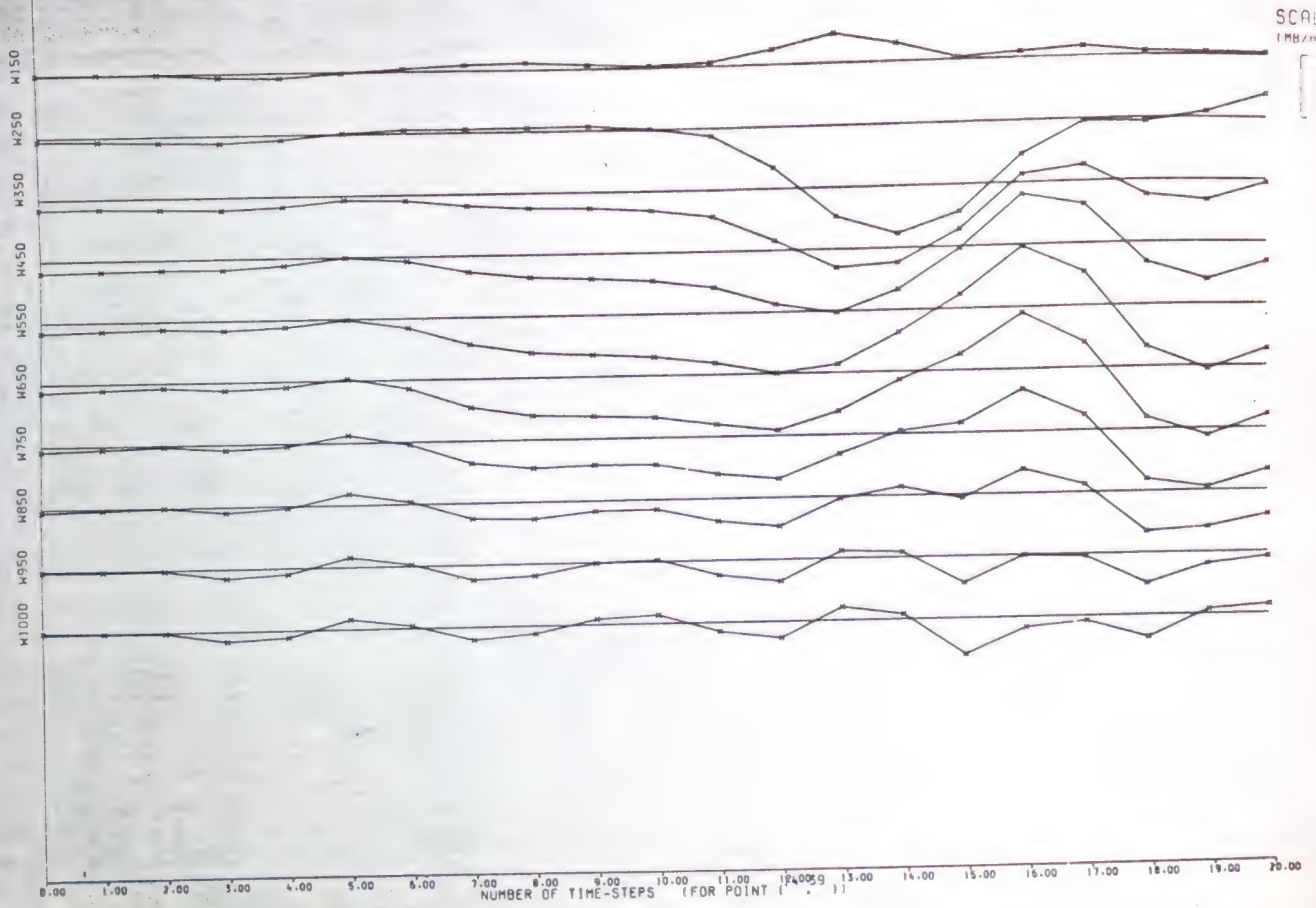

HORIZONTAL LINES REPRESENT ZERO VALUES AT EACH LEVEL

FIGURE 18c VERTICAL VELOCITY $\omega = \frac{Dp}{Dt}$ AT POINT B DURING 1ST FOUR HOURS OF . . . .

FORECAST FOLLOWING 4½ HOURS OF DYNAMIC INITIALIZATION. DATA TIME 12Z 16/5/75

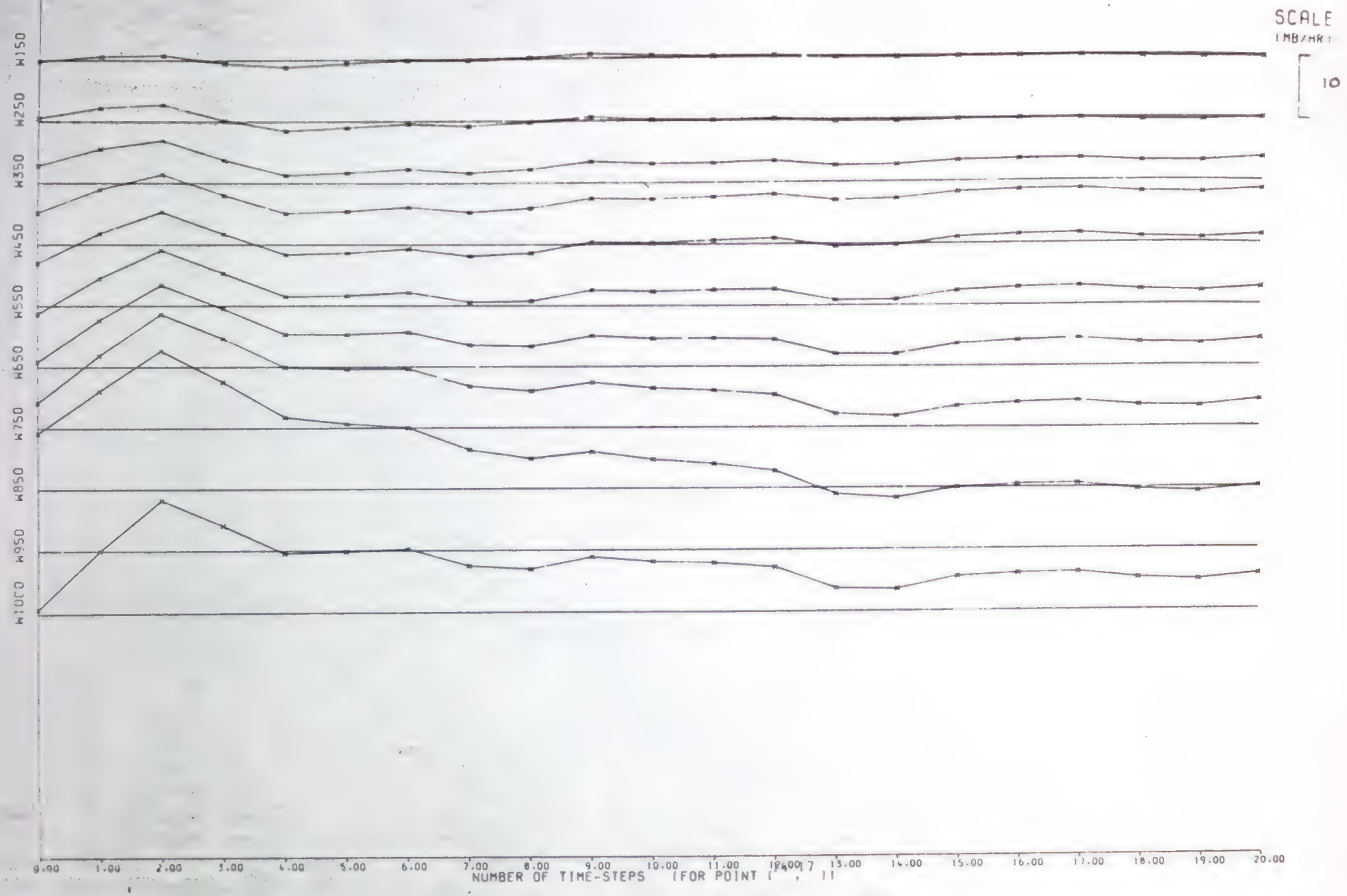

HORIZONTAL LINES REPRESENT ZERO VALUES AT EACH LEVEL.

FIGURE 18d VERTICAL VELOCITY $\omega = \frac{Dp}{Dt}$ AT POINT (3) DURING 1ST FOUR HOURS OF OPERATIONAL FORECAST, DATA TIME 12Z 16/5/75

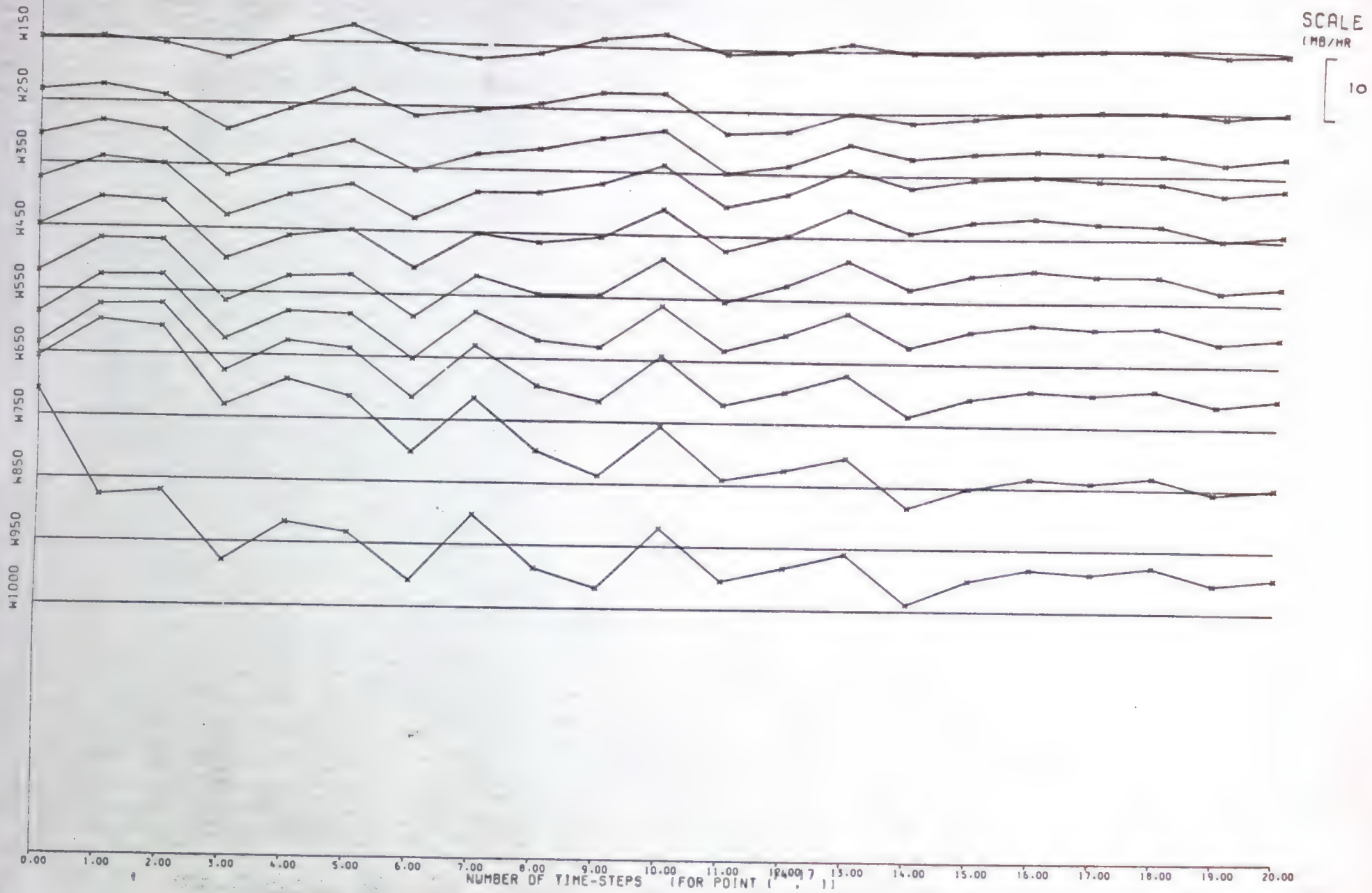

HORIZONTAL LINES REPRESENT ZERO VALUES AT EACH LEVEL

FIGURE 19a. HEIGHTS AT ALL LEVELS FOR POINT C DURING 1ST 6 HOURS OF FORECAST FOLLOWING 4½ HOURS OF DYNAMIC INITIALIZATION. (RELATIVE TO INITIAL VALUES) DATA TIME 12Z 16/5/75

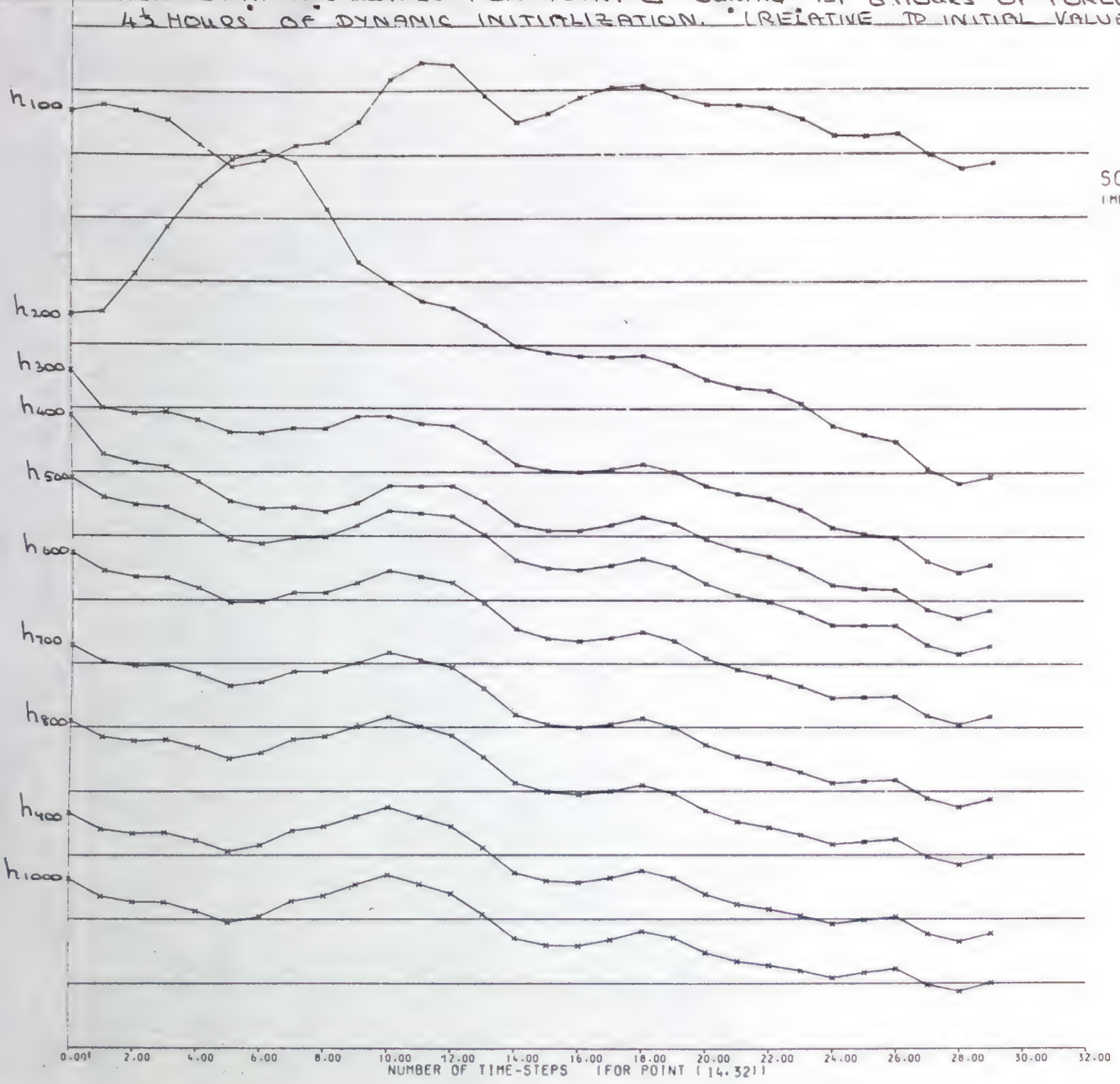

SCALE (METRES) 10

ALL CURVES ARE ON THE SAME SCALE BUT WITH THE ORDINATES DISPLACED

FIGURE 196. HEIGHTS AT ALL LEVELS FOR POINT C DURING 1ST 6 HOURS OF OPERATIONAL FORECAST (RELATIVE TO INITIAL VALUES) DATA TIME 12Z 16/5/75

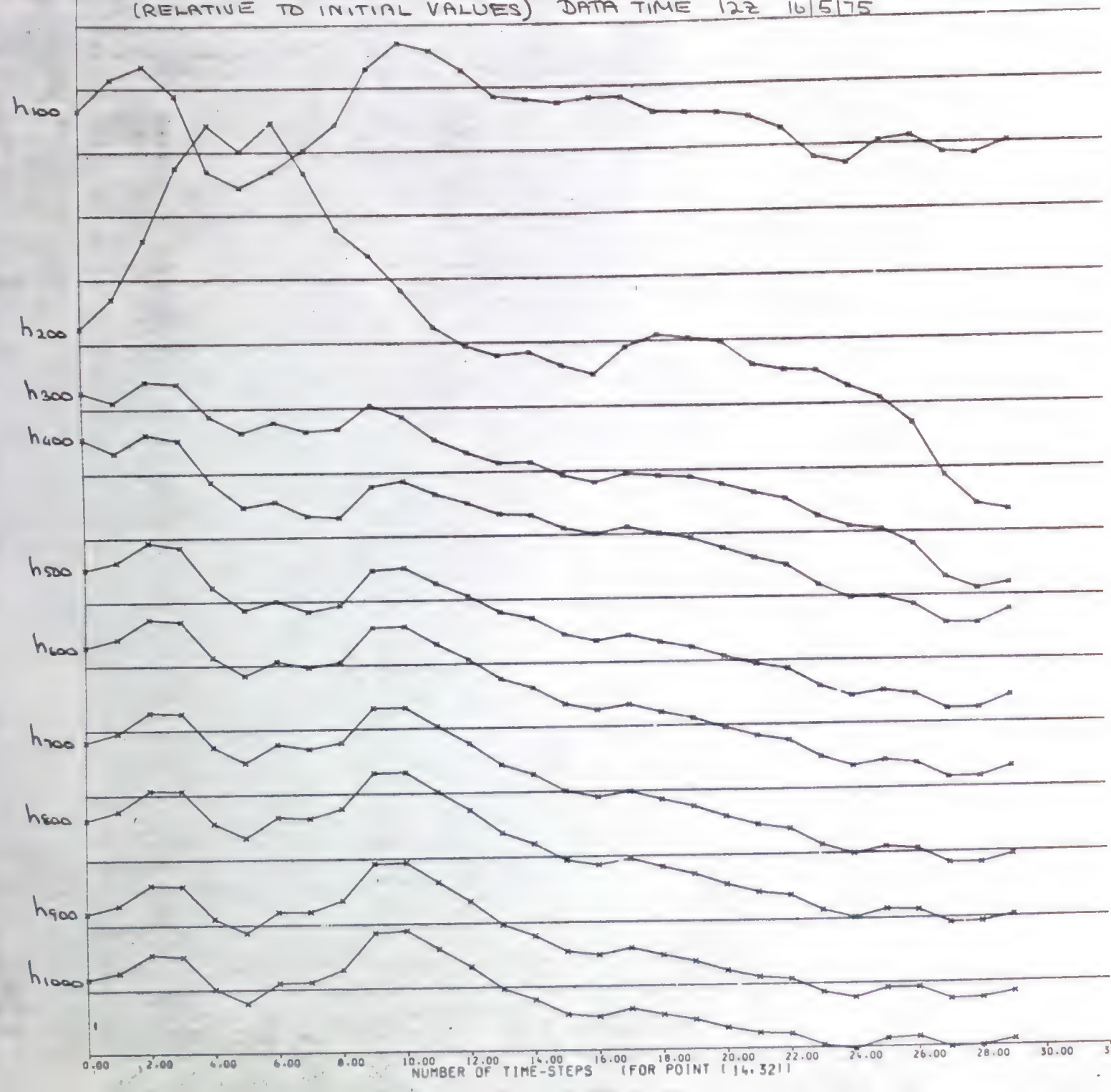

SCALE (METRES)

10

ALL CURVES ARE ON THE SAME SCALE BUT WITH THE ORDINATES DISPLACED.

FIGURE 20a. HEIGHTS AT 5 LEVELS, RELATIVE TO THEIR INITIAL VALUES DURING THE 1ST 6 HOURS OF FORECASTS. AT POINT D DATA TIME 12Z 16/5/75

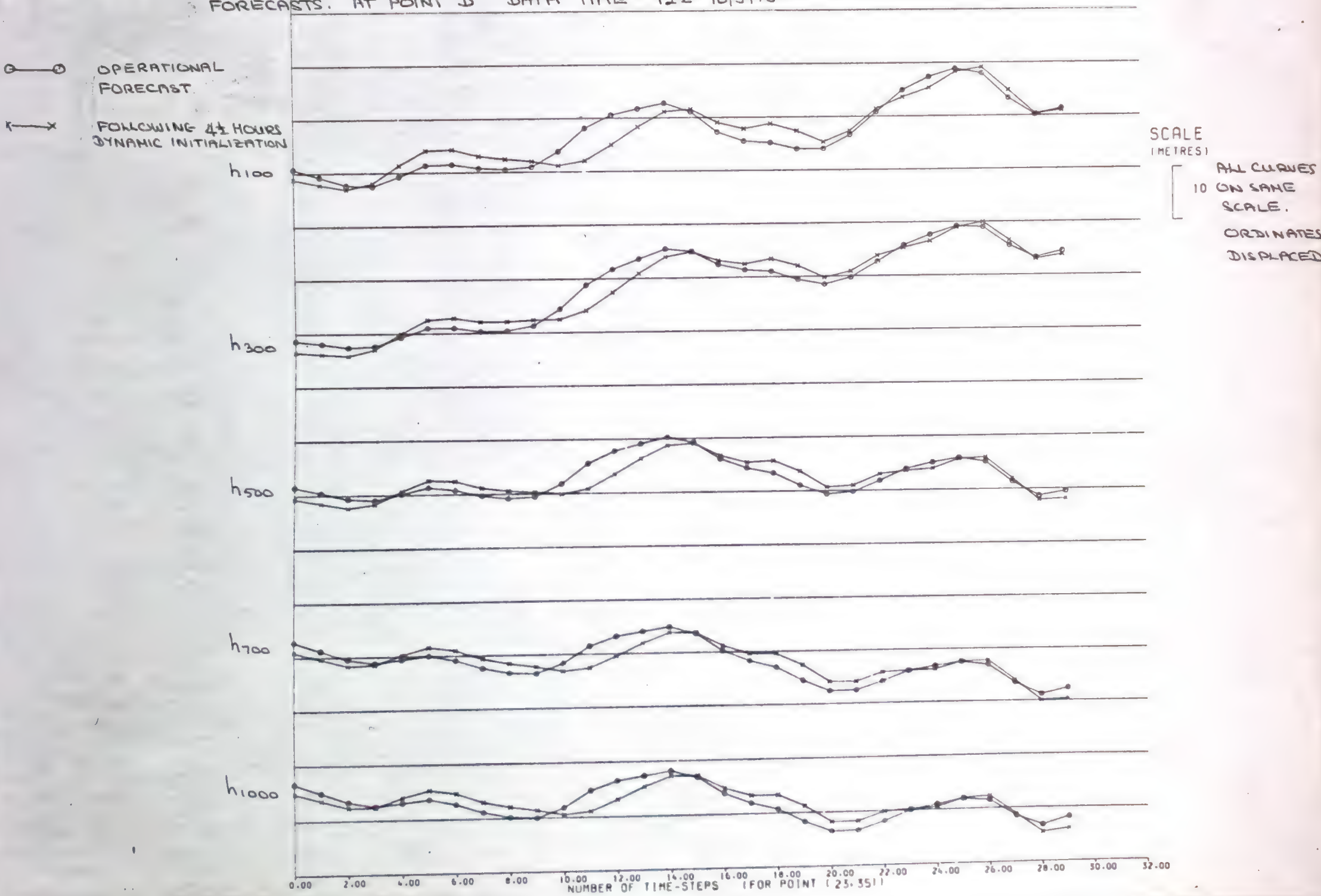

FIGURE 206. HEIGHTS AT 5 LEVELS, RELATIVE TO THEIR INITIAL VALUES, DURING 1ST 6 HOURS OF FORECASTS.
AT POINT E DATA TIME 12Z 16/5/75

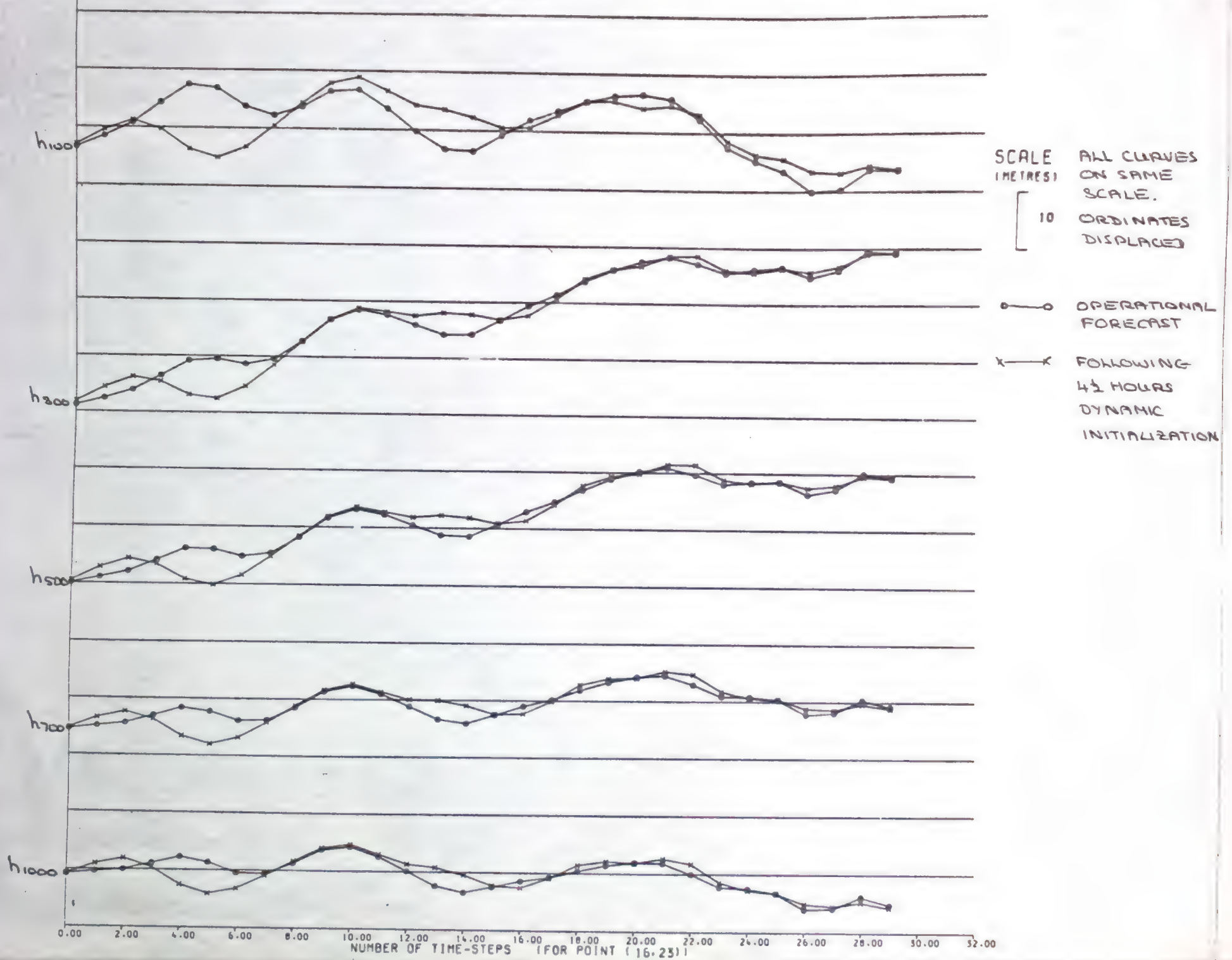

FIGURE 21. HEIGHTS AT ALL LEVELS, RELATIVE TO THEIR INITIAL VALUES, AT POINT C, DURING 1ST 6 HOURS OF FORECAST WITH PHYSICAL PROCESSES REMOVED, FOLLOWING 4½ HOURS OF DYNAMIC INITIALIZATION. DATA TIME 12Z 14/5/75

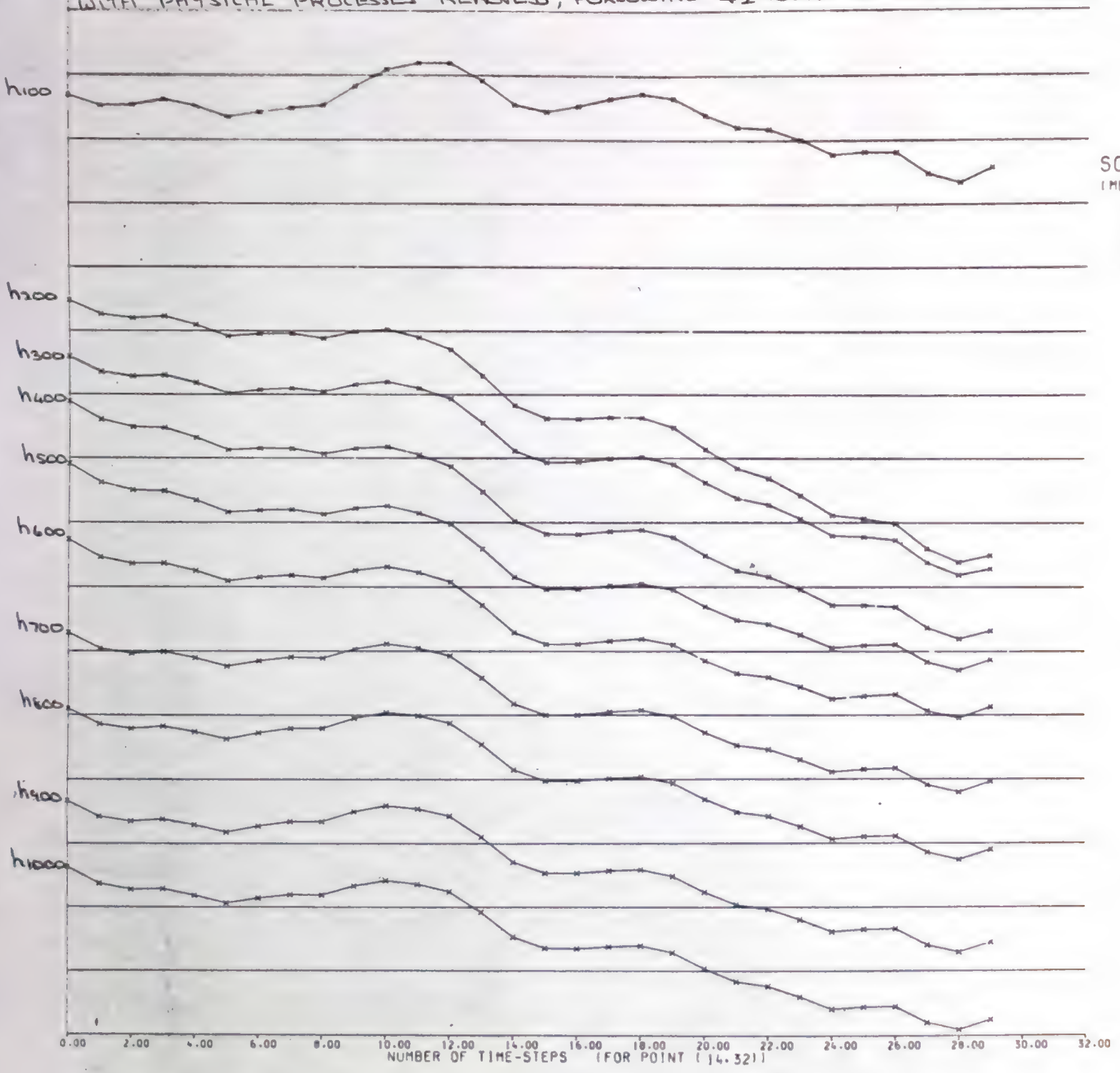

FIGURE 22. HEIGHTS AT ALL LEVELS, RELATIVE TO THEIR INITIAL VALUES, AT POINT C, DURING 1ST 6 HOURS OF FORECAST WITH PHYSICAL PROCESSES REMOVED AND NO BOUNDARY UPDATING, FOLLOWING 4½ HOURS OF DYNAMIC INITIALIZATION. DATA TIME 12Z 16/5/75.

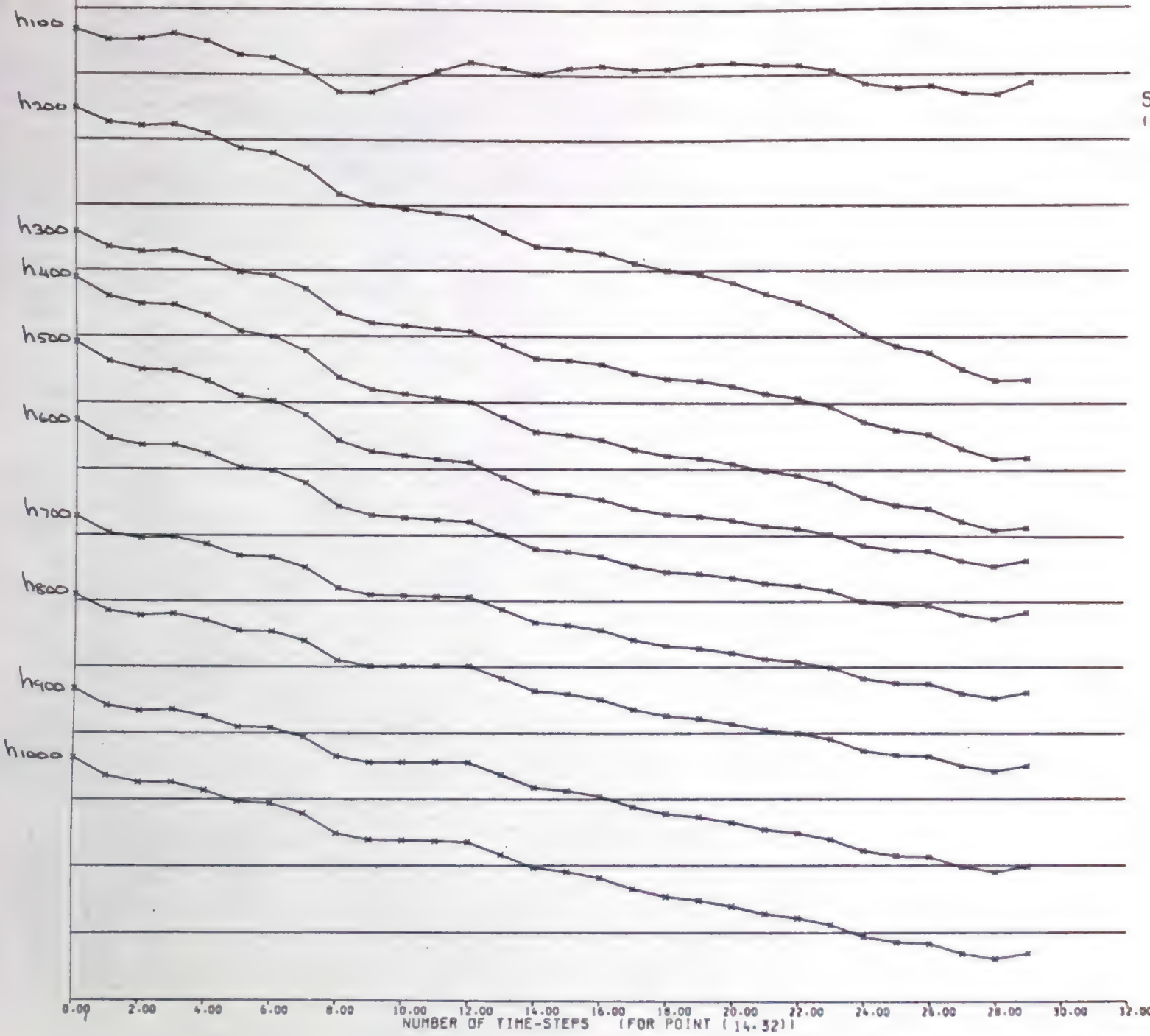

SCALE (METRES)

10

ALL CURVES ARE ON SAME SCALE BUT WITH ORDINATES DISPLACED

FIGURE 23a. HEIGHTS AT 5 LEVELS, RELATIVE TO THEIR INITIAL VALUES, DURING 1ST 6 HOURS OF FORECASTS AT POINT C.
DATA TIME 12Z 16/5/75.

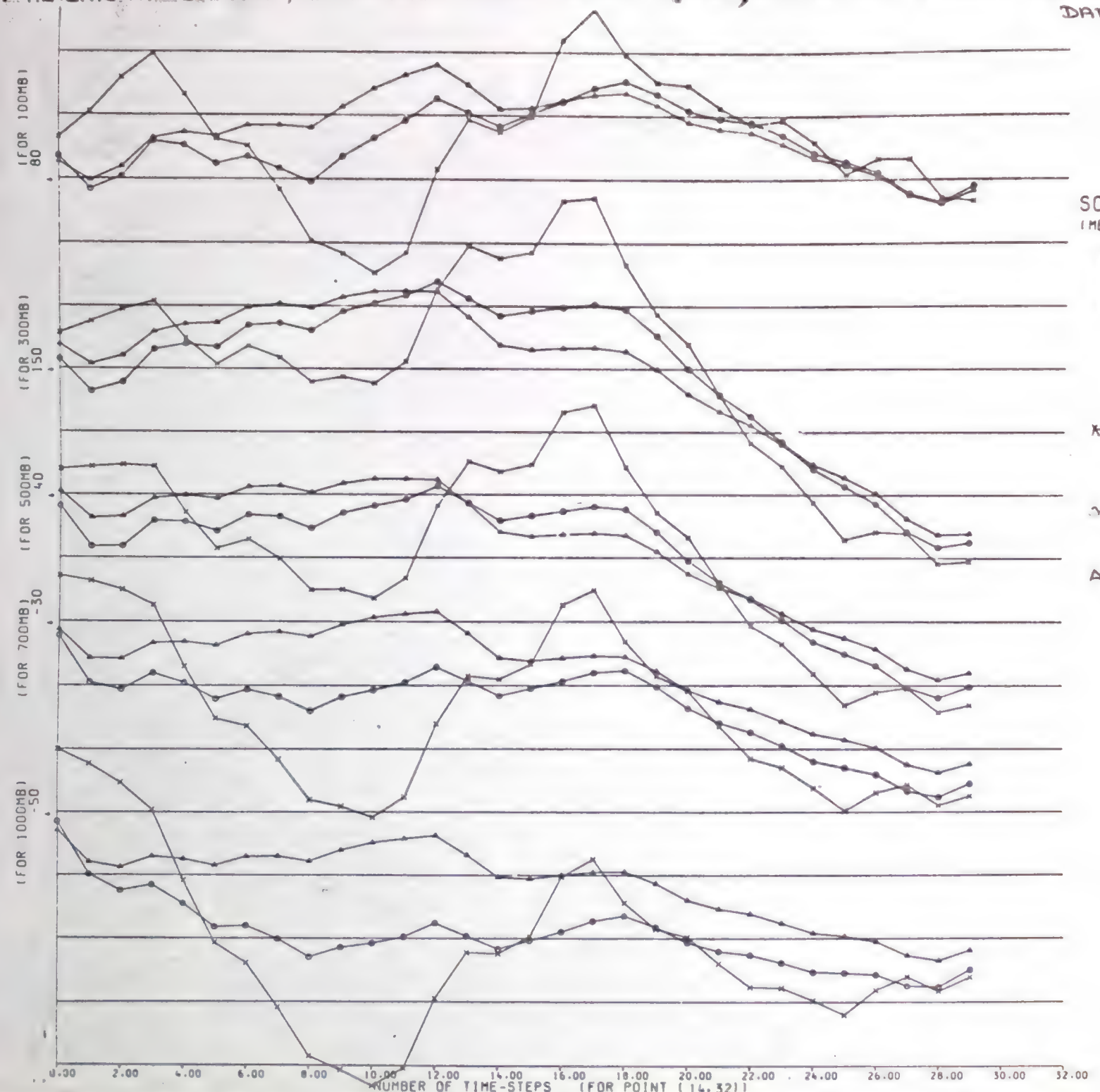

SCALE (METRES) 10

ALL CURVES ON SAME SCALE BUT ORDINATES DISPLACED. VALUE OF ORDINATE FOR EACH LEVEL IS DIFFERENCE FROM ICAO STANDARD ATMOSPHERE HEIGHT.

(1) ANALYSED HEIGHTS GEOSTROPHIC WINDS NO INITIALIZATION

(2) AS (1) WITH 7½ HOURS INITIALIZATION

(3) AS (1) WITH 31½ HOURS INITIALIZATION

FIGURE 236. HEIGHTS AT 5 LEVELS RELATIVE TO THEIR INITIAL VALUES, DURING 1ST 6HOURS OF FORECASTS AT POINT E.
DATA TIME 12Z 16/5/75

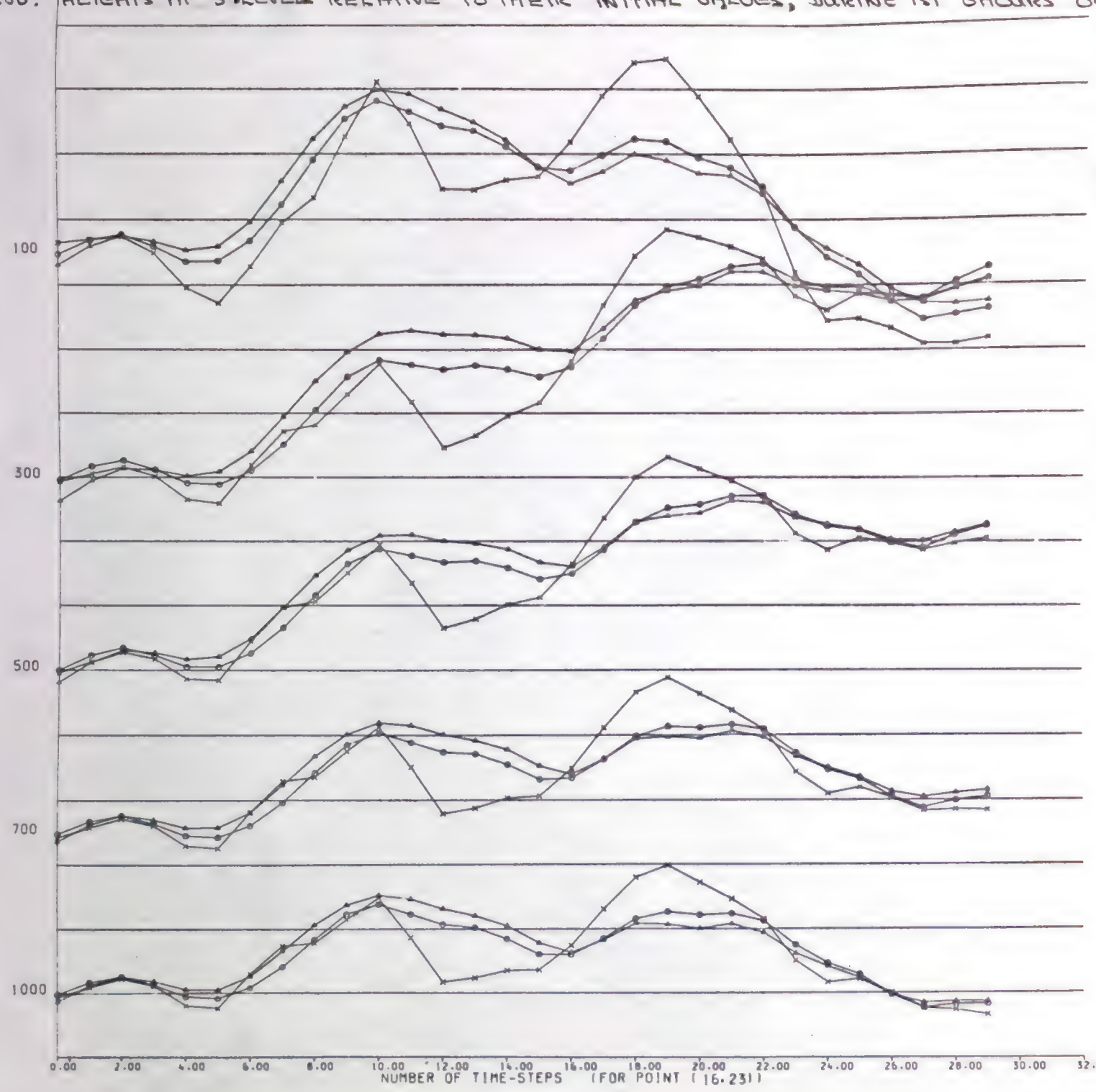

SCALE (METRES) 10

ALL CURVES ON SAME SCALE BUT ORDINATES DISPLACED

(1) ANALYSED HEIGHTS GEOSTROPHIC WINDS NO INITIALIZATION

(2) AS (1) WITH 7½ HOURS INITIALIZATION

(3) AS (1) WITH 31½ HOURS INITIALIZATION.

FIGURE 24. 1000MB HEIGHT DURING FIRST 6 HOURS OF FORECASTS FROM DIFFERENT INITIALIZATIONS DATA TIME 00Z 18/11/76

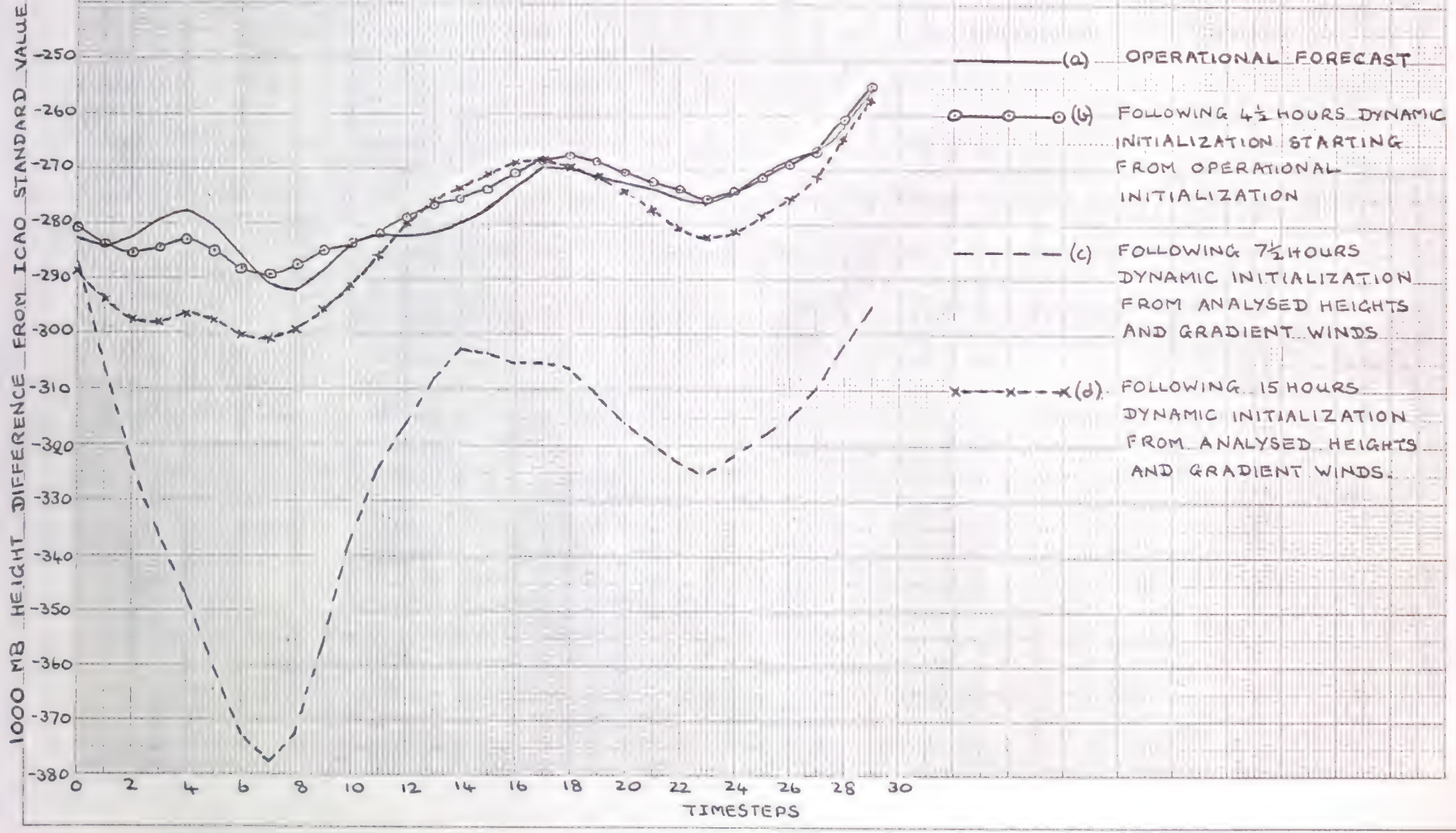

FIGURE 25a OPERATIONAL INITIALIZATION (a)

SURFACE PRESSURE

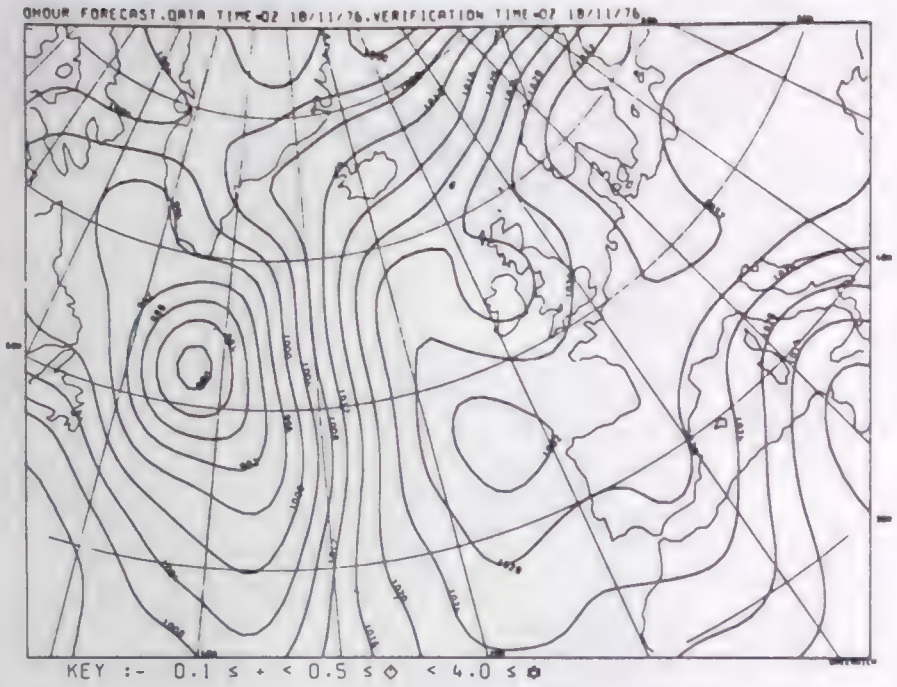

300 MB CONTOURS ISOPLETH INTERVAL=12 DECAMETERS

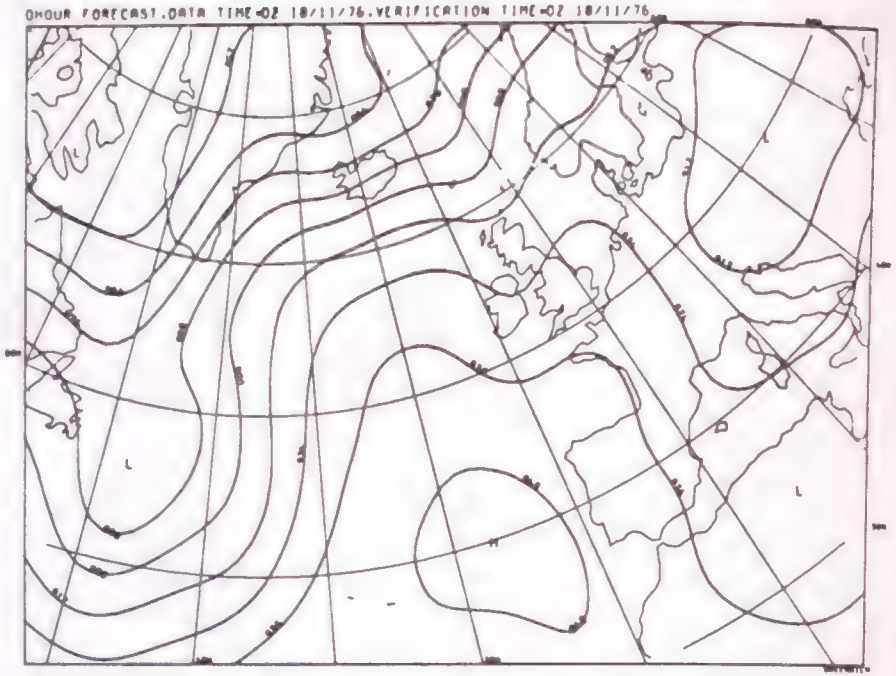

300 MB ISOTACHS ISOTACH INTERVAL=5 M/S

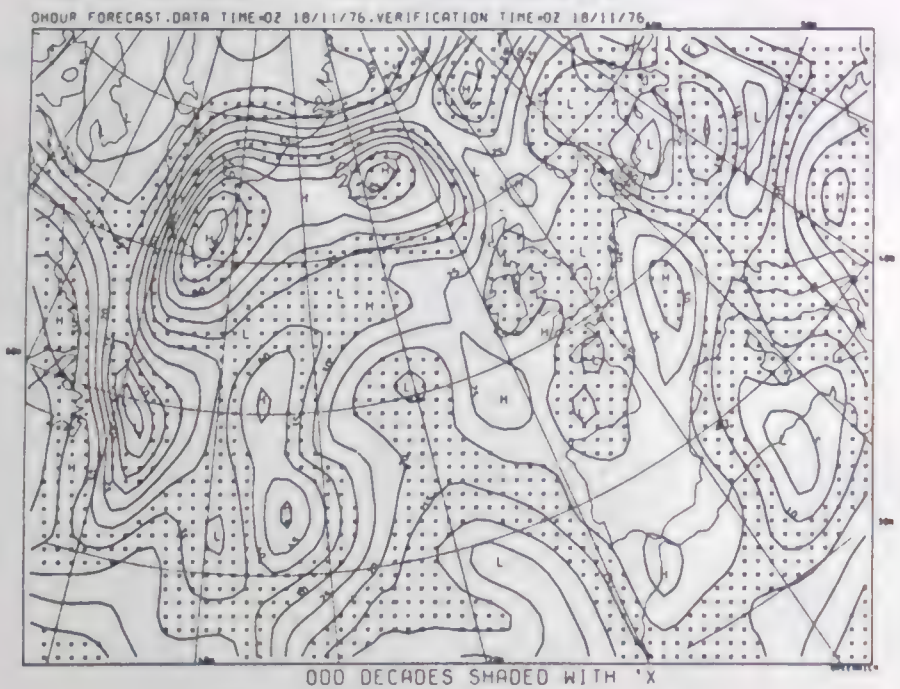

FIGURE 25 b 15 HOURS OF DYNAMIC INITIALIZATION FROM ANALYSED HEIGHTS AND GRADIENT WINDS (d)

SURFACE PRESSURE

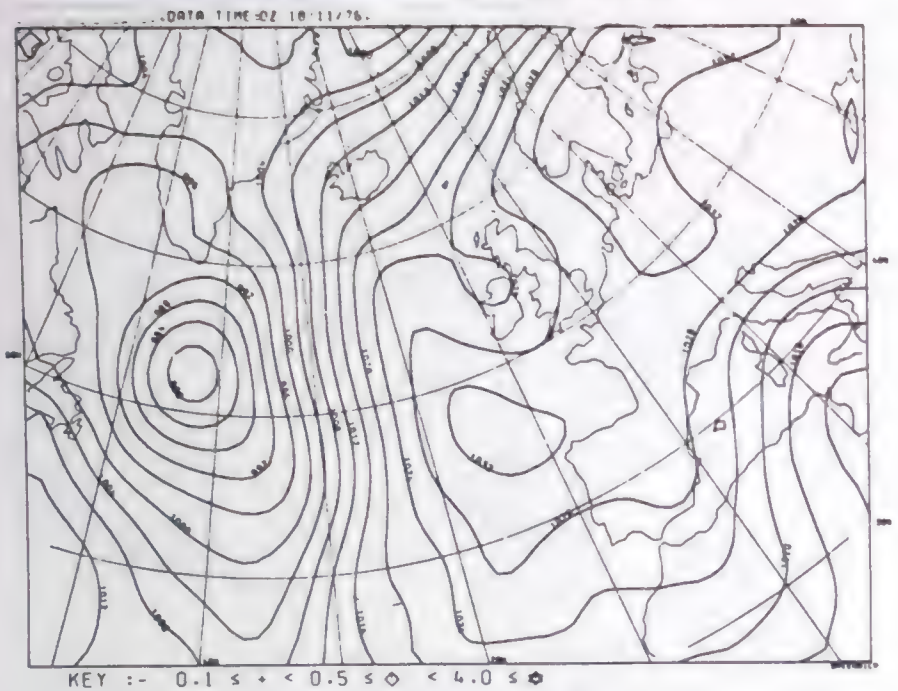

KEY :- 0.1 ≤ + < 0.5 ≤ ◇ < 4.0 ≤ ✪

300 MB CONTOURS ISOPLETH INTERVAL=12 DECAMETERS

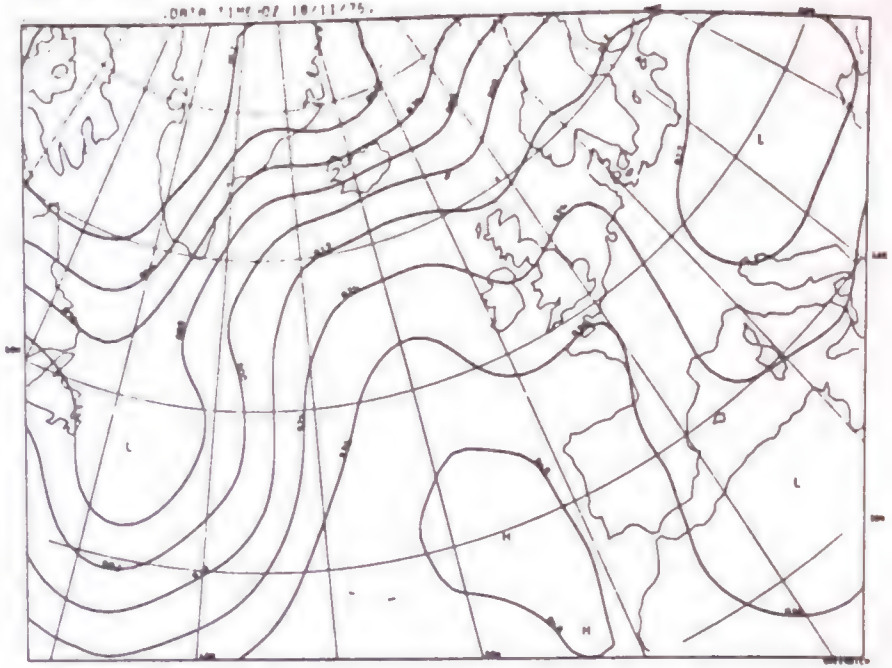

300 MB ISOTACHS ISOTACH INTERVAL=5 M/S

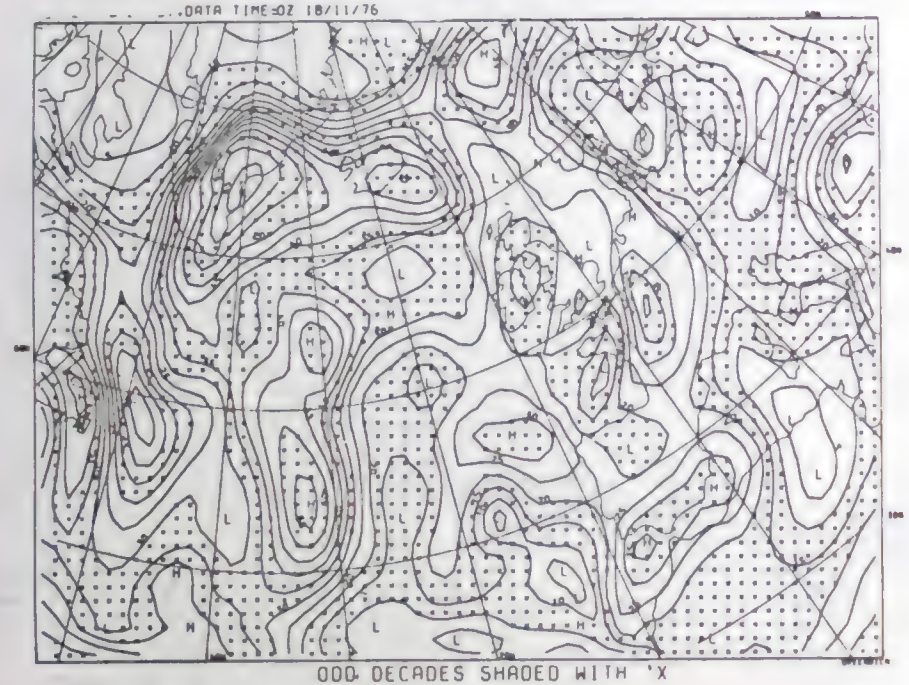

000 DECADES SHADED WITH 'X

FIGURE 26a ..... OPERATIONAL FORECAST (a)

TOTAL RATE OF RAIN (MM/HR) AND SURFACE PRESSURE

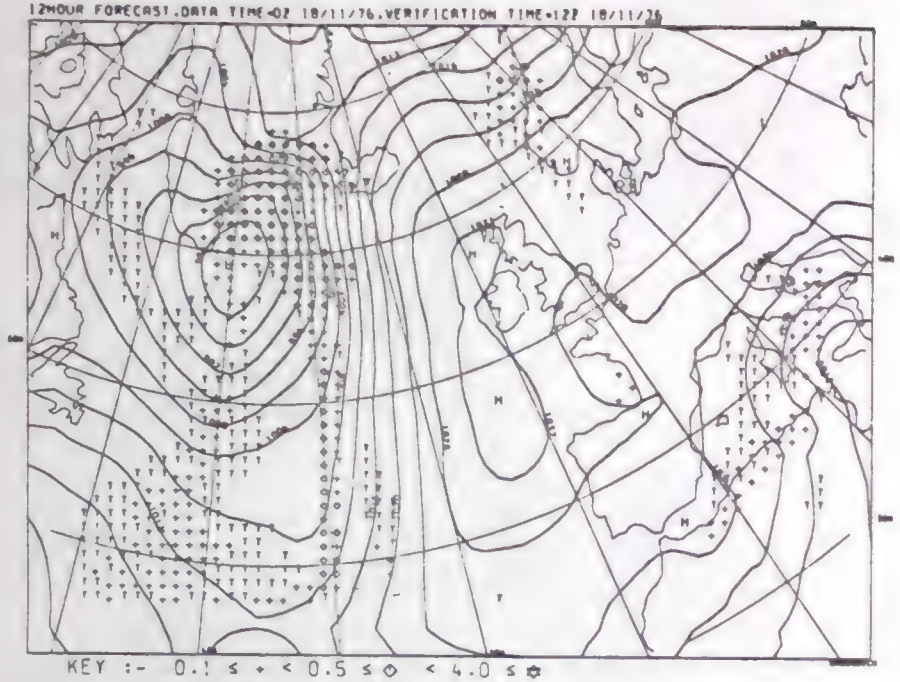

300 MB CONTOURS !SOPLETH INTERVAL=12 DECAMETERS

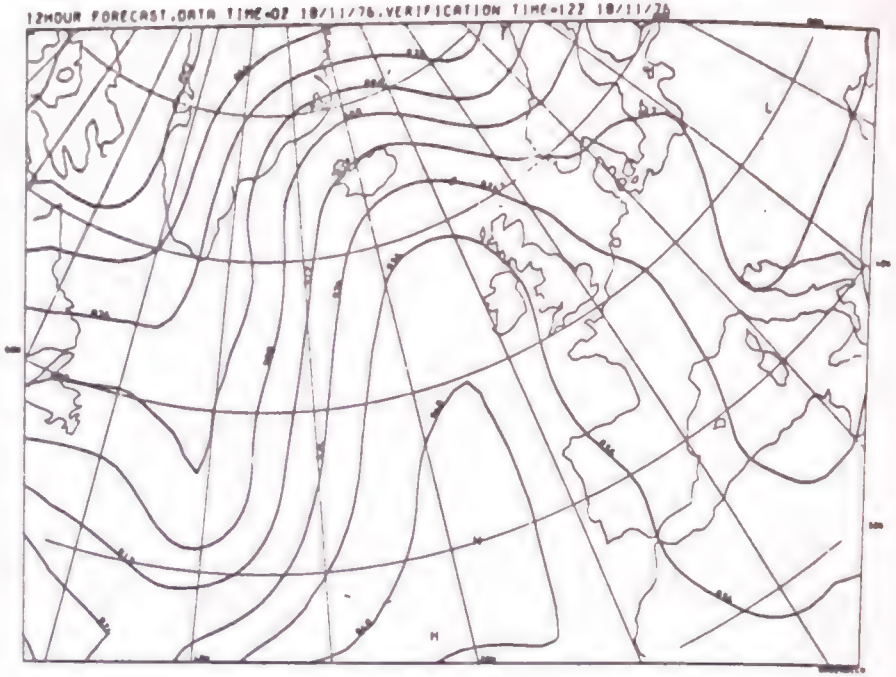

300 MB !SOTACHS !SOTACH INTERVAL=5 M/S

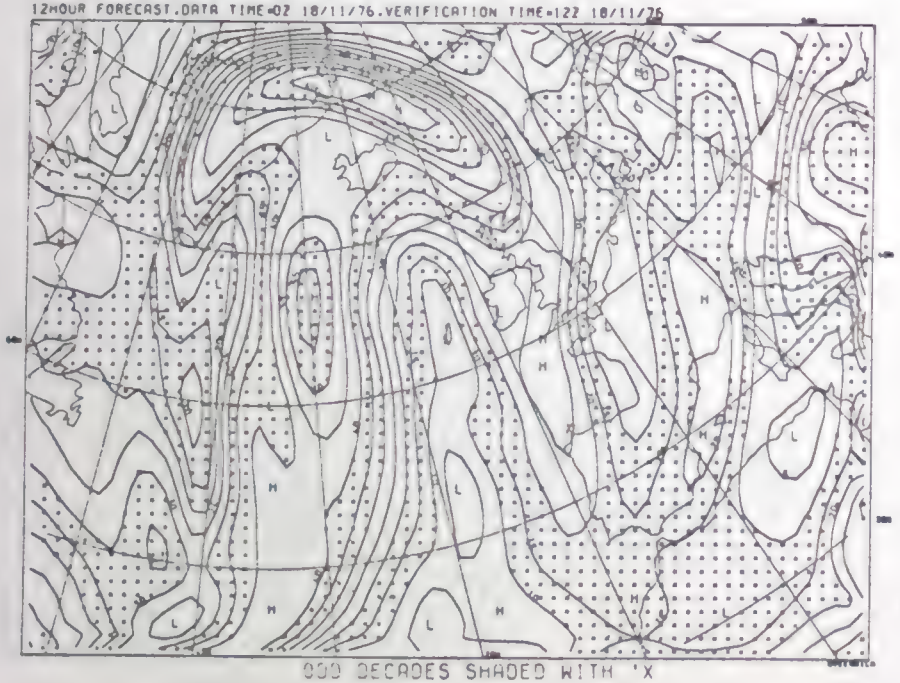

12 HR ACCUMULATED RAIN (MM) IN PERIOD T+0 TO T+12

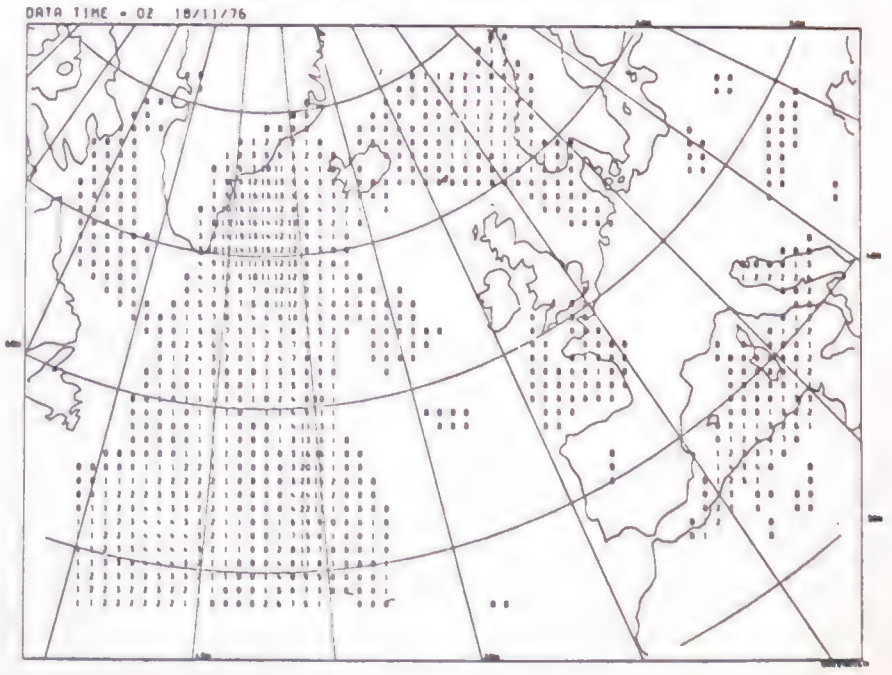

FIGURE 26G 12-HOUR FORECAST FROM 15 HOURS OF DYNAMIC INITIALIZATION FROM ANALYSED HEIGHTS AND GRADIENT WINDS (d)

TOTAL RATE OF RAIN (MM/HR) AND SURFACE PRESSURE

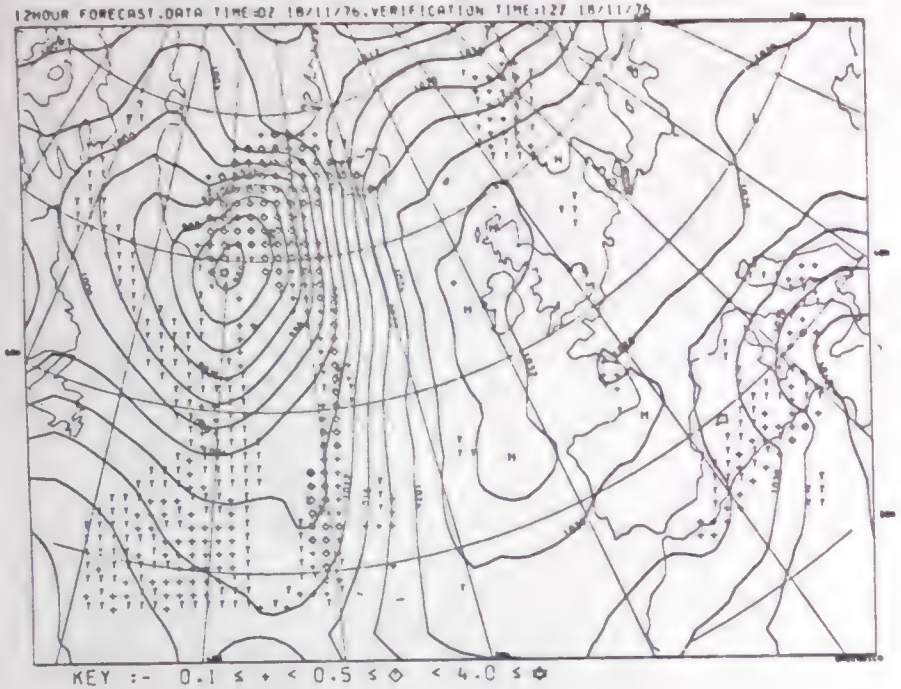

KEY :- 0.1 ≤ + < 0.5 ≤ ◇ < 4.0 ≤ ✿

500 MB CONTOURS ISOPLETH INTERVAL=12 DECAMETERS

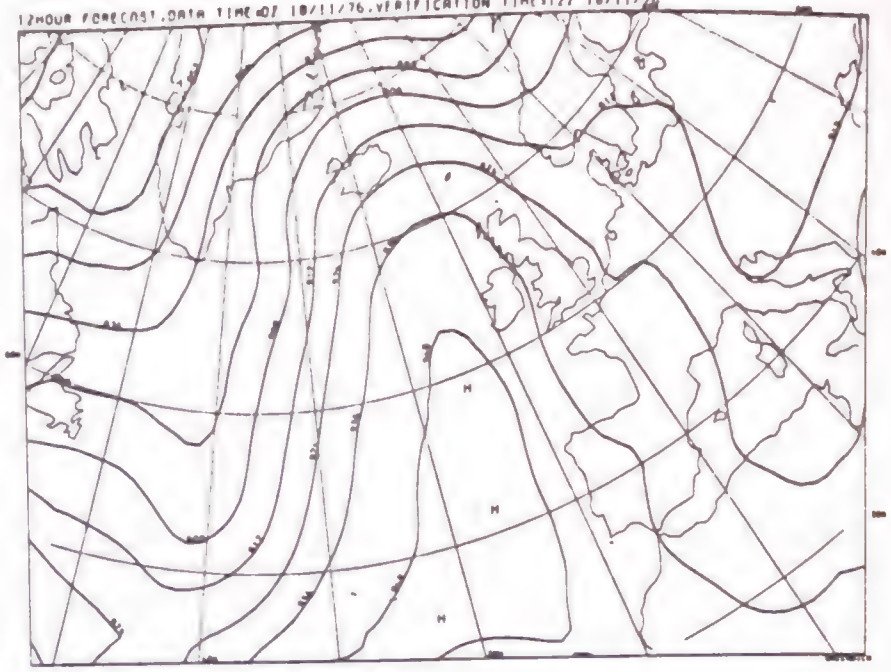

300 MB ISOTACHS ISOTACH INTERVAL=5 M/S

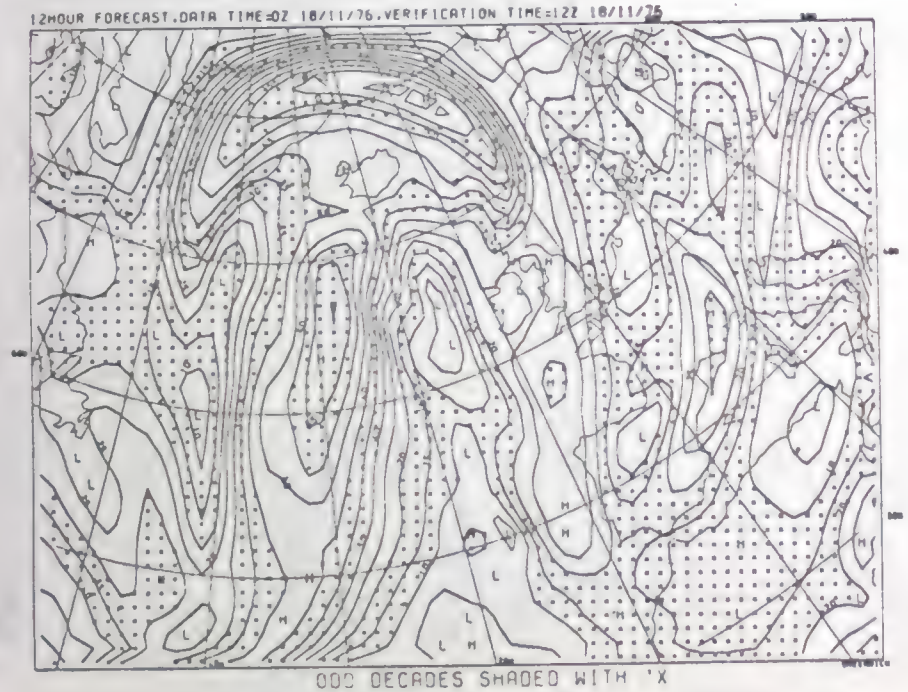

000 DECADES SHADED WITH 'X

12 HR ACCUMULATED RAIN (MM) IN PERIOD T+0 TO T+12

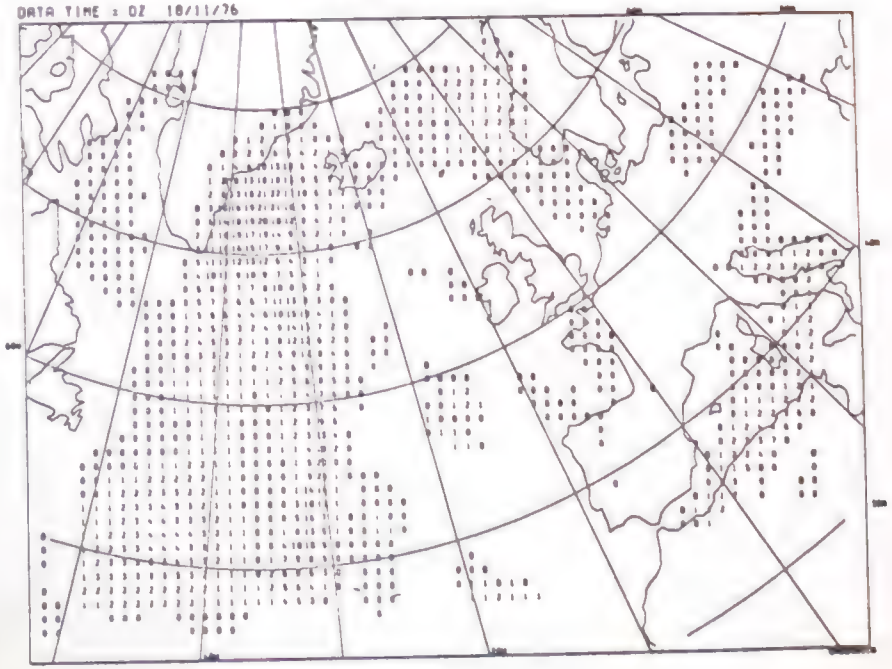

FIGURE 27a OPERATIONAL FORECAST (a)

TOTAL RATE OF RAIN (MM/HR) AND SURFACE PRESSURE

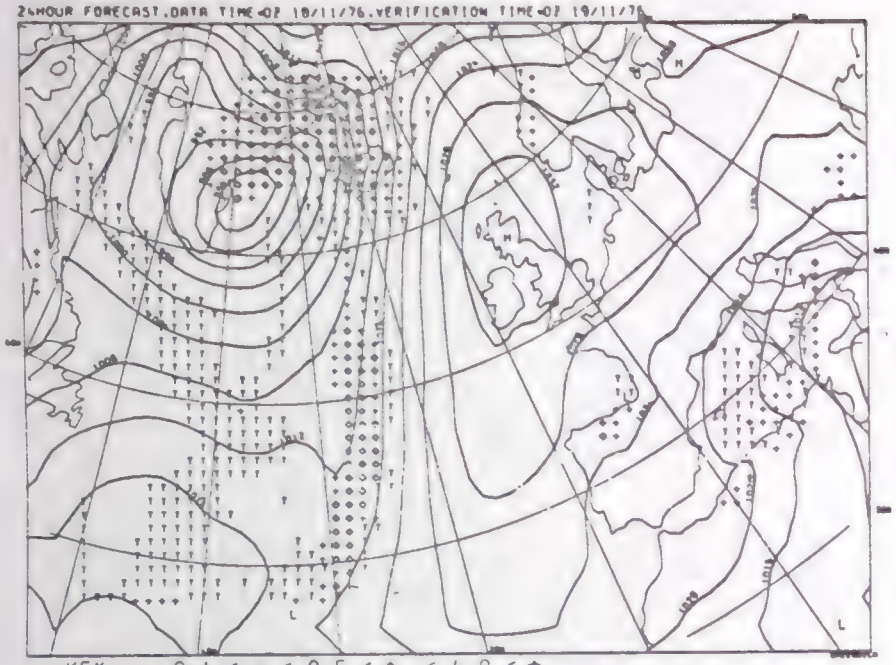

KEY :- 0.1 ≤ + < 0.5 ≤ ◇ < 4.0 ≤ ✪

300 MB CONTOURS ISOPLETH INTERVAL=12 DECAMETERS

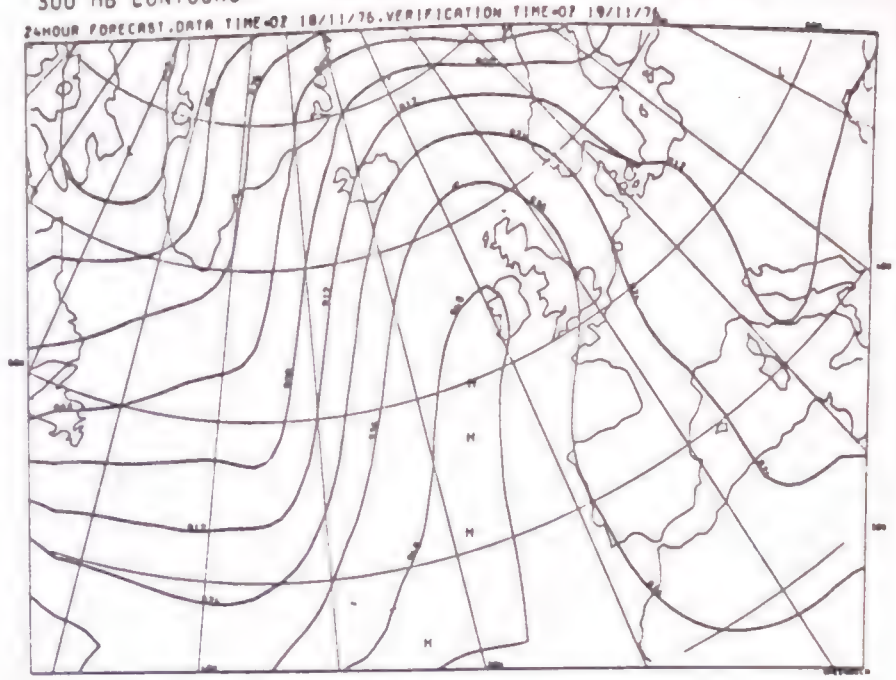

300 MB ISOTACHS ISOTACH INTERVAL=5 M/S

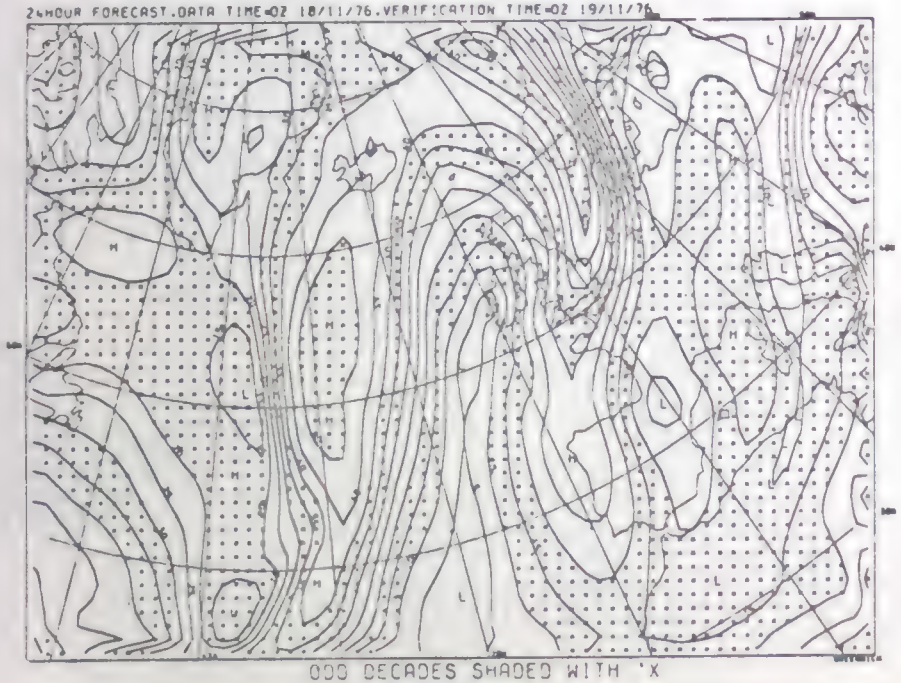

000 DECADES SHADED WITH 'X

6 HR ACCUMULATED RAIN (MM) IN PERIOD T+18 TO T+24

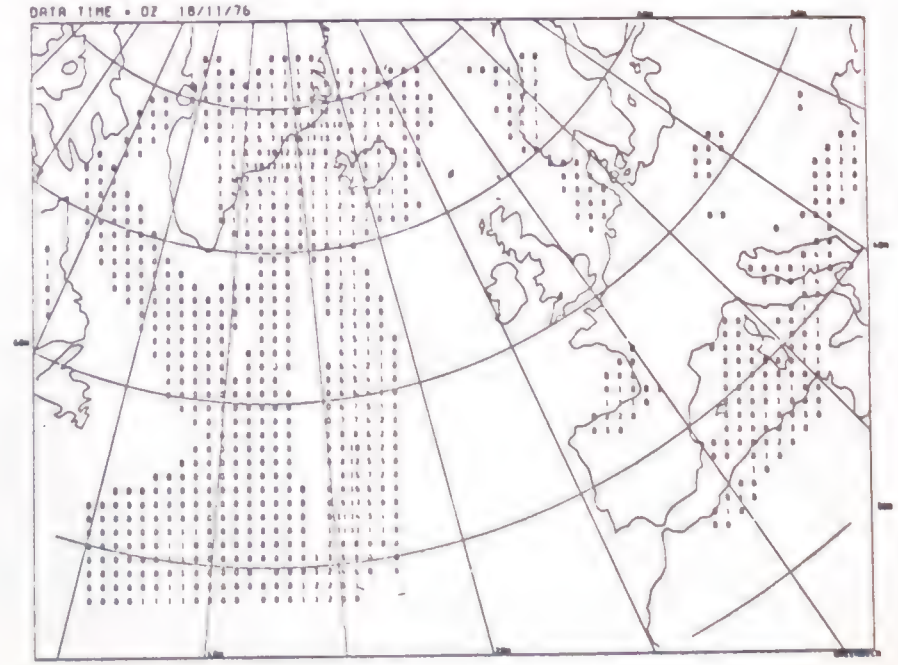

FIGURE 27(d) 24-HOUR FORECAST FROM 15 HOURS OF DYNAMIC INITIALIZATION FROM ANALYSED HEIGHTS AND GRADIENT WINDS

TOTAL RATE OF RAIN (MM/HR) AND SURFACE PRESSURE

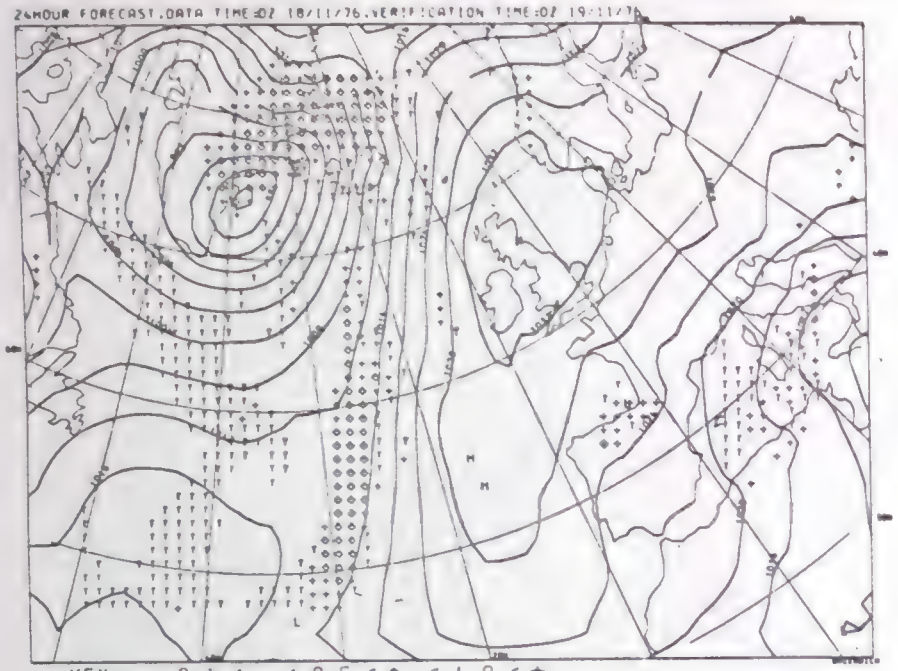

KEY :- 0.1 ≤ + < 0.5 ≤ ◇ < 4.0 ≤ ✡

300 MB CONTOURS ISOPLETH INTERVAL=12 DECAMETERS

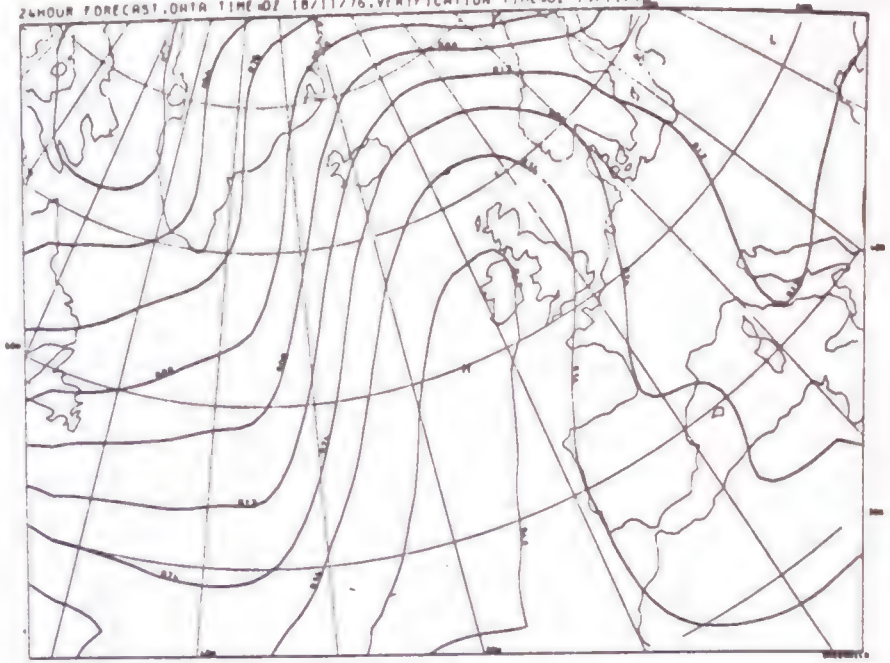

300 MB ISOTACHS ISOTACH INTERVAL=5 M/S

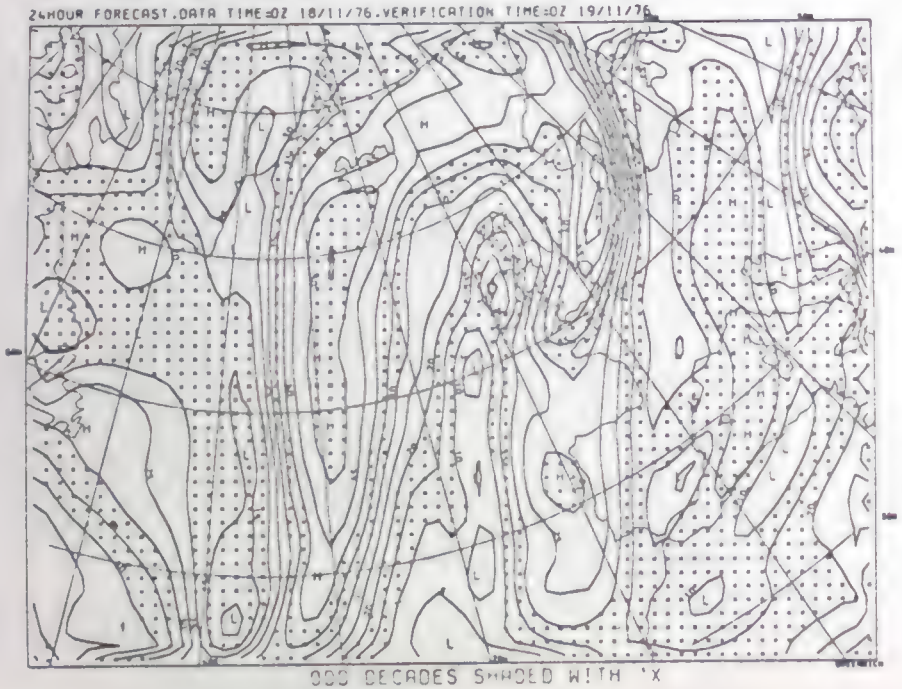

000 DECADES SHADED WITH 'X

6 HR ACCUMULATED RAIN (MM) IN PERIOD T+18 TO T+24

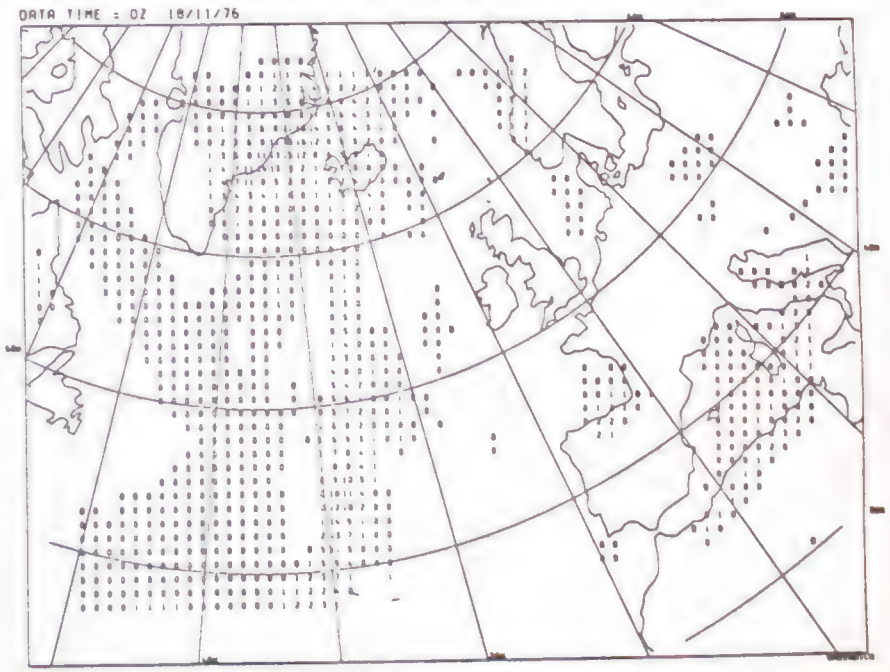

FIGURE 28

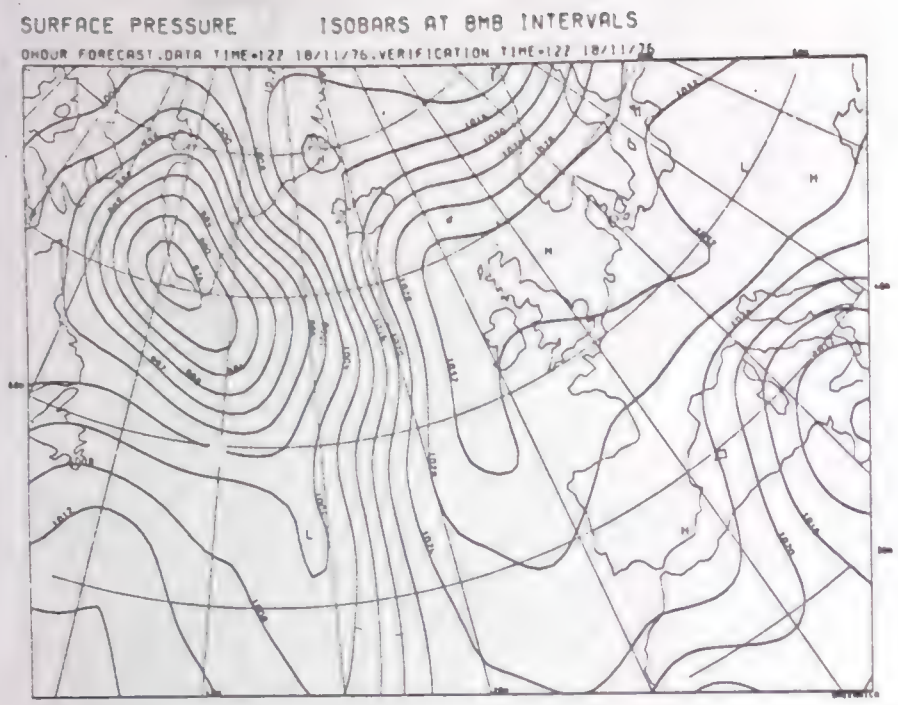
SURFACE PRESSURE ISOBARS AT 8MB INTERVALS
0HOUR FORECAST.DATA TIME=122 18/11/76.VERIFICATION TIME=122 18/11/76

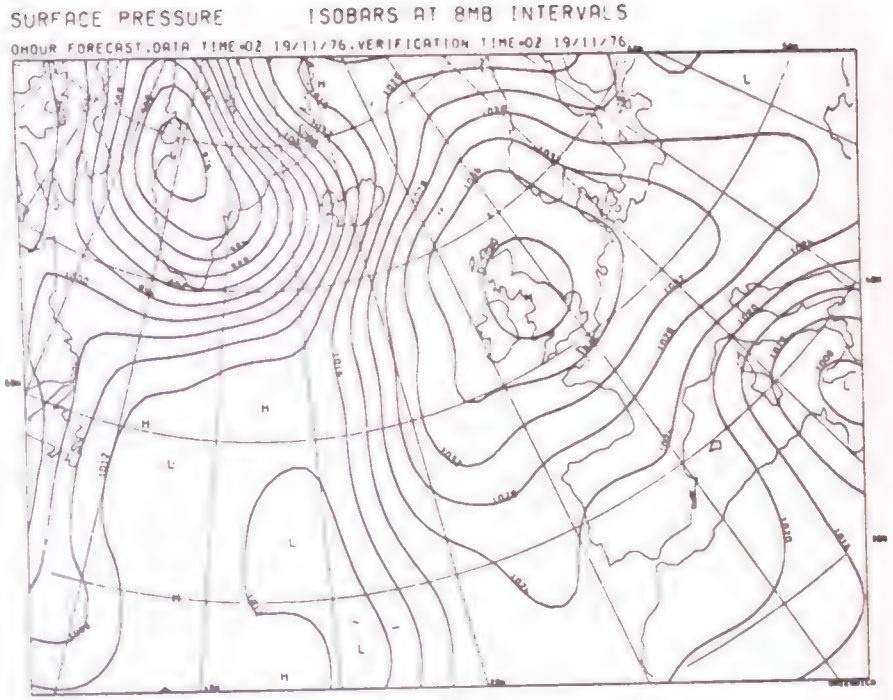
SURFACE PRESSURE ISOBARS AT 8MB INTERVALS
0HOUR FORECAST.DATA TIME=02 19/11/76.VERIFICATION TIME=02 19/11/76

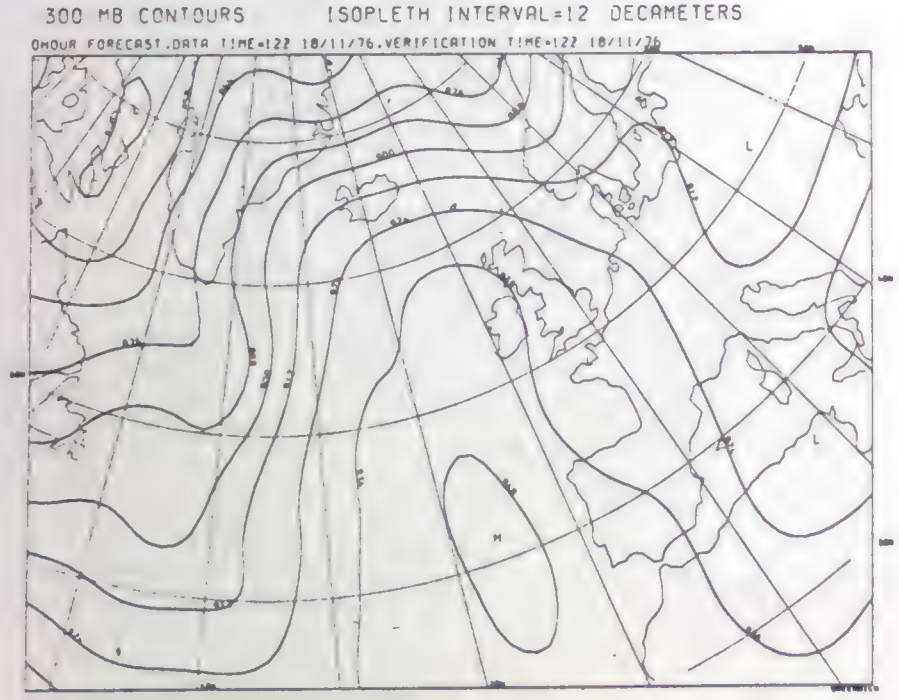
300 MB CONTOURS ISOPLETH INTERVAL=12 DECAMETERS
0HOUR FORECAST.DATA TIME=122 18/11/76.VERIFICATION TIME=122 18/11/76

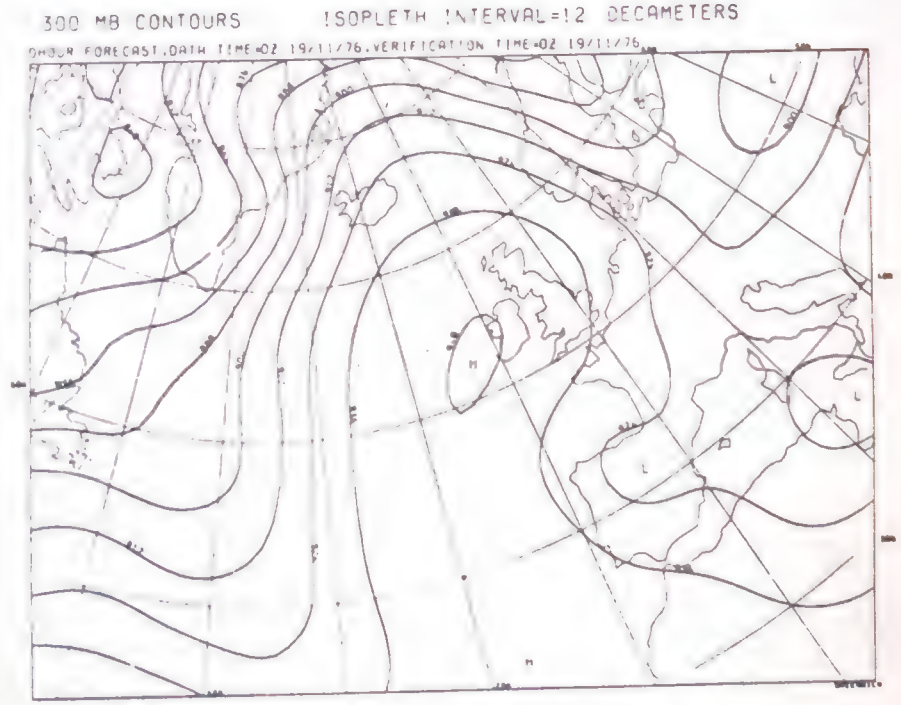
300 MB CONTOURS ISOPLETH INTERVAL=12 DECAMETERS
0HOUR FORECAST.DATA TIME=02 19/11/76.VERIFICATION TIME=02 19/11/76

FIGURE 29 .. SURFACE PRESSURE AT A POINT IN THE ATLANTIC DURING FORECASTS FOLLOWING A WIND DATA ASSIMILATION.

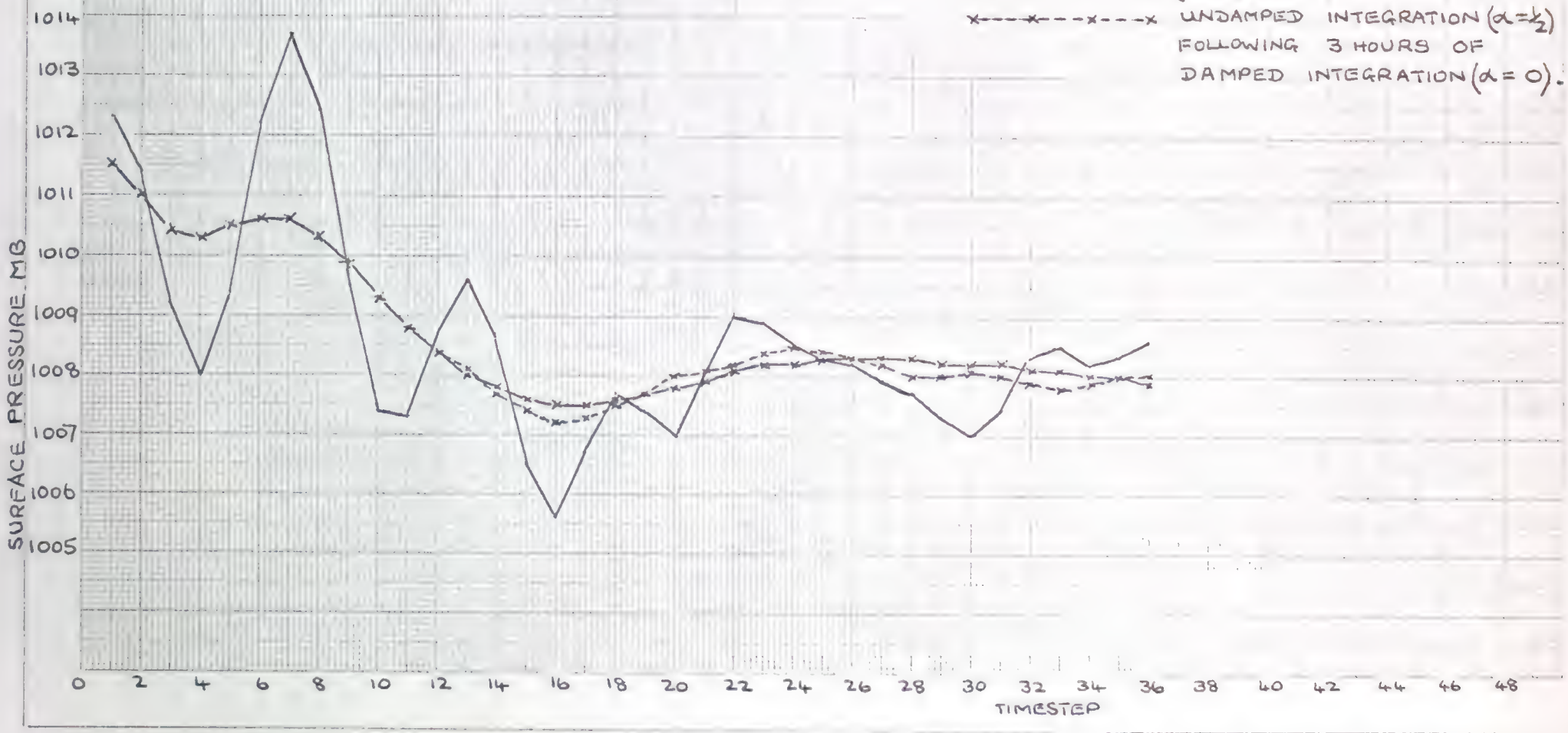

FIGURE 30. SURFACE PRESSURE AT A POINT IN THE ATLANTIC DURING FORECASTS WITH AND WITHOUT DYNAMIC INITIALIZATION.

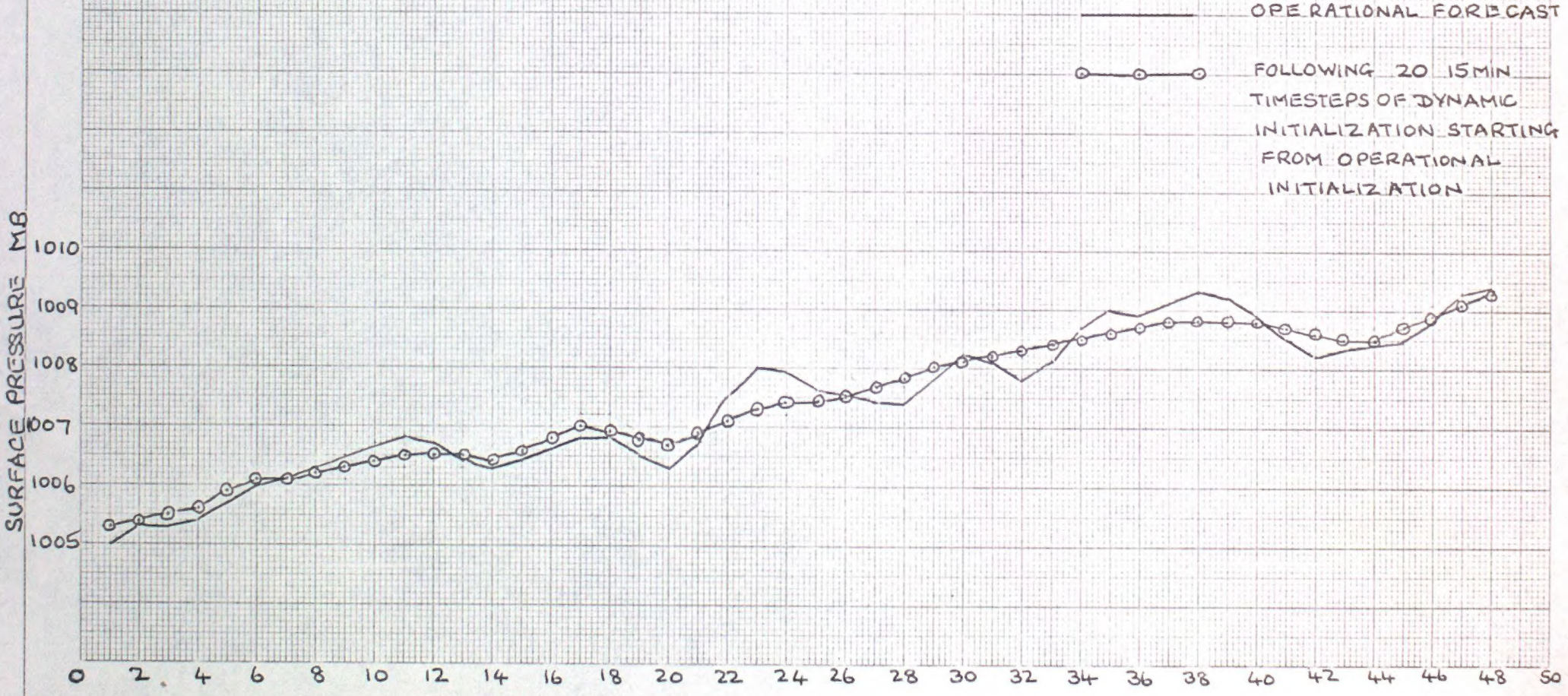

FIGURE 31a OPERATIONAL INITIALIZATION

SURFACE PRESSURE ISOBARS AT 4MB INTERVALS

0 HR.FORECAST. DATA TIME 12 Z 30 / 12 / 75. VERIFICATION TIME 12 Z 30 / 12 / 75

SI VERSION

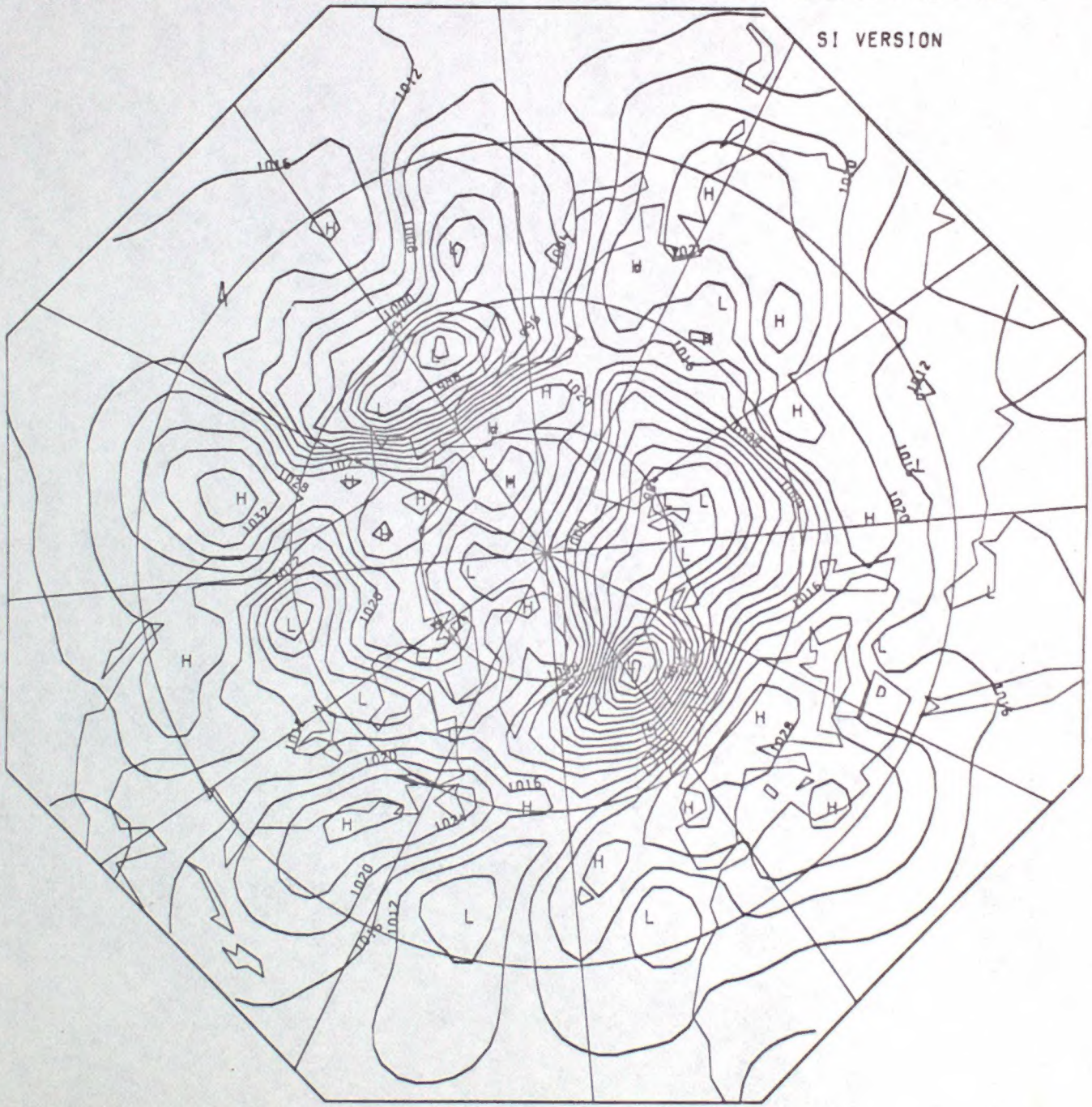

*FIGURE 316 OPERATIONAL INITIALIZATION FOLLOWED BY TWENTY 15-MIN TIMESTEPS (5 HOURS) OF DYNAMIC INITIALIZATION

SURFACE PRESSURE ISOBARS AT 4MB INTERVALS

5 HR. ~~FORECAST~~. DATA TIME 12 Z 30 / 12 / 75. VERIFICATION TIME 12 Z 30 / 12 / 75

DYNAMIC INIT

SI VERSION

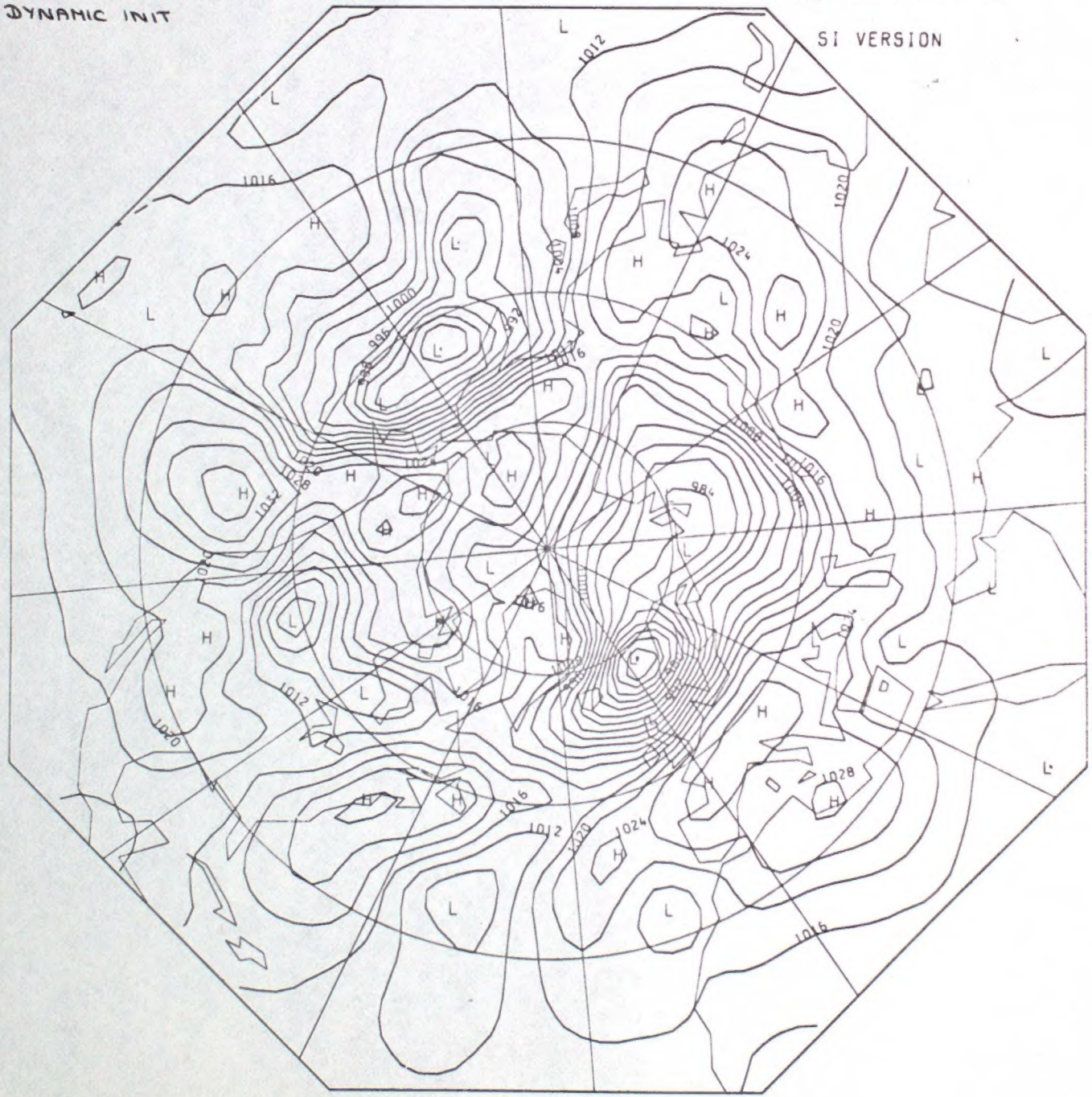
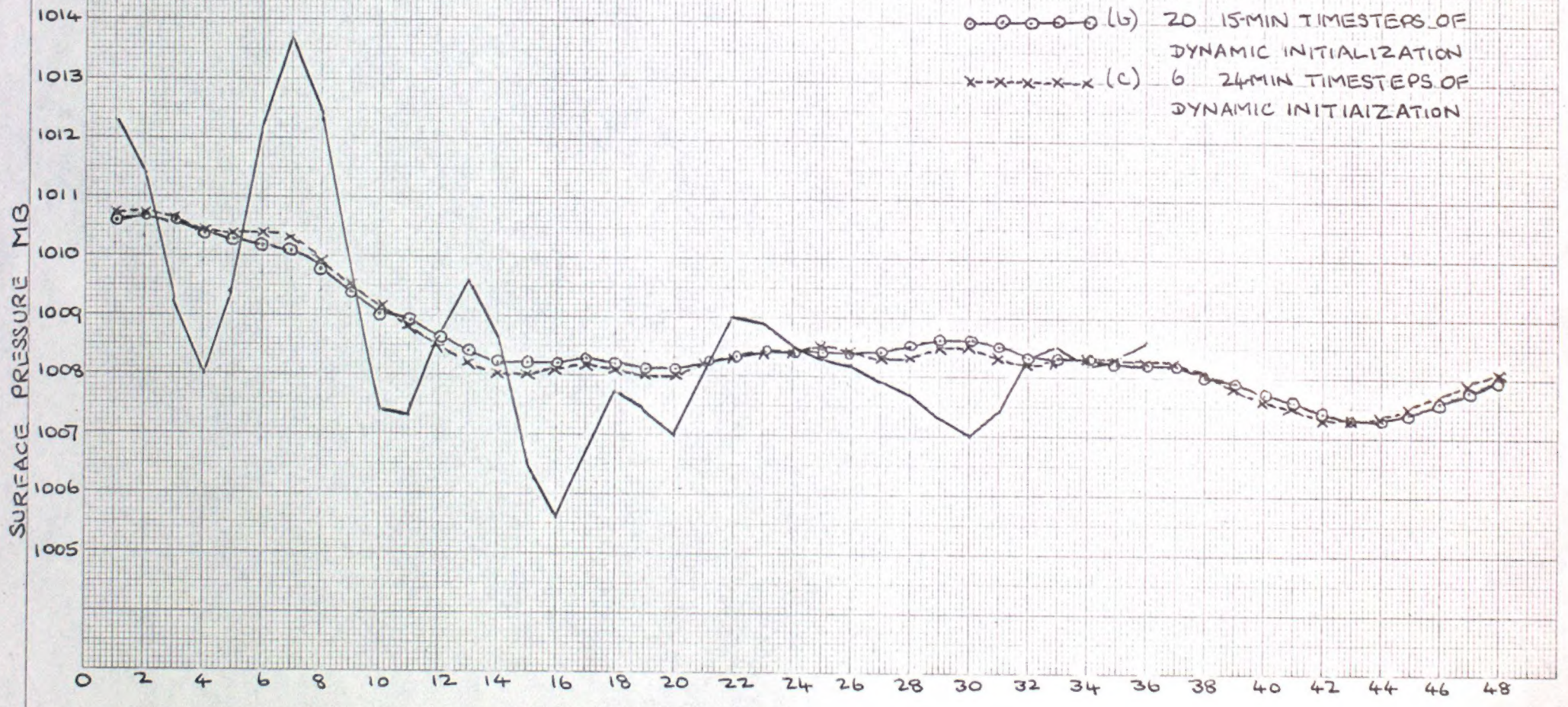
FIGURE 32. SURFACE PRESSURE AT A POINT IN THE ATLANTIC DURING FORECASTS FROM WIND ASSIMILATION WITH VARYING AMOUNTS OF INITIALIZATION